PHASE III FINAL REPORT

VOLUME 1

A VHF COMMUNICATION SYSTEM FOR A LOW ALTITUDE SATELLITE UTILIZING A DATA RELAY SATELLITE SYSTEM

MAY 1971

Contract No. NAS 5-11602

Goddard Space Flight Center
Technical Monitor / Paul Heffernan

Prepared By:
Project Manager / Dennis Eggert
Hughes Aircraft Company
Space and Communications Group
For
Goddard Space Flight Center
Greenbelt, Maryland

HUGHES
HUGHES AIRCRAFT COMPANY

PREFACE

This volume reports the results of one portion of Phase III of the Study of a Low Altitude Satellite Utilizing a Data Relay Satellite System. Phase I involved an investigation of the many technical considerations associated with a low altitude satellite which communicates with earth-based terminals via a data relay satellite system. Phase II consisted of a conceptual design of an earth observation spacecraft based on the results of Phase I. Phase III covered three separate study areas, one of which concerned communication to many low altitude satellites via a VHF link. This study is documented in this report.

CONTENTS

ILLUSTRATIONS

TABLES

1. INTRODUCTION AND SUMMARY

The objective of this study was to develop a VHF system concept capable of providing command access to and telemetry data from many low altitude satellites (LASs) via a data relay satellite (DRS) system. In addition, this system must allow range and range-rate determination from signal processing. This report presents the parametric analysis and rationale supporting the design choices and parameter selections leading to such a system concept.

1.1 CAPABILITIES AND CHARACTERISTICS

1) Effective command of a virtually unlimited number of LASs

2) Simultaneous telemetry transmission from 35 LASs within each DRS field of view

3) Range and range-rate tracking capability simultaneous with command and telemetry transmission

4) Performance of the above communication functions for all LAS altitudes between 100 and 2000 miles

5) Rejection of interference due to earth-based transmitters, earth-reflected signals (multipath), and other satellite transmitters

The system is based on the correlation properties of binary sequences called pseudonoise (PN) codes. A waveform corresponding to such a sequence can be correlated with a locally generated replica to separate the desired data signal from a particular transmitter from the total received signal and noise. The emphasis in this study was on the LAS system design, where simplicity, reliability, and good performance were design objectives along with weight, power, and size limitations.

The LAS communication system concept presented in this report employs a digital implementation of the delay lock discriminator method of PN code synchronization. This technique provides good performance with reliable digital techniques. Biphase modulation of the carrier by the PN coded binary signal is employed for both the command and telemetry links. More specific properties and performance data are listed below.

1) Command Link

RF bandwidth	100 kHz clear channel
Command bit rate	500 bits/sec
Probability of bit error	10^{-6}
Maximum handover acquisition time	18 seconds (performed only once per DRS viewing pass)
Chip rate (code pulse rate)	70 kilobits/sec
Code length	4095

2) Telemetry Link

RF bandwidth	1 MHz (136 - 137 MHz)
Telemetry data rate	500 bits/sec
Probability of bit error	10^{-6}
Maximum simultaneous transmissions	35 per DRS field of view
Chip rate	700 kilobits/sec
Code length	40950
RF power	2 watts

3) Tracking Performance

Range ambiguity	5450 miles
RMS range uncertainty	18 meters
RMS range-rate uncertainty	$\leq$10 cm/sec

4) LAS System Physical Parameter Estimates

Weight	3.2 pounds
Power	22 watts dc
Volume	25.5 in^3

The above estimates do not include the command decoder, telemetry encoder, antennas or power supplies

1.2 DRS REQUIREMENTS

Below are the DRS requirements for support of the LAS system with the above characteristics. These correspond to the capabilities of the Mark 1A DRS concept of Reference 1.

Communication coverage:	26 degree cone, earth centered
Minimum effective radiated power (ERP):	+26 dBw
Minimum receiver G/T:	-14 dB/°K
Coherent frequency conversion	

The requirement for coherent frequency conversion is necessary for range-rate determination from doppler shift measurement, and is important for it requires a phase-tracking receiver which maintains frequency lock of the ground-transmitted signal. Phase tracking is a well-established technique and should not present a serious problem; however, an alternate method is available. If a beacon signal, derived from the local oscillator of the DRS VHF system, is transmitted from the DRS directly to the ground, then the local oscillator drift can be compensated by ground processing. With this technique, the required third phase-tracking loop has been placed on the ground instead of on the DRS. However, either a separate beacon transmitter or frequency multiplexing is required to transmit the beacon signal to the ground.

1.3 REPORT ORGANIZATION

This report is organized in a logical progression from desired objectives to concept, implementation, and parameter selections for the LAS communication system. Section 2 presents and discusses the objectives, requirements and limitations for the VHF communication system. Section 3 treats the subject of LAS/DRS environment and shows the necessity of an interference-free frequency band for the command link. Section 4 presents an overall system concept and implementation method for the LAS VHF

system. Parametric trades are discussed in Section 5, leading to a selection of signal parameters resulting in the command and telemetry link characteristics of subsection 1.1. Section 6 presents some details of the LAS system implementation, and Section 7 provides a brief analysis of the potential tracking performance. Section 8 discusses a representative concept for the ground receiving system, and Section 9 treats the subject of antenna systems and signal combining techniques.

2. OBJECTIVES, REQUIREMENTS, AND LIMITATIONS

Necessary at the beginning of the VHF communication system design were the basic functional objectives and specific performance requirements of the system and the fundamental limitations imposed by the spacecraft and ground terminals. These basic items are outlined and briefly discussed below.

2.1 OBJECTIVES

These objectives can be separated into the two basic classes: functional and design.

2.1.1 Functional Objectives

The LAS/DRSS VHF communication system must be capable of performing the following functions. Expanded discussion on some items is presented in the following subsections.

1) LAS command capability

2) Spacecraft and housekeeping telemetry data transmission

3) Signal transponding for range and range-rate determination

4) Simultaneous support of a minimum of 40 low altitude satellites

5) Capability of direct ground communication of items 1, 2, and 3 for backup/emergency purposes

2.1.2 Design Objectives

In developing a communication system capable of providing the above functions, the following design objectives furnished guidelines:

1) Communication link performance independent of LAS orientation and attitude control

2) Substantial growth potential to accommodate additional LASs

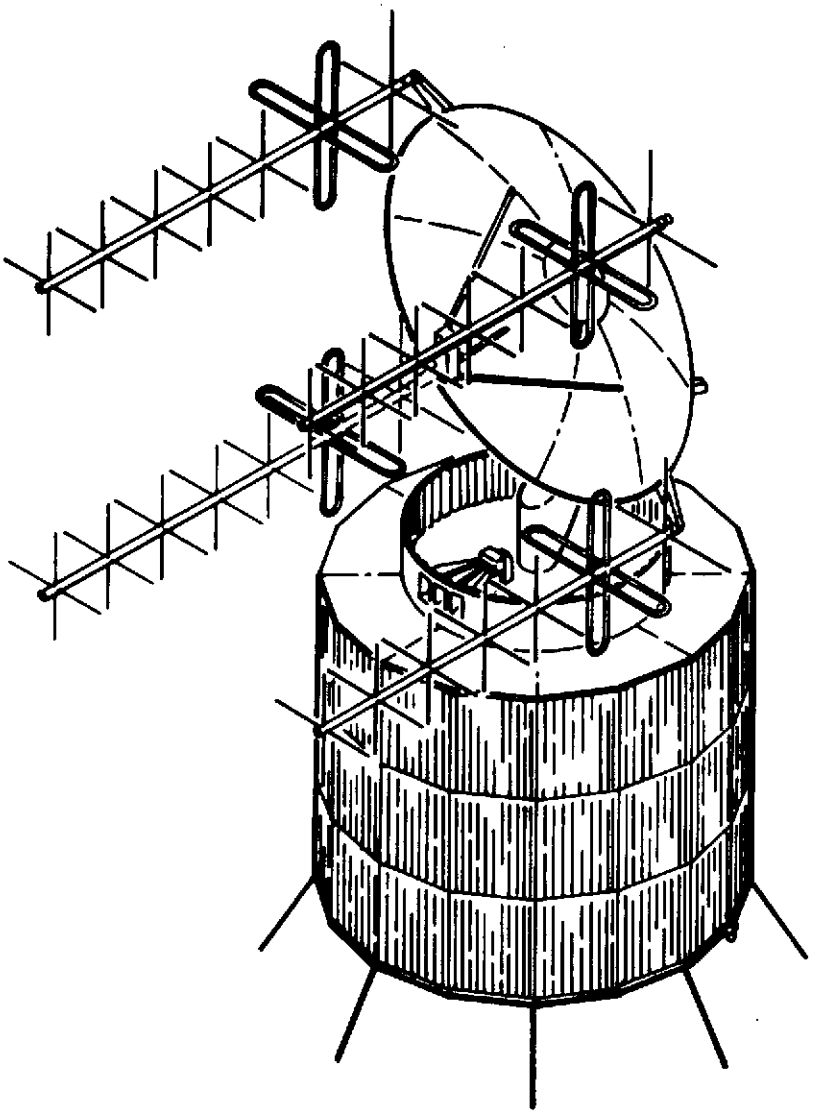

Figure 2-1. NASA, GSFC Mark 1A DRS Concept

3) Standardize the VHF communication system for all LASs.

4) Minimize problems associated with frequency allocations.

5) Minimize LAS system complexity.

6) Maximize LAS communication coverage.

Some of these items (such as 3, 4, 5, and 6 above) present conflicts resulting in engineering tradeoffs. These trades are discussed later in Section 5 as they arise in the analysis.

2.2 SPACECRAFT LIMITATIONS

2.2.1 Low Altitude Satellites

Fundamental to the above objectives is the requirement that this system be capable of providing tracking, telemetry, and command (TT&C) support to all NASA scientific and application LASs. Since every possible LAS structural configuration cannot be anticipated, this requirement is an amplification of design objective 1 above; i.e., the system operation should not require an attitude-stabilized spacecraft. If employed on such a vehicle, command access and telemetry monitoring should be possible in the event of an attitude control system failure.

A further restriction is imposed on the LAS system weight and power. The smallest booster (Scout) can put vehicles of 400 pounds or less into low altitude orbits. Vehicles of this class typically have power generation systems providing 150 watts or less. It is not clear what portion of the LAS weight and power should be allocated to the VHF communication system. Certainly, for the smaller vehicles where this system provides the entire communication capability, these fractions may be as high as 20 and 50 percent, respectively. For larger spacecraft with additional communication subsystems for wideband payload data, the fractions will be smaller, but the total weight and power capacity will be correspondingly larger. In general, it appears that the LAS transmitted RF power must be less than 10 watts. The design developed in this study assumed an RF power of 2 watts.

2.2.2 Data Relay Satellites

The Goddard Mark 1A concept of Reference 1 has been used to provide a representative DRS capability. In that reference, the Mark 1A concept, shown in Figure 2-1, is estimated to weigh 805 pounds and provide 260 watts of power, and the VHF transmitter RF power is specified as 20 watts. This RF power is consistent with the rationale that for a DRS with moderate communication capability (such as the Mark 1A), 40 to 70 watts of dc power will be used for DRS-to-LAS VHF transmission; and with measured VHF transmitter efficiencies of 30 to 40 percent, the radiated power will lie between 12 and 30 watts. In the link analysis of this study, the Mark 1A RF power of 20 watts is used.

The VHF communication system of the DRS will require a two-way repeater of the frequency translation type. Of some concern for this study is whether the frequency conversions in the repeater should or should not be phase coherent. A coherent repeater uses a phase-locked loop in the ground-signal receiver so that all frequency conversions will bear a known relationship to a ground-transmitted reference. Such a system allows accurate range-rate determination with a relatively simple signal design. An incoherent DRS repeater will require more complex ground and LAS equipment, more complex signal design, and greater bandwidth (for the same performance). One alternative for an incoherent repeater requires that some multiple of the free-running local DRS oscillator be transmitted to the ground on a separate beacon. This will allow the long-term oscillator drift to be properly accounted for in the range-rate determination process. In this study, it is assumed that either the latter technique or a coherent repeater will be used by the DRS.

2.3 COMMAND AND TELEMETRY DATA

Commands to the LAS and low rate data from the LAS are conveniently and most frequently transmitted using binary-coded signals. It was assumed in this study that the commands at the ground station and telemetry data at the LAS will be available in digital form. Further, this study did not treat the signal encoding/decoding process, but was limited to a parametric variation of the bit rate of the resulting digital signals.

2.3.1 Command

Functional objective 4 is interpreted as not requiring simultaneous command transmission to 40 LASs, but allowing command of any specific LAS when desired, and allowing all to be commanded within a short period. For instance, at a rate of 500 bits/sec with a 50 bit command sequence, ten LASs could be commanded within 1 second and all 40 within 4 seconds. A command capability such as this appears to be quite satisfactory.

The alternate requirement of simultaneous command does not appear to be necessary, and it would require a system of considerably greater complexity than the one developed in this study. Thus, sequential command capability was taken as the preferred approach because it allows the optimum use of available DRS VHF transmitter power. Note from the above example that quick access is possible at relatively low command bit rates. The command bit rate is allowed a limited variation in the parameteric analysis of subsection 5.1.

2.3.2 Telemetry

The possibilities for telemetry data are more varied. As shown later, the limited capacity of the LAS/DRSS VHF link will not allow high bit rate transmissions from small satellites. Of course, large satellites can provide greater transmitter power to achieve higher bit rates, but this higher power may interfere with and seriously degrade the telemetry transmissions

from smaller satellites. Inasmuch as one of the design objectives is to standardize the on-board VHF communication system for all LASs, a transmitter power should be chosen consistent with both the capabilities of low power NASA scientific and application satellites and sufficient link data capacity. In the telemetry link analysis of Section 5, an LAS ERP of 0.0 dBw is assumed which implies a transmitter power of 2 or 3 watts, depending on the omnidirectional antenna configuration and capability.

The functional objective for simultaneous ground reception of telemetry data from a minimum of 40 LASs is interpreted as an overall system requirement. If 40 LASs are in orbit, on the average, only 20 to 25 will be visible from a single DRS. Thus, 40 represent a peak load for a single DRS with small probability of occurrence. If a system of two or more DRS are employed, and if each can relay 25 to 35 simultaneous telemetry transmissions without degradation due to mutual interference, then the DRS system can accommodate more than 40 simultaneous transmissions. Thus, the simultaneous telemetry relay design objective for each DRS field of view was allowed a range of 25 to 35. Note in subsection 1.1 that the upper limit was achieved.

2.4 TRACKING

Tracking refers here to the determination of the LAS range and range rate via the communication link. In lieu of establishing absolute requirements for the LAS/DRSS tracking system, the performance of the Goddard Range and Rate System (GRARR) (Reference 2) was used as a guide in this study. This system modulates a carrier with several distinct frequencies. The combined signal is received by the LAS directly from the ground and repeated directly to the ground. The estimated performance is shown in Figures 2-2 and 2-3. In Figure 2-2, the two curves correspond to the highest baseband frequency used to modulate the carrier. In Figure 2-3, the effect of varying the noise bandwidth, B_n, and the measurement rate can be seen. These performance estimates were used as guidelines for comparing the performance of the system developed in this study.

2.5 ANTENNAS

For continuous communication capability with many LASs, the DRS antenna radiation pattern must cover the earth and a spherical region about it. If LAS altitudes are assumed to be less than 2000 miles, the resultant sphere of 6000 mile radius subtends a cone with a vertex angle of about 26 degrees. Since an antenna with this 3 dB beamwidth has a peak gain of approximately 16 dB, the minimum gain over the required field of view is about 13 dB. The LASs are assumed to have omnidirectional antennas with gains less than 0 dB.

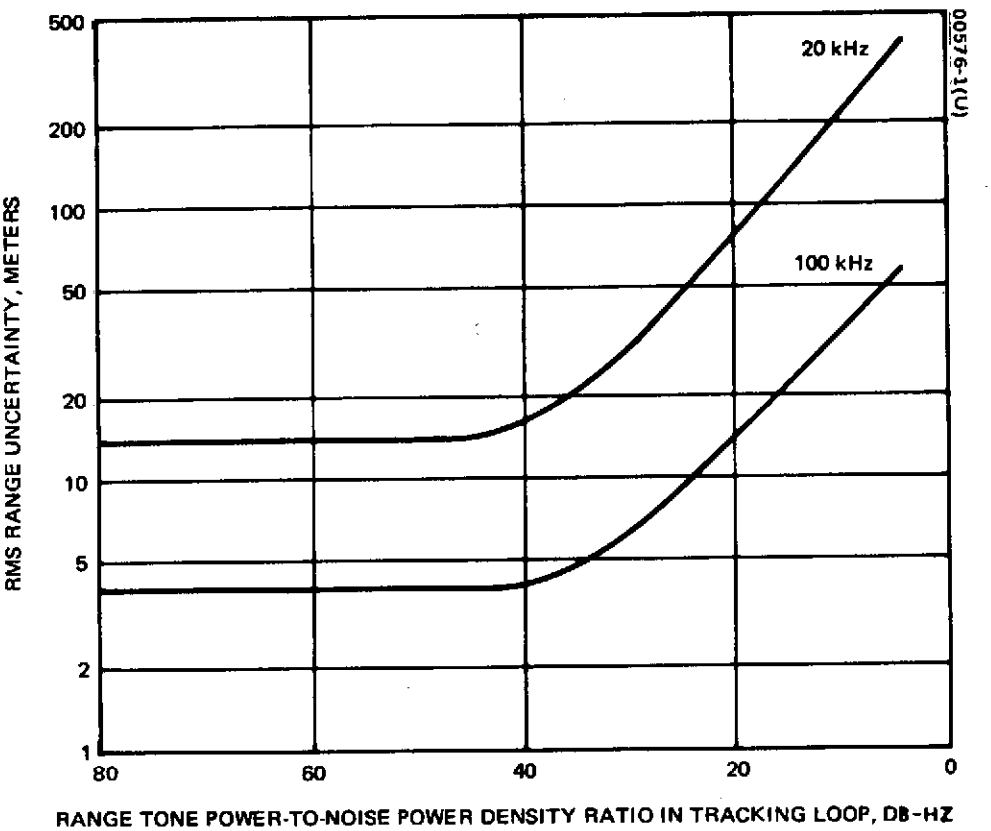

Figure 2-2. Range Instrumental Accuracy of GRARR VHF System (Figure 4-43 of Reference 2)

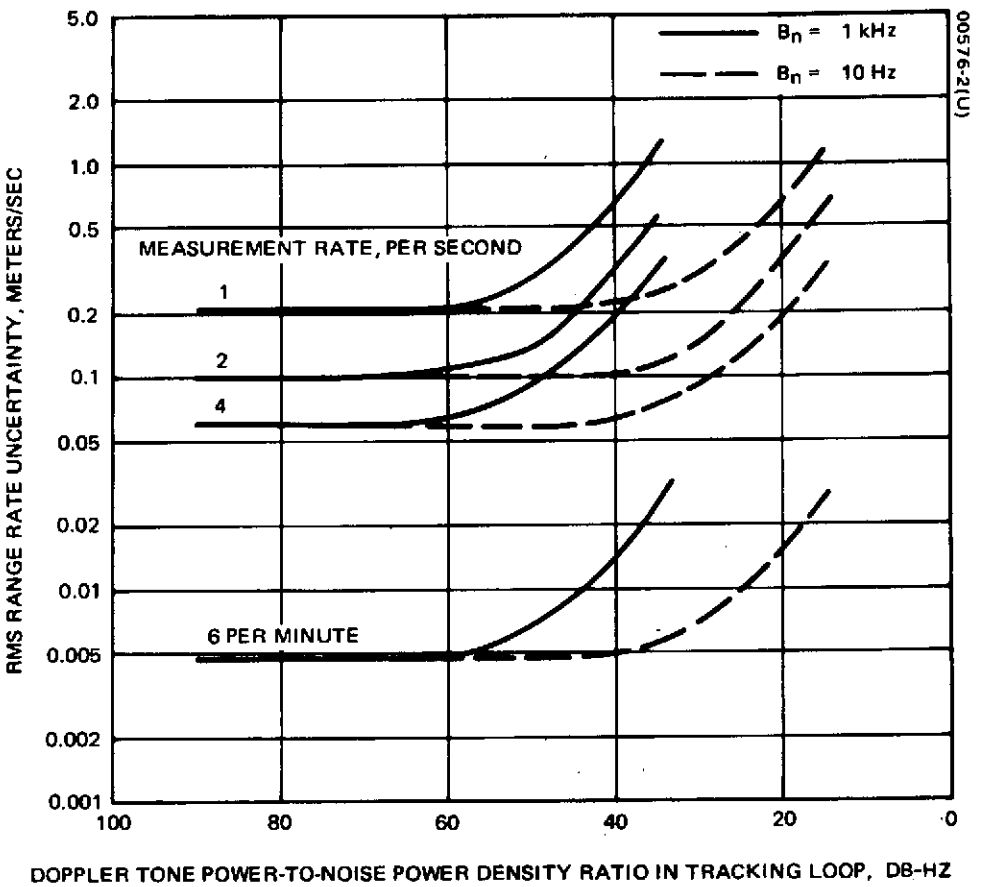

Figure 2-3. Range Rate Instrumental Accuracy of GRARR VHF System

(Figure 4-46 of Reference 2)

2.6 FREQUENCY AND BANDWIDTH

At present, NASA has two frequency bands for command and telemetry purposes. The band 148 to 149.9 MHz is used for command, and the band 136 to 138 MHz for telemetry to the ground. With a DRS system, the 148 to 149.9 MHz band would be used for commands transmitted from the DRS to the LAS. The LAS data transmission to the DRS would occupy a portion of the 136 to 138 MHz band. The system developed in this study is not strongly dependent upon the use of these frequency bands, but the interference present in them resulted in some design choices that may not be appropriate for other frequency ranges.

In general, with the fixed gain antennas described in the previous subsection, link capacity is increased as the frequency is decreased. Thus, the use of the lowest possible frequencies is advantageous. The VHF frequencies above are the lowest currently available for the space applications of NASA and were assumed as the nominal frequency bands for command and telemetry in this study.

3. ENVIRONMENT

VHF transmissions between LASs and a system of geosynchronous delay satellites will be at a substantial disadvantage relative to conventional VHF transmissions direct to the ground due to a combination of environmental conditions which include the substantially greater distances involved and natural and man-made electromagnetic interference. While the former derives from geometrical considerations common to all communications systems employing synchronous satellites, the latter is in many ways peculiar to the VHF LAS/DRS system under study here. The two sources of electromagnetic interference in VHF LAS/DRS links are ground-based emitters operating in the same frequency bands as LAS/DRS transmissions and reflections by the earth of LAS and DRS transmitted signals.

In this section, both sources of interference are discussed. First, as a basis for the discussion and for later link and tracking analysis, some major aspects of the LAS/DRSS geometry are required.

3.1 GEOMETRY

The geometrical quantities of interest for communication system analysis include the range, range rate, visibility of the LAS by a DRSS, and a number of angles helpful for specifying relative antenna orientations and for defining the earth reflection process. Related to the range and range rate are the doppler shift and doppler rate. The first three are discussed in detail in References 3 and 4; the results most important to this study are repeated here for completeness.

3.1.1 Separation Angle and Visibility

A useful quantity in the LAS-DRS communication geometry is the separation angle, ϕ, shown in Figure 3-1. This angle is related to the other orbital angles shown in the figure by

$$\cos \phi = \cos \theta \cos (\psi - \lambda) + \cos i \sin \theta \sin (\psi - \lambda) \qquad (1)$$

The separation angle is a function of both the range between the two satellites and LAS altitude. The relationship between the maximum separation angle and LAS altitude is shown in Figure 3-2.

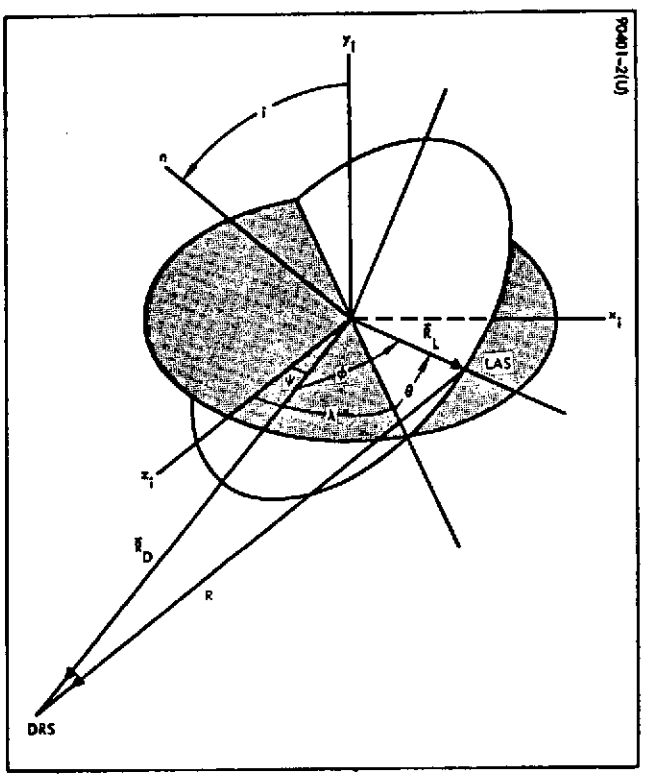

Figure 3-1. Orbital Parameters

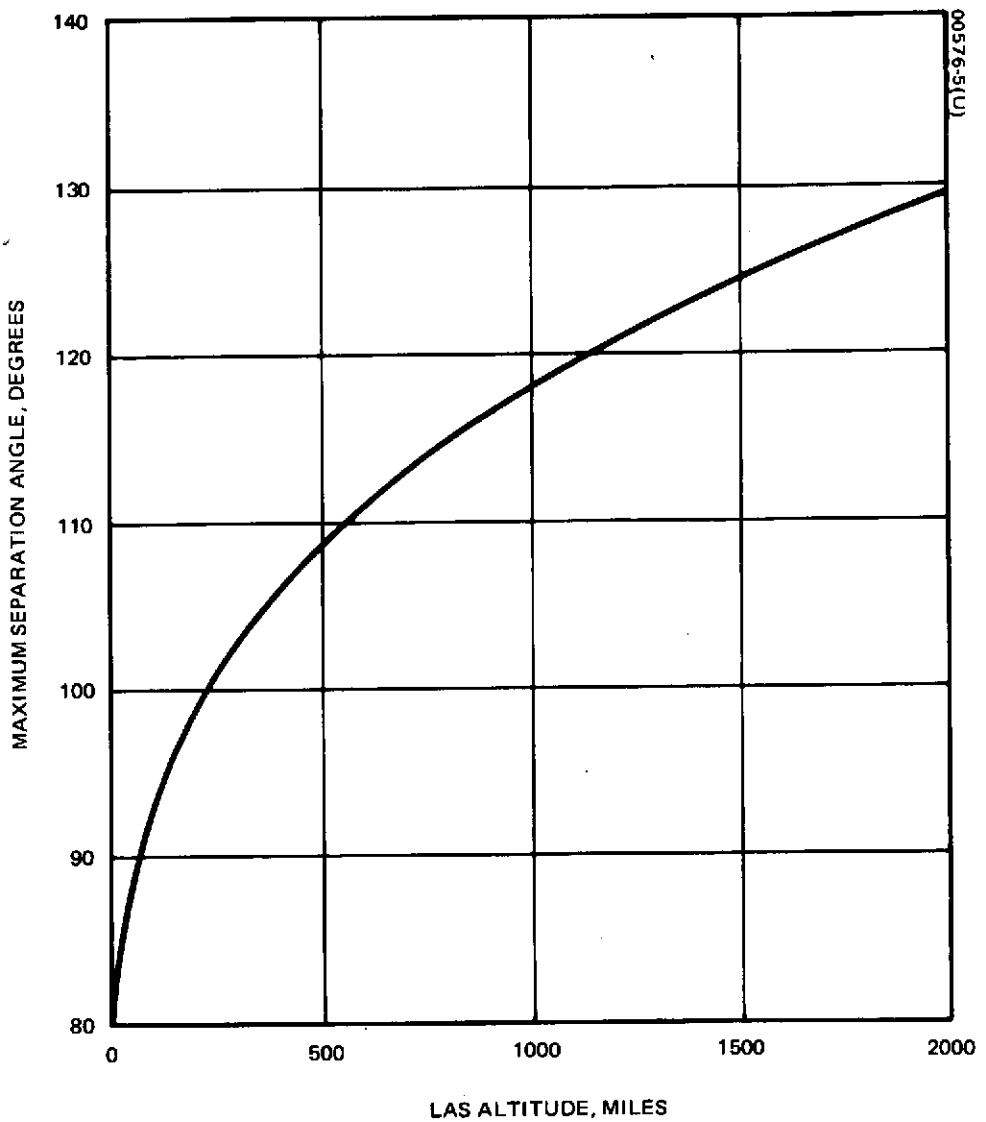

Figure 3-2. Maximum Separation Angle as Function of Altitude

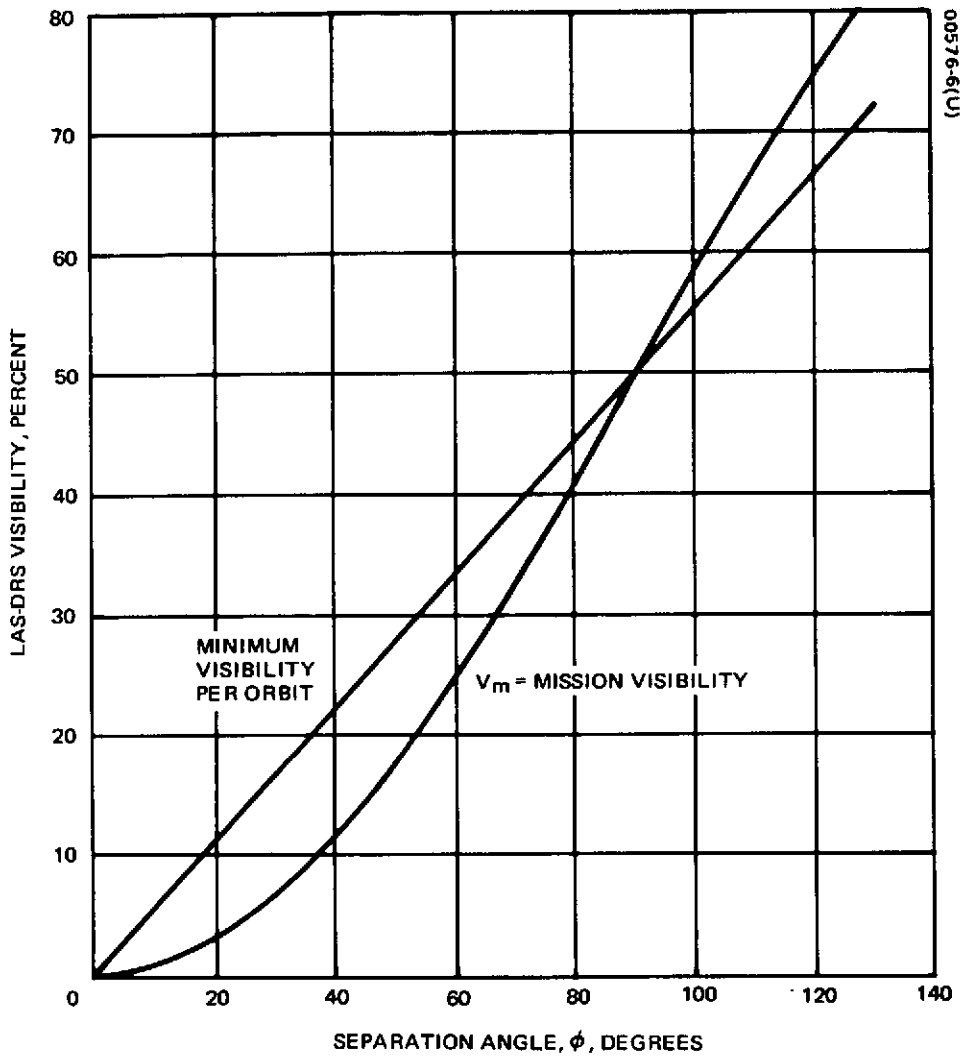

Figure 3-3. Visibility From Single DRS

Now, if communication were limited to separation angles less than some specified value, ϕ_{max}, both maximum range and minimum visibility would be determined. The minimum visibility in any single orbit, V_o, is given approximately by

$$V_o = \frac{\phi}{180} \tag{2}$$

where ϕ is given in degrees. The total mission visibility is given by the portion of a sphere intersected by a cone of half-angle ϕ with vertex at the sphere's center. From an elementary mensuration formula, it can then be shown that the long-term average or mission visibility, V_m, is given by

$$V_m = \frac{(1 - \cos \phi)}{2} \tag{3}$$

The relationships given by Equations 2 and 3 are illustrated in Figure 3-3. Note, that for $\phi \geq 90$ degrees, the mission visibility is greater than the minimum orbital visibility.

3.1.2 Range

The range, R, or distance between the LAS and a DRS is a function of the separation angle, ϕ, and the LAS altitude and is given by

$$R^2 = R_D^2 + R_L^2 - 2R_D R_L \cos \phi \tag{4}$$

where

R_D = 26,200 miles

$R_L = R_e + h$

R_e = 3963.2 miles

h = LAS altitude in miles

Equation 4 is illustrated in Figure 3-4.

The maximum value of ϕ, which is determined by the LAS altitude, establishes the maximum range. The relationship between the LAS altitude and this maximum range to a DRS is shown in Figure 3-5. If three or more DRSs are used and are symmetrically spaced, then the maximum range to any one occurs when the LAS orbit radius is perpendicular to R_s. Because of the relatively large values of R_s and R_e, the effect of low altitudes on this range is small as shown in Figure 3-5. This range is less than 26,900 miles for LAS altitudes less than 2000 miles.

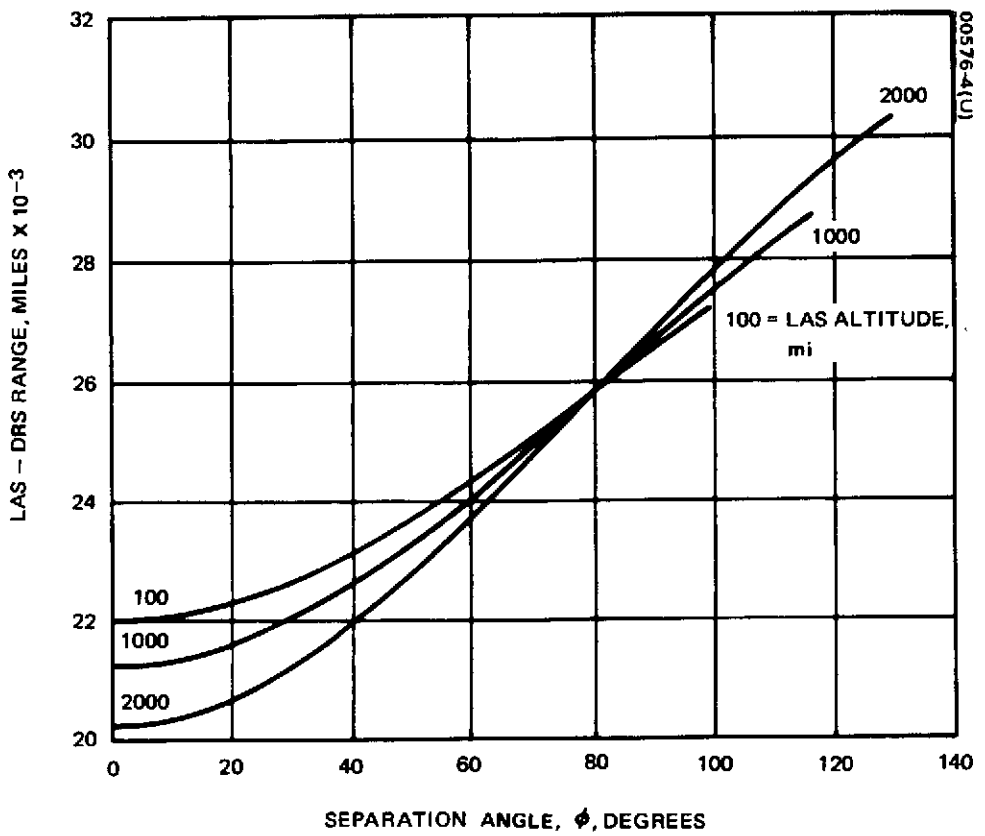

Figure 3-4. Range as Function of Separation Angle

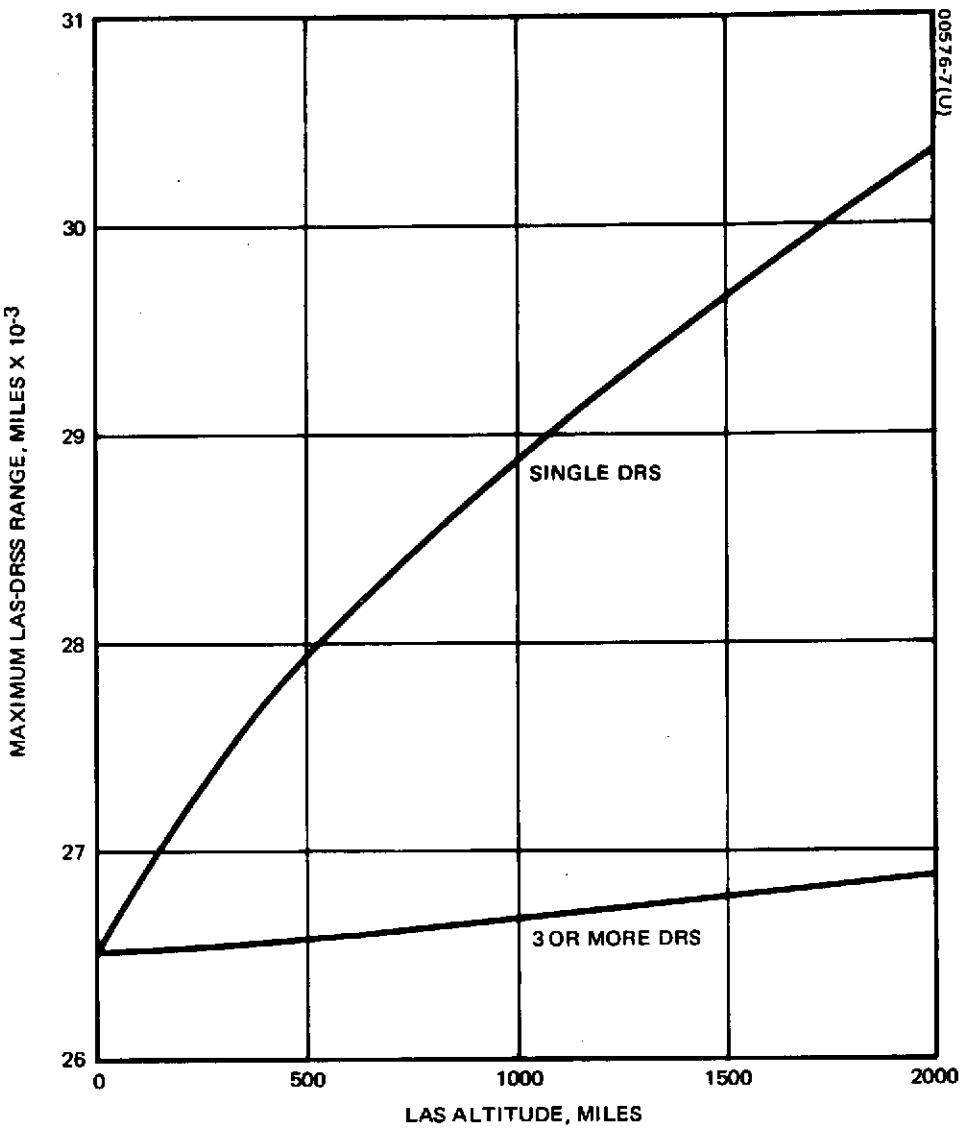

Figure 3-5. Maximum LAS-DRS System Range

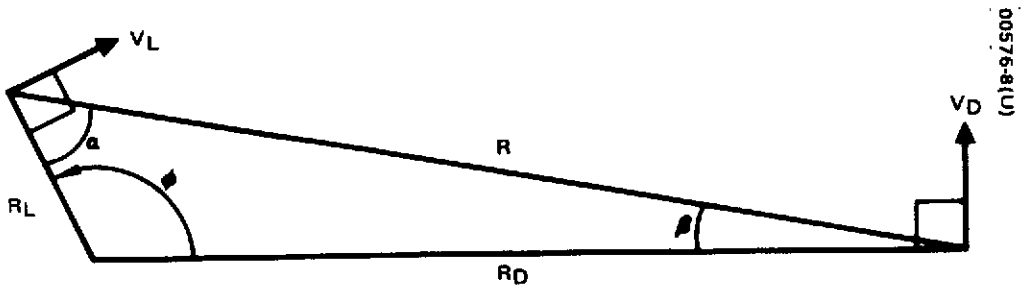

Figure 3-6. Maximum Range Rate Geometry

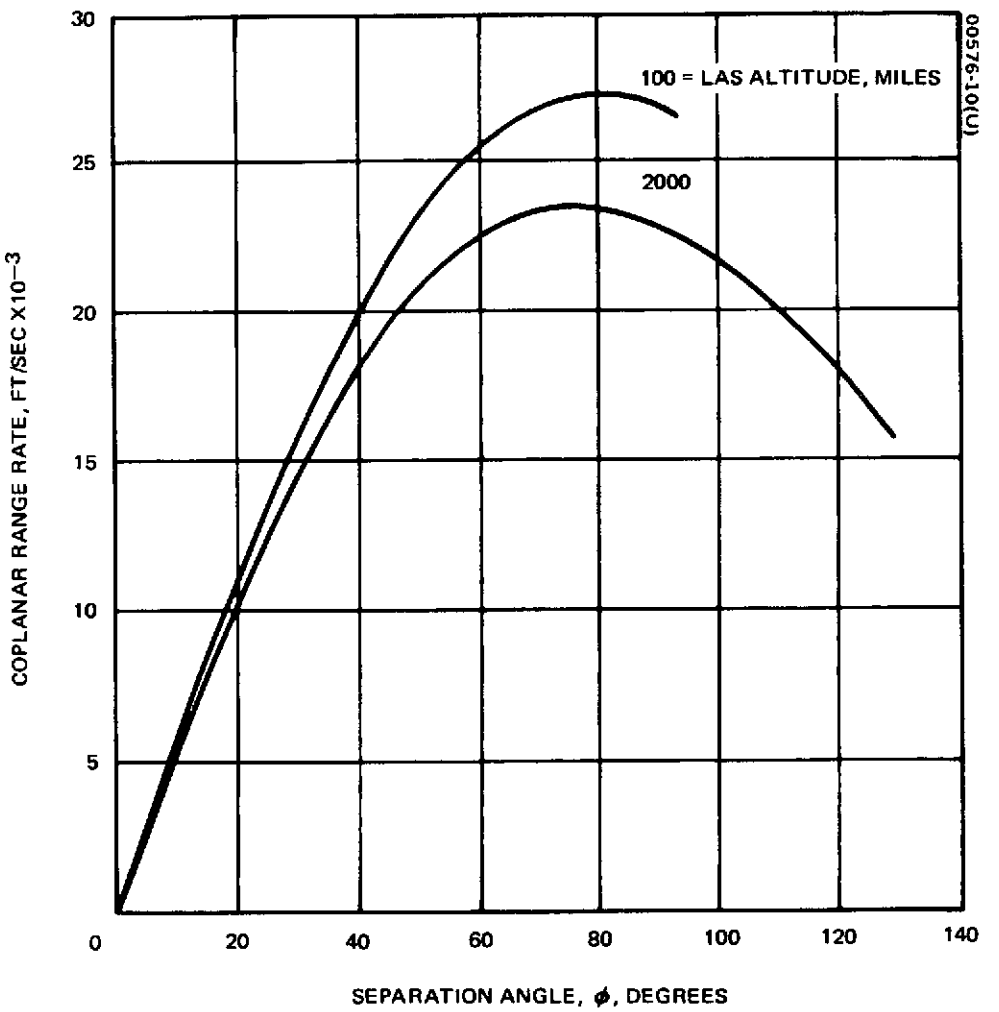

Figure 3-7. Coplanar Range Rate

3.1.3 Range Rate

The range rate is the component of the relative velocity vector of the two satellites which is parallel to the range vector, R. The maximum possible range rate occurs if the orbits of the two satellites are coplanar. This case is shown in Figure 3-6. Referring to this figure, it can be shown that

$$\dot{R} = \left(\frac{V_L R_D + V_D R_L}{R} \right) \sin \phi \qquad (5)$$

Using Equation 5, the range rate for circular LAS orbits as a function of ϕ is shown in Figure 3-7. Note that the peak rate occurs at separation angles between 75 and 85 degrees. The speed, V_D, of the DRS is approximately 10,100 fps and LAS speed, V_L, is a function of its altitude for circular orbits. This latter relationship is shown in Figure 3-8.

An LAS may have an elliptical orbit within the altitude bounds of 100 and 2000 miles. If the perigee is 100 miles and the apogee is 2000 miles, it can be shown that the maximum speed, which occurs at perigee is 27,900 fps. Using Figures 3-2 and 3-7 and Equation 5, it can be shown that the maximum range rate for this special case is approximately 29,700 fps. A more common case involves a circular polar LAS orbit and an equatorial DRS orbit. For this case, the maximum range rate is the LAS orbit speed given by Figure 3-8.

3.1.4 Doppler Shift

The doppler shift is the change in received frequency from the transmitted frequency. It is a function of the range rate and carrier frequency and, ignoring relativistic effects, is given by

$$\Delta f = \frac{\dot{R}}{c} f \qquad (6)$$

where f is the transmitted frequency and c is the speed of light $= 9.84 \times 10^8$ fps. Using Equations 5 and 6, the doppler shift can be calculated as a function of the separation angle, LAS altitude, and transmission frequency. However, for this treatment, maximum values are sufficient.

Using the extreme case of the eccentric LAS orbit coplanar with the DRS orbit, the maximum doppler shifts at 137 and 149 MHz are 4.13 and 4.5 kHz, respectively. In a coherent transponding system, where the transponder's transmitter frequency is a function of the received frequency, these values must be doubled for the two-way transmission. Further, this shift will both increase and decrease the frequency; thus, the total two-way variation in frequency will be, at maximum, 16.5 and 18 kHz, respectively.

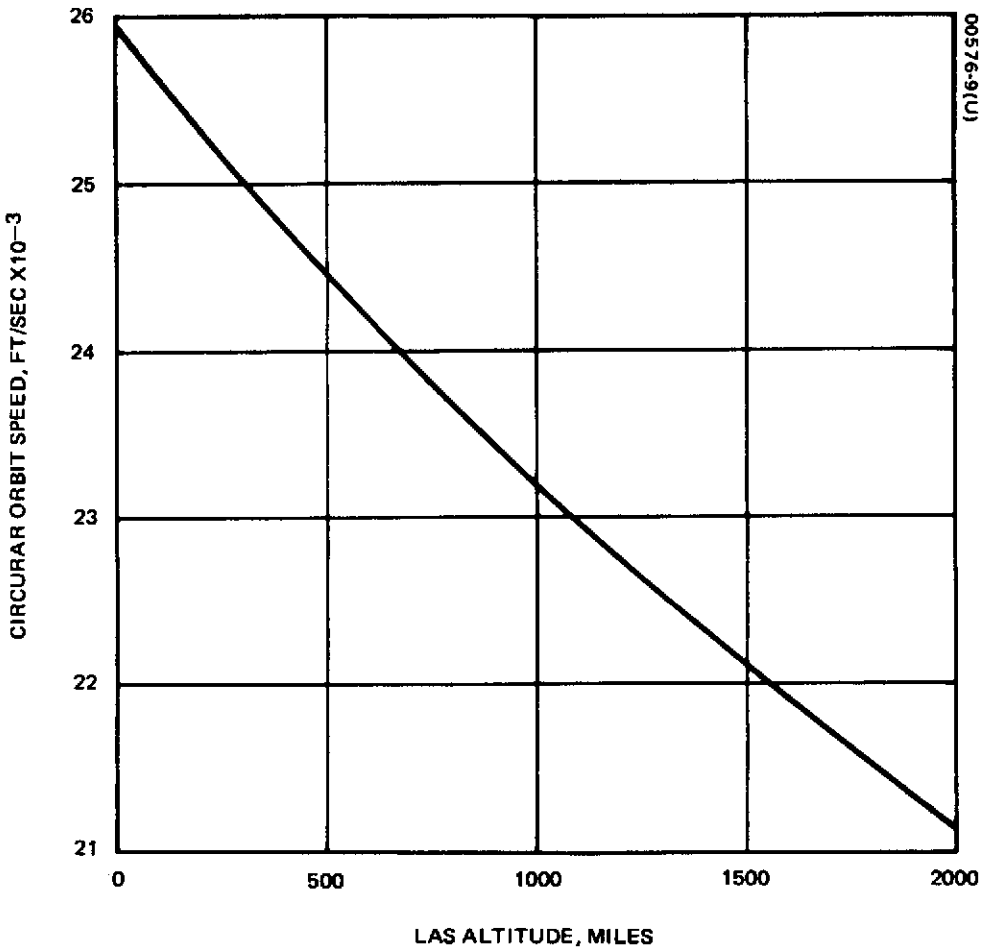

Figure 3-8. Circular Orbit Speed as Function of Altitude

For a circular, polar LAS orbit with an altitude of 400 miles, the two-way variation at 140 MHz is approximately 15 kHz.

3.1.5 Doppler Rate

Of concern for analyzing the behavior of phase-locked loops is the rate of change of the frequency. This is related to the second derivative with respect to time of the range. Referring again to Figure 3-6, it can be shown that

$$\ddot{R} = \left(A\dot{\phi}\ \frac{\cos\phi}{R} - \frac{R_L R_D}{R^3} \sin^2\phi \right) \tag{7}$$

where

$$A = V_L R_D + V_D R_L \tag{8}$$

The rate of change in frequency which is equal to the rate of change of doppler shift is given by

$$\dot{f} = \frac{d}{dt}(\Delta f) = \frac{\ddot{R}}{c} f \tag{9}$$

For circular orbits, $\ddot{R}$ is a function of the separation angle and so, too, is $\dot{f}$. For f = 140 MHz, the frequency rate is shown in Figure 3-9 as a function of ϕ.

3.2 MULTIPATH

The term "multipath" refers to a communication link in which there exists more than one signal propagation path between the signal source and the receiver. In LAS-DRS communication, there are basically two paths between the satellites, as shown in Figure 3-10: a direct path and a path by reflection from the earth's surface. The total reflecting surface may be envisioned as many smaller reflecting surfaces; hence, the overall reflection path is a collection of many reflection paths. The signal received via this reflection path is delayed and distorted with respect to the received, directly transmitted signal.

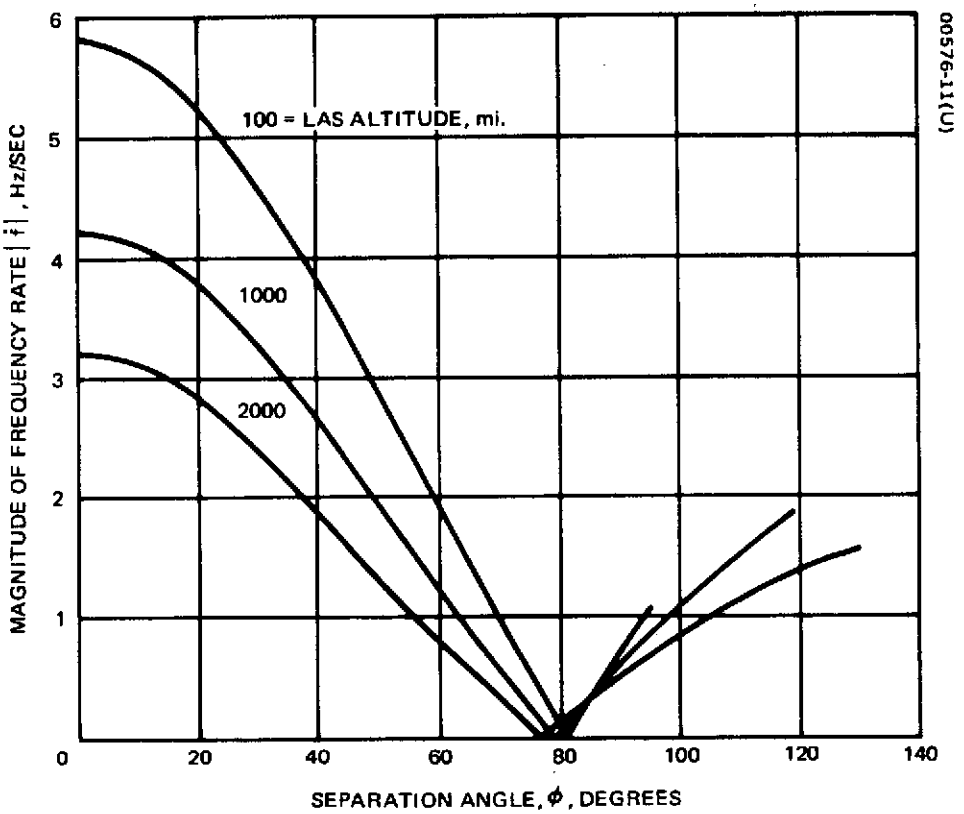

Figure 3-9. Magnitude of Rate of Change of Received Frequency

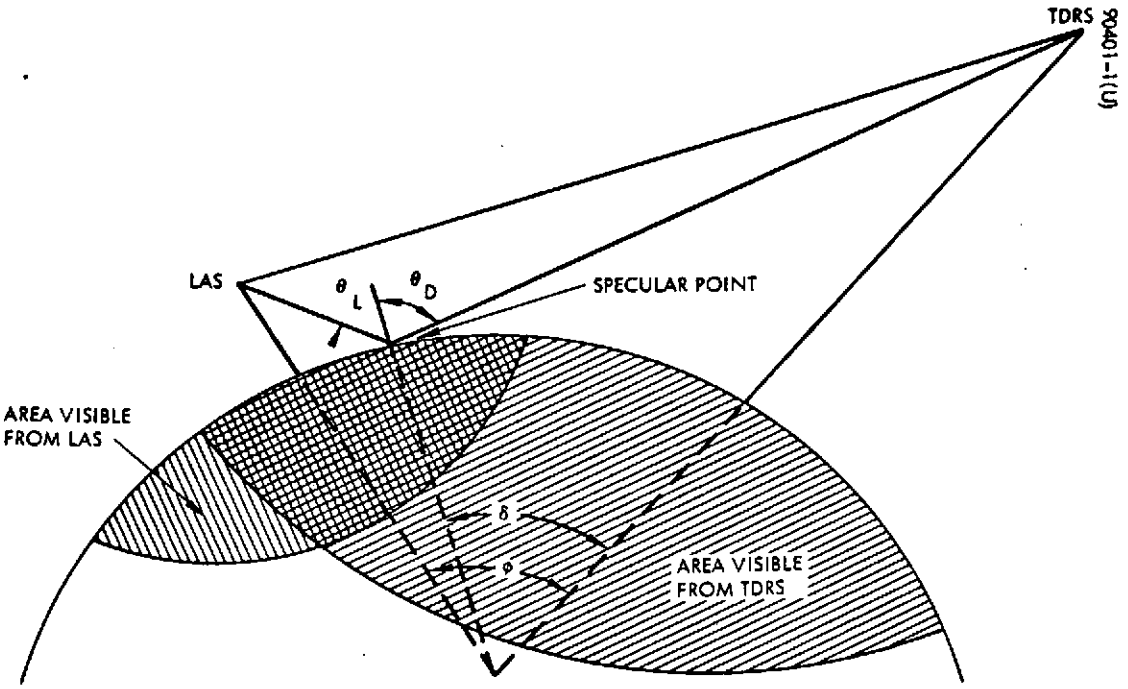

Figure 3-10. LAS-DRS Geometry

In a study performed under this same contract and documented in Reference 3, this phenomenon is discussed in considerable detail, and estimates of the reflected power and its time and frequency characteristics are presented. Some of those results most relevant to the communication objectives of this study are repeated here. Three aspects of the reflected signal provide a useful characterization; they are

1) Power transmission — the total power reflected by the earth to the receiver

2) Time response — received reflected power as a function of time

3) Frequency effects — multipath effect on a fixed frequency signal

In the statistical model of reflection discussed in Reference 3, the following parameters influence these characteristics:

1) Geocentric LAS-DRS separation angle, ϕ

2) LAS altitude, h

3) Transmission frequency, f

4) Surface electrical properties (sea or land)

5) RMS surface slope (roughness factor, η

6) RMS surface height variation, σ

7) Antenna polarizations

The separation angle, altitude, and transmission frequency have been mentioned above. For this study, the frequency will be assumed to have a nominal value of 140 MHz. An analysis of electromagnetic reflection from a surface shows that for typical electrical properties, sea water is a much better reflector than land. Since the sea covers about 70 percent of the earth's surface, an LAS-DRS communication system must be designed to operate over this surface. The surface roughness parameters, σ and η, have established ranges, but typical values are $\eta = 0.1$ radian and $\sigma = 1.0$ meter.

Part of the reflected signal is phase-coherent with the direct signal and part has a randomly varying phase. The coherent reflected power is a function of the separation angle and of the ratio of the rms surface height variation and wavelength. Linear antenna polarization may be defined with respect to the plane of Figure 3-10. Horizontal polarization implies that the electric field vector lies perpendicular to this plane, and for vertical polarization, the electric field vector lies in the plane. If an antenna is considered omnidirectional, then the magnitude of these vectors in all directions within the plane is the same.

3.2.1 Reflected Power

A quantity useful for evaluating the received reflected power with respect to the received direct power is called the relative power and is defined as the ratio of the two. Figure 3-11 shows an estimate of the relative power as a function of separation angle and altitude. The worst case occurs for low altitudes when the separation angle is zero, i.e., the DRS is directly above the LAS. From Figure 3-11, it can be seen that the incoherent reflected power is only about 1 dB less than the directly received power for this condition and an altitude of 100 miles. Figure 3-12 shows the effect of varying surface roughness for an LAS altitude of 300 miles.

3.2.2 Time Response

The time response is most conveniently referenced to the specular point reflection, where the specular point is the surface point where θ_R and θ_D of Figure 3-10 are equal. It can be shown that energy reflected from this point is delayed less than that reflected from any other point. Thus, energy reflected from surrounding points will be delayed slightly longer, causing a time spreading of a transmitted signal.

A simple calculation using the maximum and minimum ranges shown in Figure 3-4 for LAS altitudes of less than 2000 miles shows that the direct path time delay lies between 0.108 and 0.16 second. Both the direct and specular point time delay can be computed as a function of the separation angle, but a more meaningful quantity is the time difference between the two delays. This difference, defined as the specular differential time delay, is shown in Figure 3-13 as a function of separation angle. The system described later takes advantage of this time delay to discriminate against this interference.

For comparison purposes, Figures 3-14 and 3-15 present estimates of a reflected impulse for two different roughness conditions. The curves of Figure 3-14 are normalized to the specular point so that only the shapes are shown. Comparing these figures with Figure 3-13, it can be seen that for the majority of geometrical conditions ($\phi \leq 80$ degrees) the time spreading is at least an order of magnitude less than the specular differential delay and will be two orders of magnitude less under moderate surface roughness conditions ($\eta \leq 0.05$).

3.2.3 Frequency Response

The doppler shift of the direct signal has been discussed in subsection 3.1 above. The doppler shift of the reflected signal may be separated into two components as was done for the time response: 1) the doppler shift of the specular point reflection and 2) the frequency spreading about the specular point reflection. As was discussed in the previous subsection,

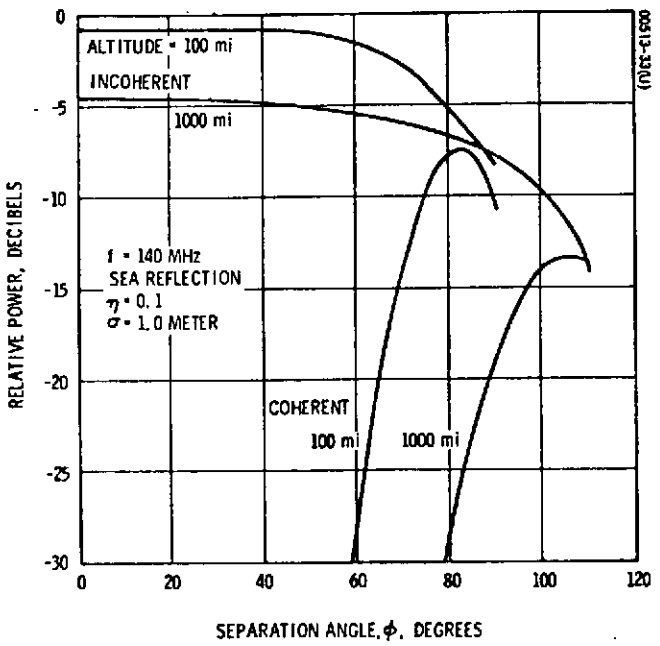

a) Horizontal Polarization

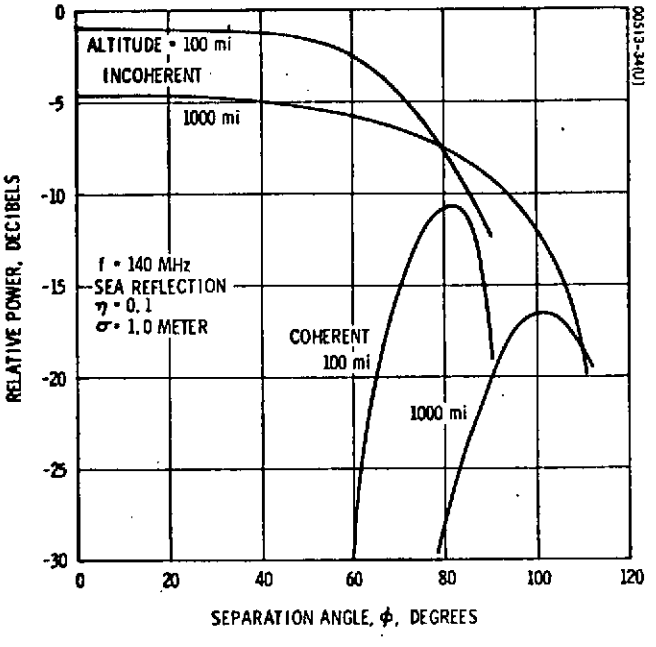

b) Vertical Polarization

Figure 3-11. Relative Multipath Power

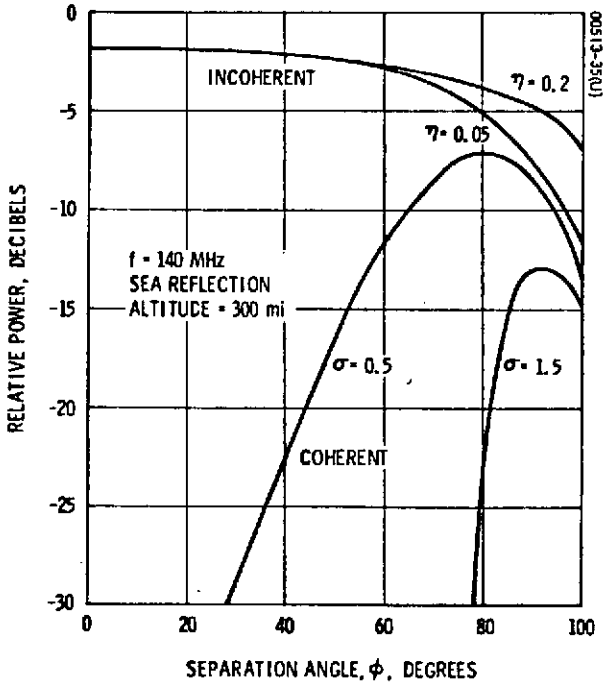

a) Horizontal Polarization

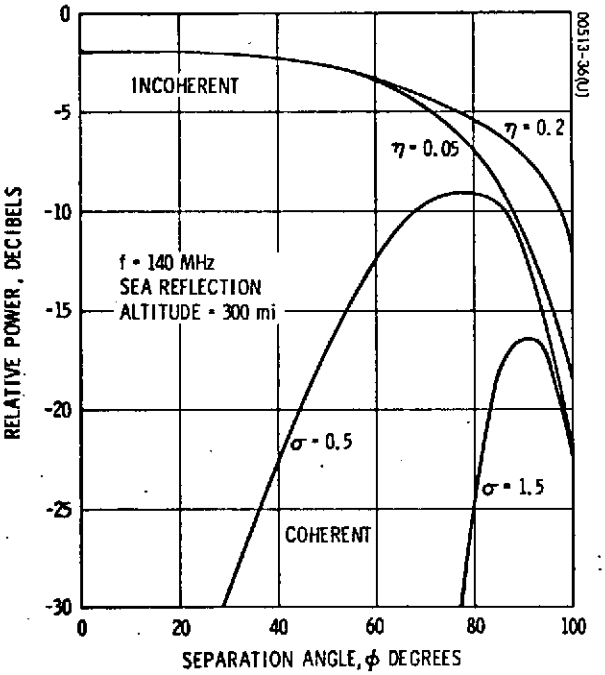

b) Vertical Polarization

Figure 3-12. Effect of Roughness Factor and RMS Surface Variation

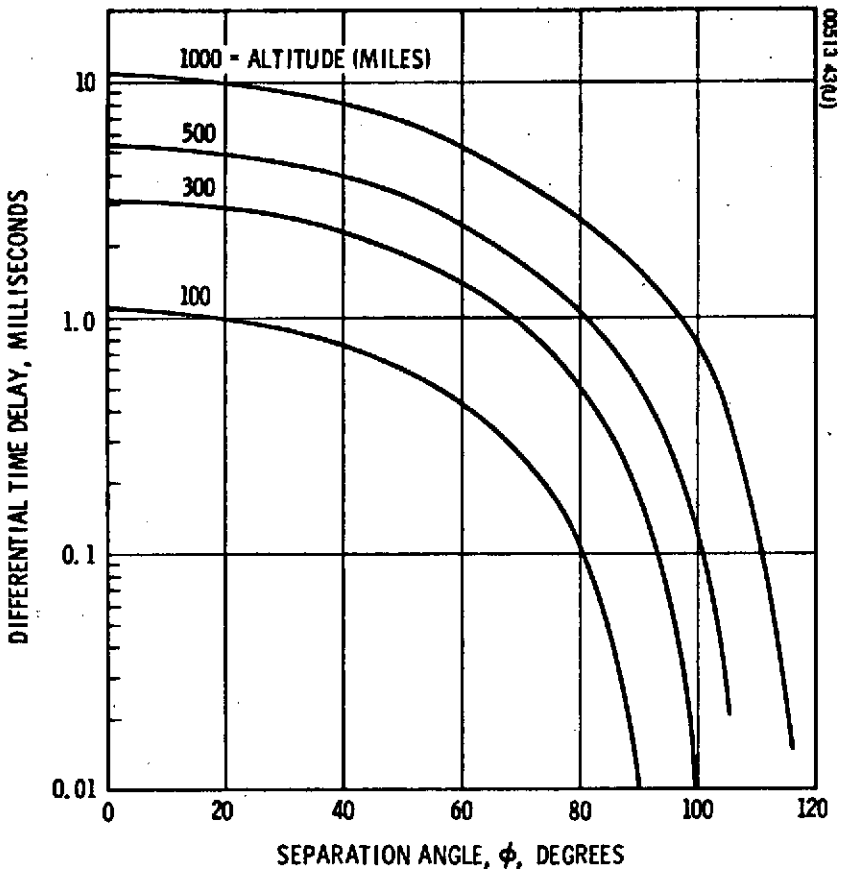

Figure 3-13. Specular Differential Time Delay

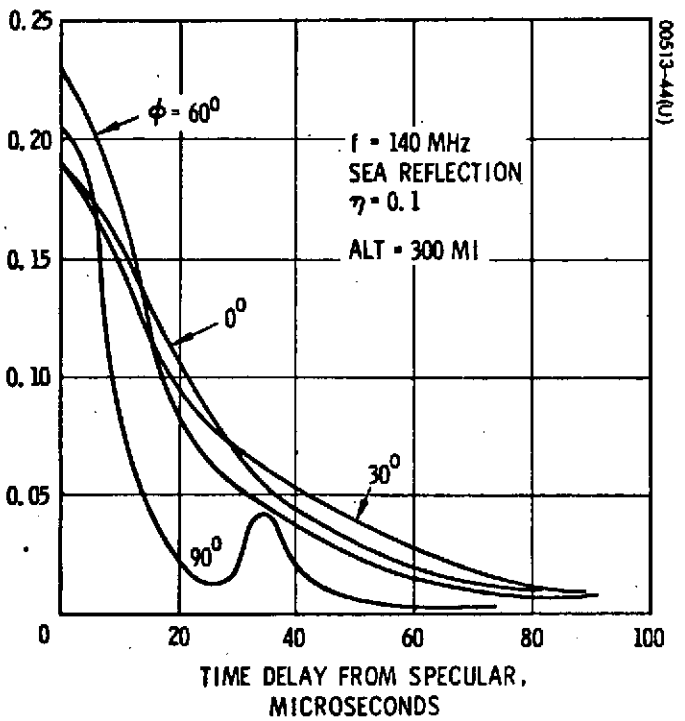

Figure 3-14. Time Response for Horizontal Polarization

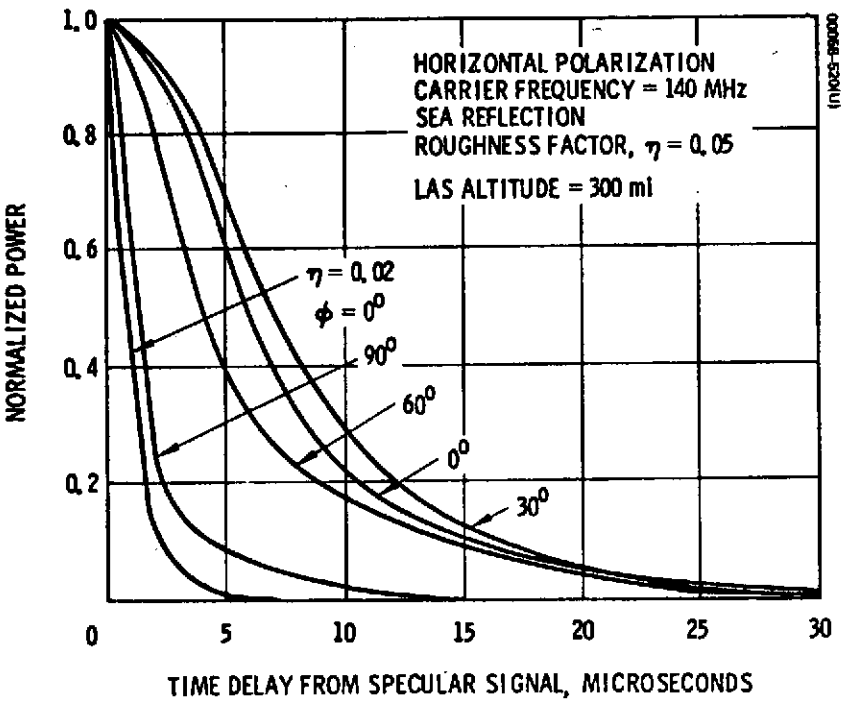

Figure 3-15. Normalized Power Time Response for Horizontal Polarization

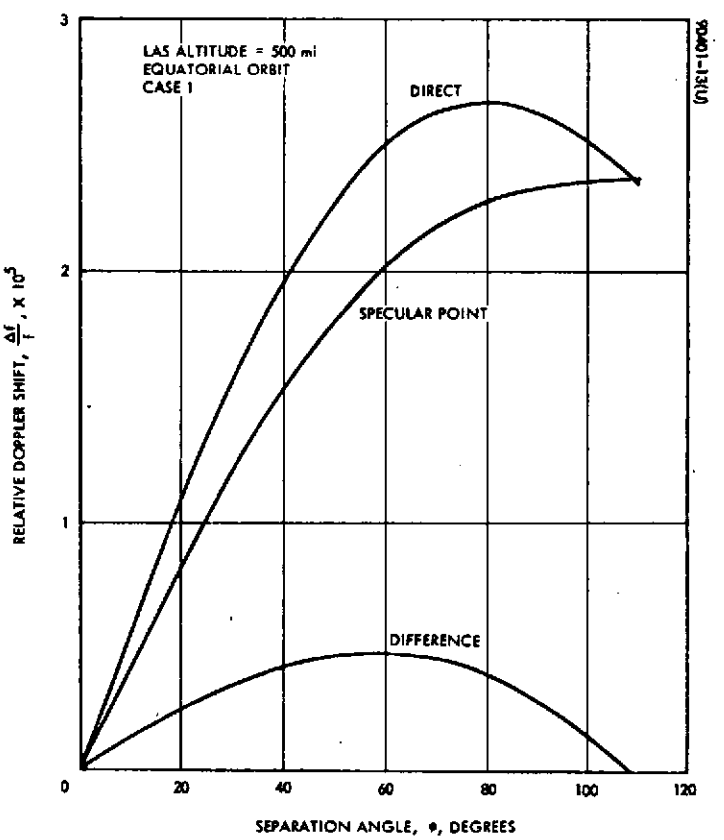

Figure 3-16. Relative Specular Doppler Shift, Case 1

the doppler shift depends on the relative orientations of the two satellite velocity vectors, and the transmission path. To illustrate the frequency effects and to provide bounds for these effects, two geometrical cases are considered here:

Case 1: The velocity vectors of both the LAS and DRS lie in the transmission plane and are pointed toward each other. This is the most extreme case and, assuming that the DRS is in an equatorial orbit, would require that the LAS also have an equatorial orbit with opposite orbital motion.

Case 2: The velocity vector of the LAS is in the transmission plane, while the DRS velocity is normal to it. This case corresponds to an LAS polar orbit and the DRS lying in the LAS orbit plane.

Figure 3-16 shows the relative doppler shift of both the direct and specular reflection paths for Case 1 and an LAS altitude of 500 miles. Of particular interest in analyzing the communication problem due to multipath interference is the difference between these two doppler shifts. This difference is shown in Figure 3-16 and again, with an expanded scale, in Figure 3-17. Figure 3-17 also shows the relative differential doppler for Case 2 and a modified Case 2 corresponding to the LAS velocity vector making a 45 degree angle with the transmission plane. Figure 3-18 shows the relationship between the relative specular differential doppler shift and altitude for Case 2. Figure 3-19 shows the actual doppler shift in Hertz for Case 2 at 140 MHz and also illustrates the effect of LAS altitude.

Since the scattering region can be visualized as many small contiguous scattering patches, the reflection path to a given patch will differ from other paths. Consequently, the doppler shift will be different for each patch with a received reflected frequency spectrum being the composite effect upon a single transmitted frequency. Since for LAS/DRS geometry the scattering region is nearly symmetrical about the specular point, it is expected that the received reflected spectrum will be nearly symmetrical about the power density from the specular point. Typical spectra for the reflected signals are shown in Figure 3-20. For a frequency of 140 MHz, most of the reflected signal power will be contained in a bandwidth less than 800 Hz, depending on the separation angle and surface roughness.

3.2.4 Omnidirectional Antenna

For this study, a representative omnidirectional antenna consisting of a whip array was used to compute relative frequency distribution of the relative power. The measured patterns of the antenna are shown in Figure 3-21, and the resultant distributions for different conditions are shown in Figure 3-22. These distributions were obtained by calculating the relative

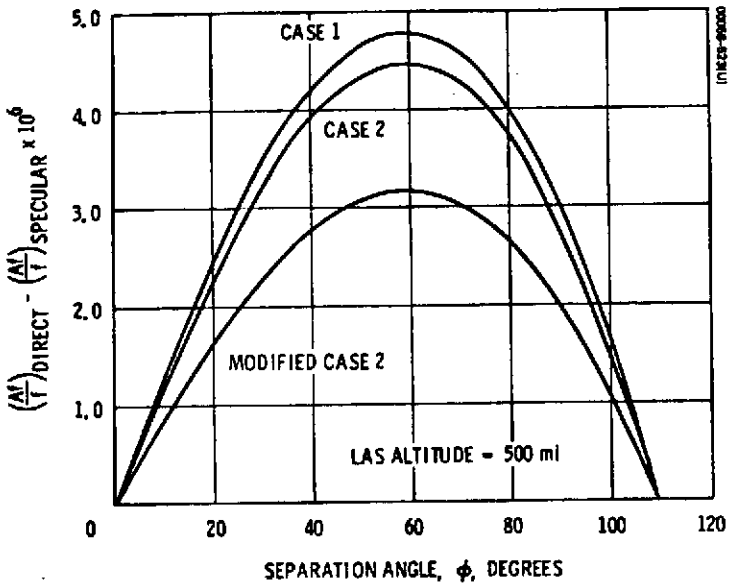

Figure 3-17. Relative Specular Differential Doppler Shift Versus Separation Angle, ϕ

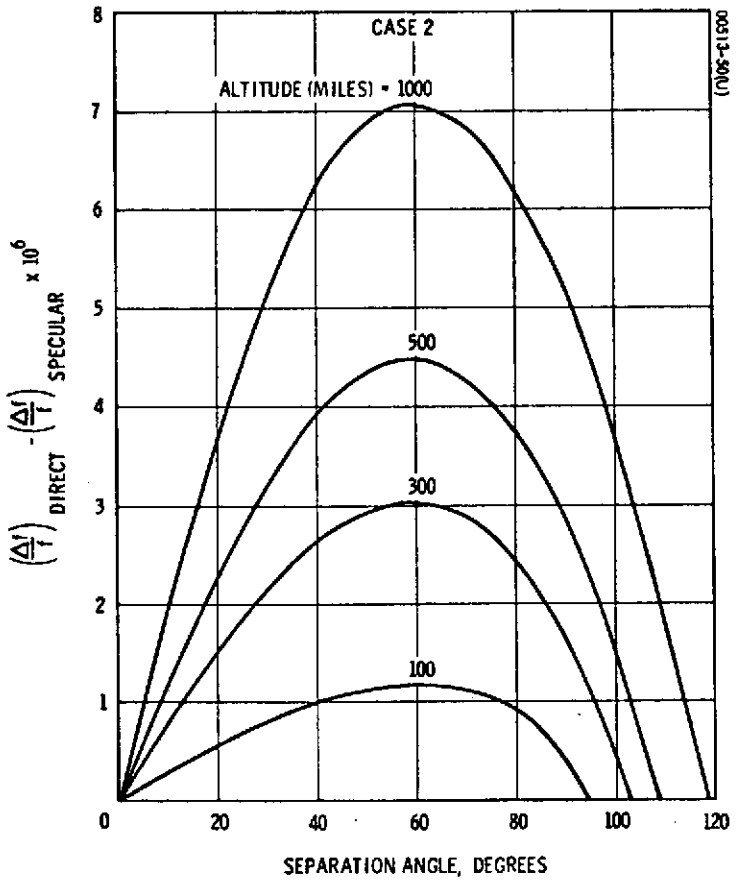

Figure 3-18. Relative Specular Differential Doppler Shift, Case 2

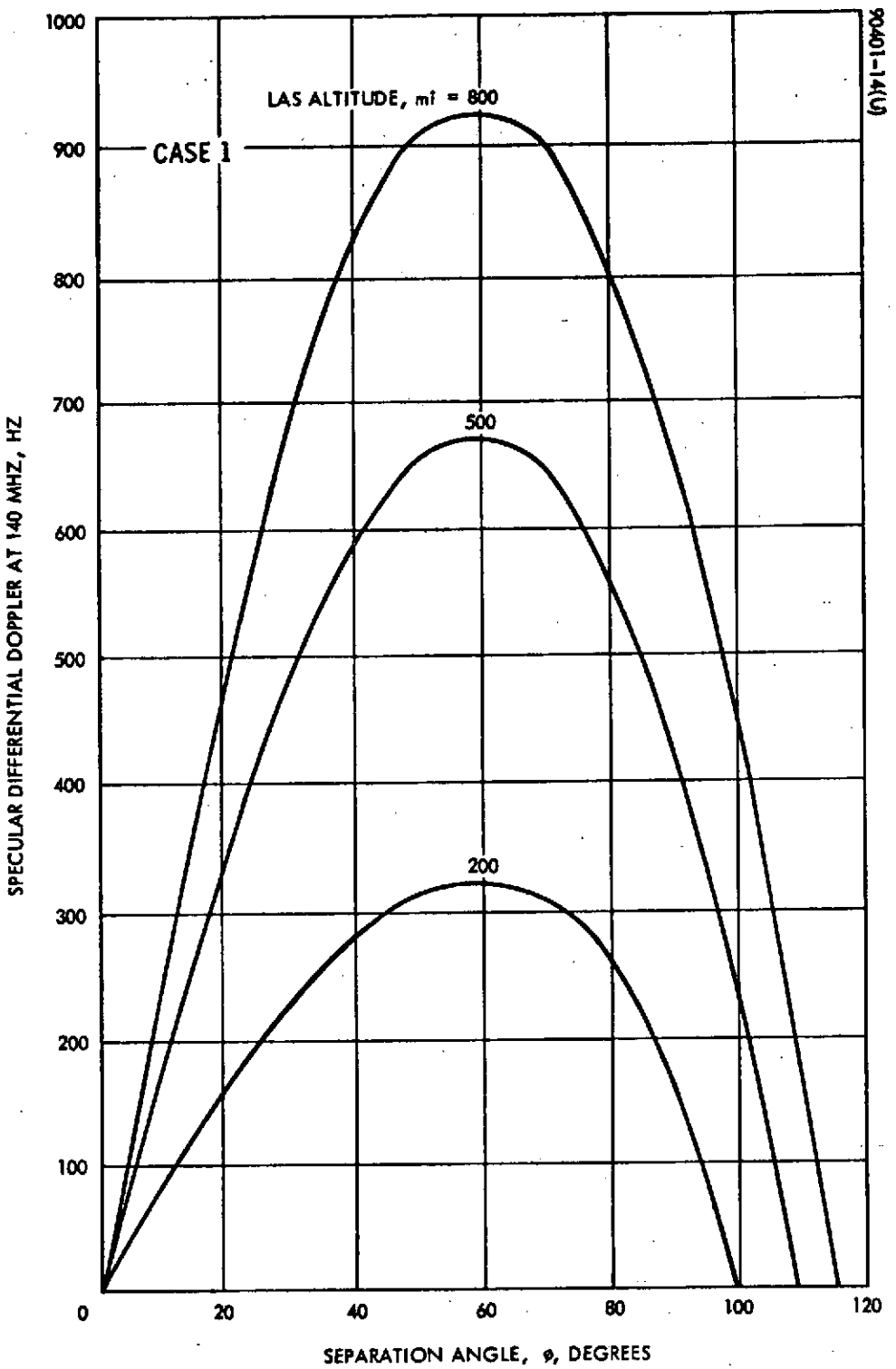

Figure 3-19. Specular Differential Doppler Shift at 140 MHz

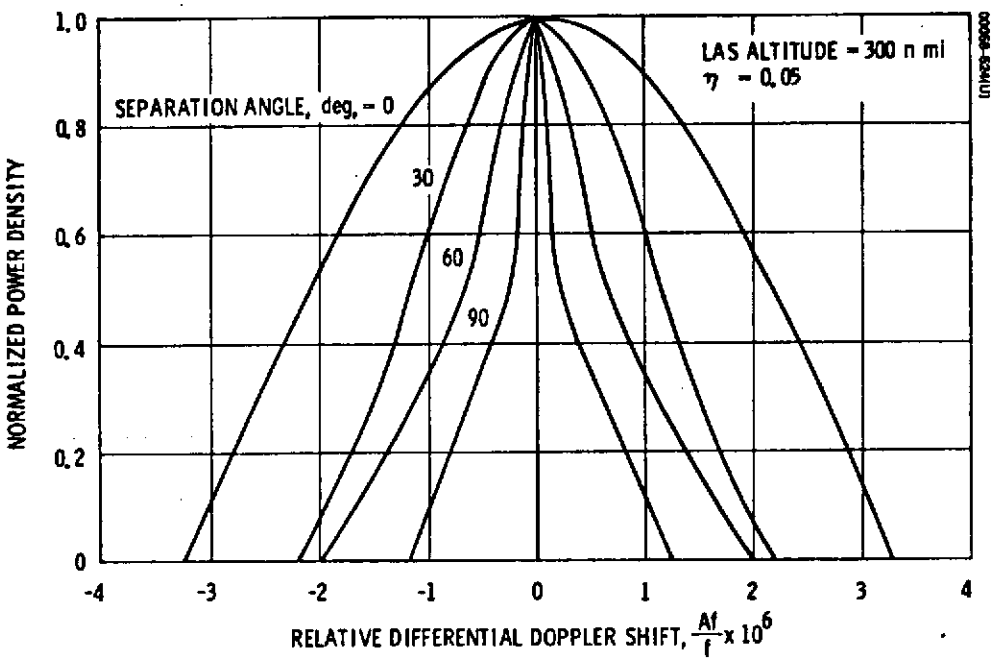

Figure 3-20. Typical Reflected Signal Spectra, Case 3

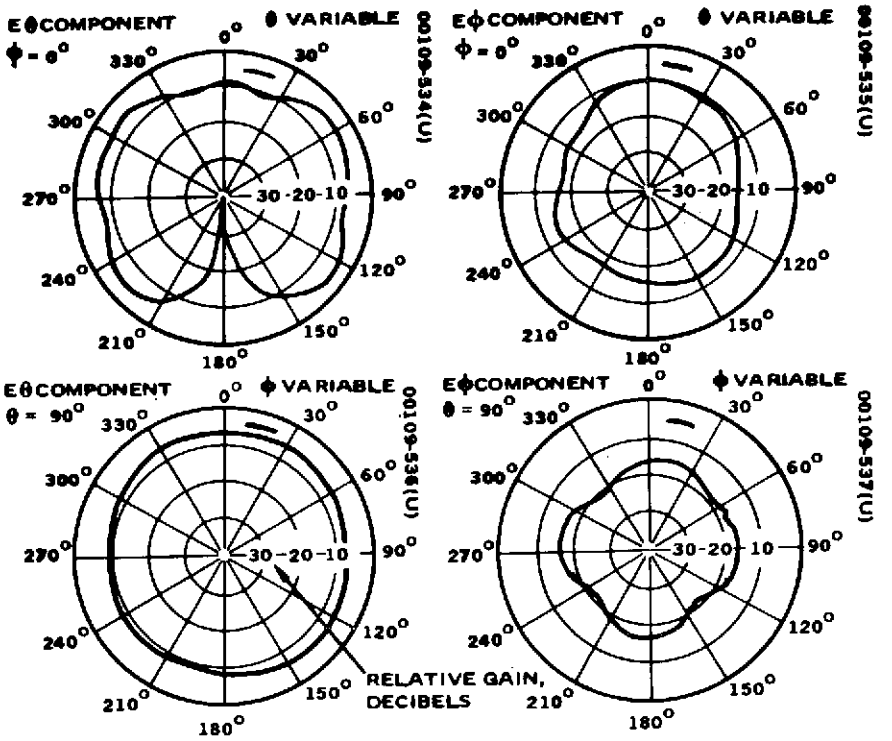

a) Frequency = 137 MHz

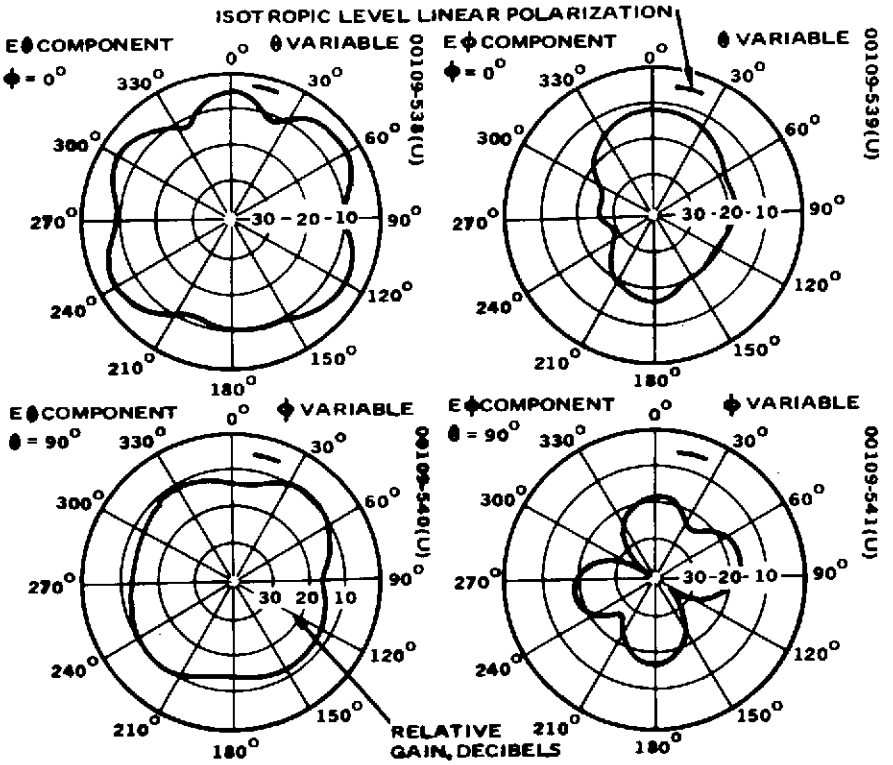

b) Frequency = 148 MHz

Figure 3-21. Measured VHF Linearly Polarized Components of Multiple Whip Antenna System for ATS

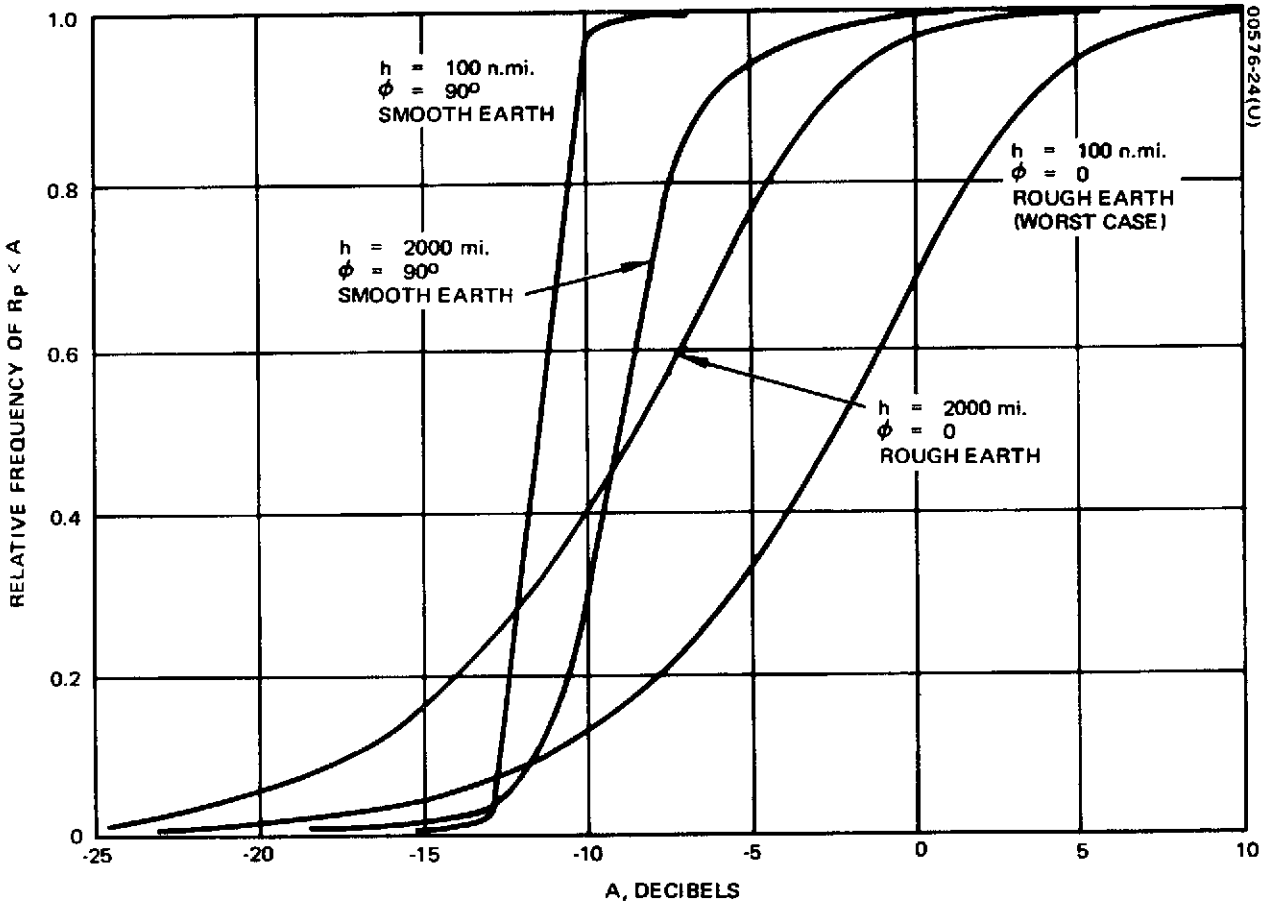

Figure 3-22. Relative Frequency Distribution of Relative Power for Typical Omnidirectional Antenna

frequency of the relative power for all orientations of the antenna. As indicated previously by Figures 3-11 and 3-12, the worst case occurs for low altitudes when the DRS is directly above the LAS. For instance, for this case, using the typical antenna, the reflected power is greater than twice the direct power ($R_p \geq 3$ dB) 14 percent of the time. A conservative communication system design might consider the 90 percent point of the worst case where $R_p \leq +4$ dB.

3.2.5 Multipath Discrimination

Four categories of techniques for discriminating against the multipath signal include: 1) antenna directivity, 2) antenna polarization, 3) frequency discrimination (filtering), and 4) time delay discrimination. The VHF system under study here is constrained to use omnidirectional antennas on all LASs, thereby eliminating the first technique as a viable approach.

Polarization discrimination is suggested by the nature of the Fresnel reflection coefficients. These are shown in Figure 3-23 for sea water. It can be seen that for most incidence angles, the reflection coefficient for vertical polarization is approximately 180 degrees different in phase than that for horizontal polarization. Thus, a circularly polarized wave — one with equal horizontal and vertical components — has its sense of rotation reversed upon reflection. Most circularly polarized antennas have at least a 20 dB rejection of circularly polarized waves of the opposite sense; therefore, an antenna adjusted to receive the direct signal will reject the reflected signal.

Practical LAS antennas cannot transmit exact circular polarization in two arbitrary different directions, and thus signal polarization will not undergo complete reversal in reflection. This can be accounted for by antenna ellipticity. Figure 3-24 presents a theoretical estimate taken from Reference 3 of the effect of polarization discrimination on the relative power as a function of separation angle for a 140 MHz transmission frequency and sea water reflection. Since the direction of the scattering region and the direct path is nearly the same for the DRS because of its relatively large distance from the earth, the polarization can be considered constant for both the direct and reflection paths. Thus, Figure 3-24a corresponds to a circularly polarized DRS antenna with respect to both the reflection and direct paths (polarization ellipticity = 0). Figure 3-24b corresponds to an LAS polarization ellipticity of -4 dB, which represents a greater amount of vertical polarization. The nine curves in each figure correspond to polarization ellipticities of the DRS antenna given in the legend. Positive ellipticities represent more horizontal polarization than vertical, and negative ellipticities imply the converse.

From Figure 3-24, it appears that circularly polarized antennas will reduce the relative power to less than -9 dB, i.e., the received reflected power will be 9 dB less than the received direct power. This technique is discussed further in Section 9.

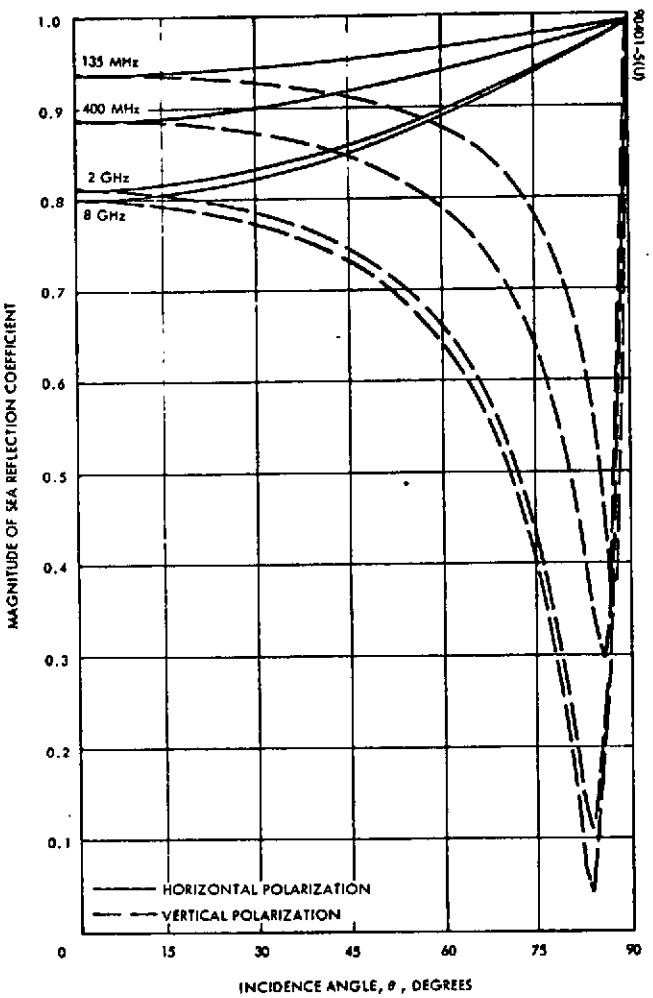

a) Magnitude

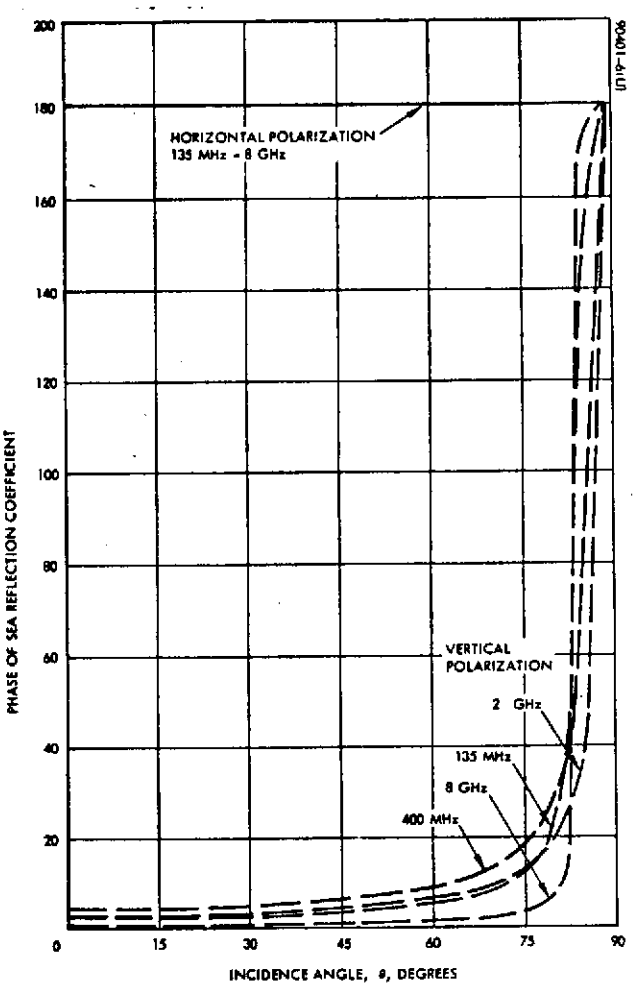

b) Phase

Figure 3-23. Sea Reflection Coefficients

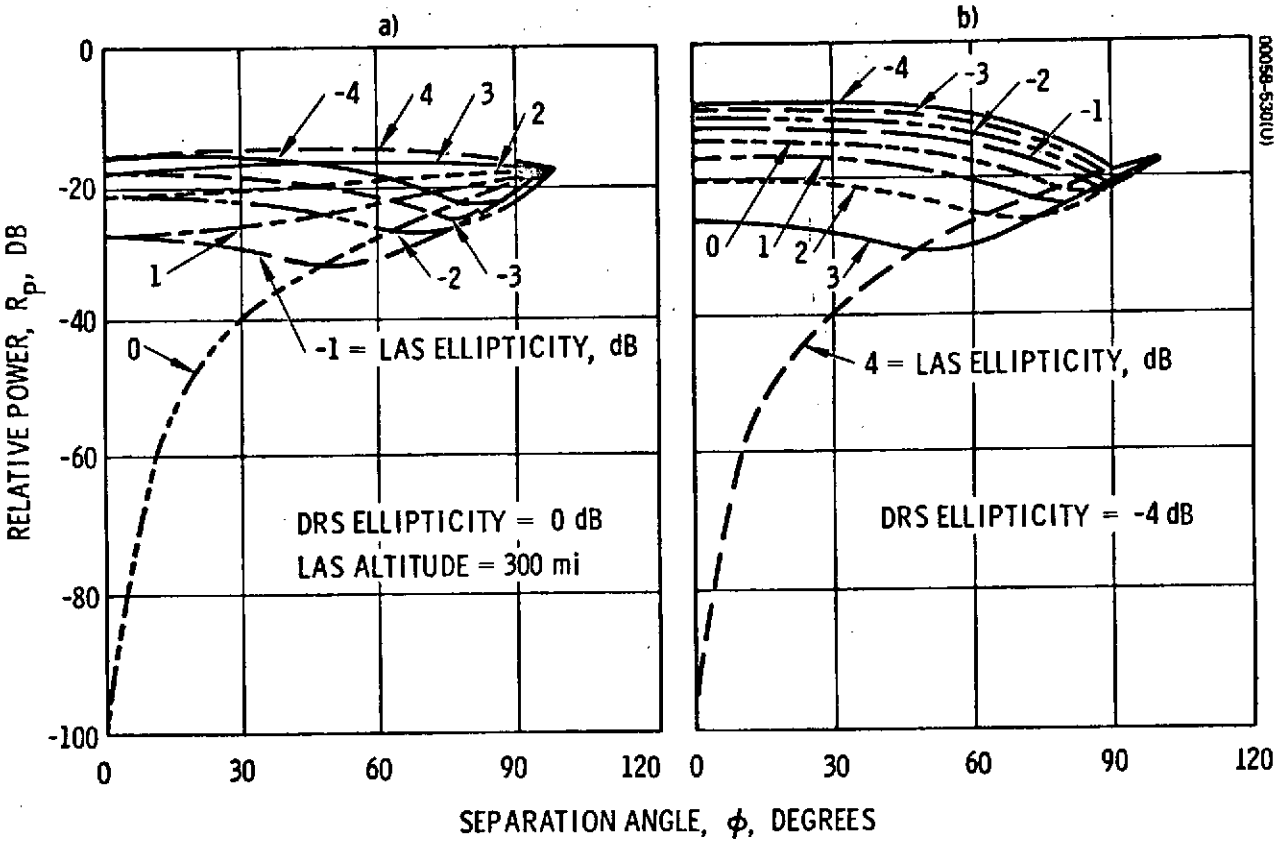

Figure 3-24. Estimated Discrimination for Sea Water Reflection at 140 MHz

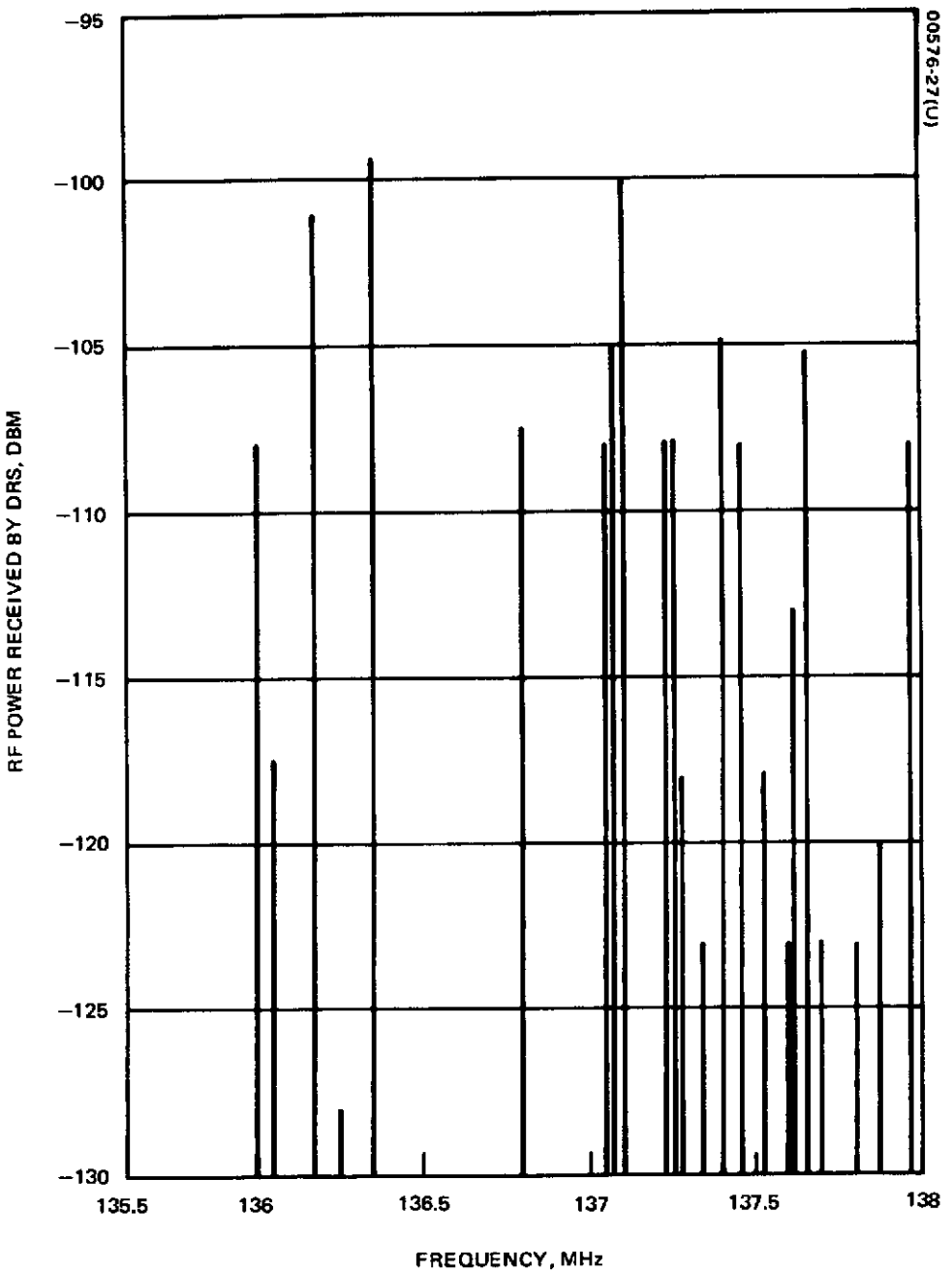

Figure 3-25. Distribution of Ground-Based Interference in Telemetry Band

(Reproduced from Reference 5)

Frequency discrimination is difficult because for small separation angles ($\phi \leq 30$ degrees) the directly received carrier frequency will lie in the power spectrum of the reflected signal. Further, the actual transmitted signal will usually have a spectrum larger than the reflected signal spreading or differential doppler shift so that the power spectra of both signals will significantly overlap even for large separation angles.

Time delay discrimination is possible because the reflected signal is delayed as discussed above and as shown in Figure 3-13. Sections 4 and 5 describe and present the analysis of a system that uses time delay discrimination.

3.3 EARTH-ORIGINATED INTERFERENCE

Earth-based transmitters radiate energy in the VHF frequency bands of interest with strength sufficient to produce serious interference. Evaluation of interference at low altitude orbits and at geostationary altitudes is incomplete, but a recent study of this interference is documented in Reference 5.

3.3.1 LAS-to-DRS Link (Telemetry Link)

According to Reference 5, a recent survey of sources visible by a DRS above the equator at 80° W longitude with an earth-coverage antenna revealed 72 potential RFI sources in the 136 to 138 MHz band within the United States alone. For these sources, Figure 3-25 shows the spectral distribution and power received at the DRS, assuming an antenna gain of 16 dB.

In Appendix D of Reference 1, this survey is also discussed; quoting from Reference 1:

> "The large number of signals and their relative power levels indicate that the central-limit theorem applies. Thus, the worst-case summed interference power will have a mean value of -92.0 dBm at the input port of the TDRS repeater with peak powers up to -80.0 dBm."

It is shown later in subsection 5.2 that with low LAS transmitter power (less than 3 watts), this interference must not exceed the receiver thermal noise power (-109 to -112 dBm) by more than 1 or 2 dB if a data rate of 500 bits/sec or greater is to be achieved. Referring to Figure 3-25, this is possible if the 13 most powerful interference sources are removed from this band, or if a portion of the band can be used where no powerful interference sources exist or are allowed. This latter technique may not be feasible since a broad spectrum is required to accommodate many LAS telemetry transmissions.

3.3.2 DRS-to-LAS Link (Command Link)

Interference in the currently available command frequency band (148 to 149.9 MHz) presents a more severe system problem than that in the telemetery band discussed above. A listing of potential RFI sources is presented in Table 3-1 taken from Reference 5. Not only are there a greater number of possible interfering sources, but the distance from these sources is much less than the distance between the LAS and DRS – about 190 times less for a 100 mile altitude.

As an example, consider a 500 mile LAS orbit and a DRS with an antenna gain of 16 dB and 20 watts of RF power as proposed for the GSFC Mark 1A DRS concept (Reference 1). Then a single 10 watt ground transmitter under the LAS with an antenna gain of 0 dB will be received with approximately 100 (20 dB) times the strength of the DRS signal.

Below is a quotation from Reference 5 concerning LAS command via a DRS in the 148 to 149.9 MHz band:

> "At present, several of the NASA spacecraft are experiencing severe interference at these command frequencies. Using command receiver AGC reading as an indicator, interference as high as -40 dBm has been reported by the OSO program. The OAO program has reported several instances in which the command code was not recognized by the spacecraft. This they believe to be due to interference sources inserting erroneous bits into the system. The operational satellite Nimbus has reported receiver saturation in their command system over portions of the globe.
>
> "A combination of the recent RFI survey and of interference reports from on-going programs, indeed, leaves an impression of impossibility of command capability from even an earth-based high power command system.
>
> "Today command receivers on most spacecraft are somewhat desensitized in an effort to overcome the 10 to 100 watt interference sources. This method is acceptable when the actual command transmitter has several kilowatts of ERP and a few hundred miles range. Neither TDRS spacecraft nor any other spacecraft can afford such sustained power levels even considering 1972 technology.
>
> "If the TDRS system is to command user spacecraft in the VHF range, a search for a less crowded portion of the spectrum must be made. Even a less crowded frequency band will require some unique command signaling technique to solve the problem precipitated when several users are simultaneously within the TDRS antenna beam. This problem of simultaneous illumination of several users while accessing only one may perhaps be resolved by the same spread spectrum and coding schemes proposed as solutions to the multipath problem."

TABLE 3-1. COMMAND LINK GROUND-BASED INTERFERENCE SOURCES*

Frequency, MHz	Total Emitters	ERP/Emitter, watts 1-9	10-19	20-29	30-39	40-49	50-59	60-69	80	>100 Watts
148.20	6		5				1			
148.21	47		7	32		1	1	6		
148.215	4		3		1					
148.22	37	11		6	16	2	2			
148.23	28	1				12	13	2		
148.24	17				16			1		
148.25	56	4	8	29	11	1	1	1	1	
148.26	3									3
148.29	176	31	18	61	22	4	34	1	4	1
148.51	53	11		35				7		
148.515	18				17		1			
148.52	149	17	53	40	22	3	5	4	5	
148.54	88	21	59	1		1	2	1	3	
148.545	12		11					1		
148.55	316	50	222	8	15	5	11	4	1	
148.56	1									1
148.575	1									1
148.59	16	1				11	4			
148.93	1						1			

*Reproduced from Reference 5.

Table 3-1 (continued)

Frequency, MHz	Total Emitters	1-9	10-19	20-29	30-39	40-49	50-59	60-69	80	>100 Watts
148.95	32	17		9			4	2		
148.988	1							1		
149.00	33		1	31				1		
149.01	285	13	32	159	52	3	22	2	1	1
149.47	40	18		22				1		
149.48	229	64	37	14	110	1	1	2		
149.49	15			9			5	1		
149.50	150	60	44	1	34	4	5	1	1	
149.51	347	83	8	77	183	2	1	3		
149.53	40	25	7			4	4			
149.54	39	28	6			3	2			
149.55	13						1	12		
149.56	70	40	5	11	3	3	4	8	1	
149.565	47			47						
149.57	100	23	35	7	9	3	7	8	9	1
154.19	3				1	1	1			

Table 3-2 presents a link analysis based on received thermal noise and is consistent with the GSFC DRS concept of Reference 1. The received command data bit energy-to-interference noise density is given by

$$\frac{E_b}{\eta_I} = \frac{S_r}{\eta_I R_c} = \frac{S_r}{L_{pI}\,\eta_{TI}\,R_c}$$

where S_r is the command signal power received by the LAS and has a nominal value of -147.6 dBw (see Table 3-2), L_{pI} is the path loss between ground interference sources and the LAS, η_{TI} is the isotropically radiated interference power density in the LAS/DRS command system frequency band, and R_c is the command bit rate. For a nominal distance of 500 miles, $L_{pI} = 4 \times 10^{-14}$ (-134 dBw).

If the number of emitters at each frequency listed in Table 3-1 are added, the total is nearly 2500. If in each 100 kHz band, transmitters visible from the LAS have a total power of 20 watts, η_{TI} = -37 dBw/Hz. Then for good quality transmission E_b/η_I must have a value of approximately 10 dB and so R_c = 23 bits/sec (13.6 dB-Hz). If the worst case parameters of Table 3-2 are used, the rate must be reduced by 6.5 dB resulting in a 5 bit/sec rate. Both of these rates are less than desired.

Other assumptions concerning the interference power, its spectral distribution, and the command link bandwidth also indicate that earth-based interference significantly degrades the command link performance or alternately limits the bit rate to undesirably low values.

3.3.3 Telemetry and Command Channel Recommendations

Based on the discussion of subsection 3.3.1 above and the later analysis of subsection 5.2, it is recommended that international controls be imposed on ground transmitters operating in the telemetry band in order that the received interference power at the DRS be no greater than the receiver thermal noise power. Low power interference sources are tolerable and will allow use of low power transmitters on the LASs. It should be emphasized that this recommendation is based on analysis indicating that desired link capacity is not possible under current potential interference conditions. The system parameters selected later with the resulting system telemetry capacity are based on the adoption of this recommendation.

Based on the observations of subsection 3.3.2 above, it is recommended here that a clear channel be obtained by NASA for DRS-LAS VHF command communication. The clear-channel bandwidth must be consistent with performance requirements as discussed in Section 5. It is also recommended that the command channel frequency be as low as possible since the power received by the LAS omnidirectional antenna is inversely proportional to the square of the carrier frequency. A clear-channel allocation in the 148 to 149.9 MHz band would be desirable since it is within a Government-owned band.

TABLE 3-2. COMMAND LINK ANALYSIS

Parameter	Nominal Value	Worst-Case Tolerance, dB
DRS ERP	+26.0 dBw	-1.0
Free-space spreading loss	-168.6 dB	-0.5
Polarization loss	-0.5 dB	-2.5
Antenna pointing losses	-1.0 dB	-1.0
Miscellaneous losses	-0.5 dB	-0.5
LAS antenna gain	-3 dB	-1
Received signal power	-147.6 dBw	-6.5
LAS system noise temperature	1000°K	
Receiver thermal density	-198.6 dBw/Hz	
Signal power/noise density	51.0 dB - Hz	-6.5
Allowance for ground-to-DRS link degradation	-1.0 dB	
Overall P/η	50.0 dB - Hz	-6.5

4. SYSTEM CONCEPT AND OPERATION

The previous section has shown that the system geometry and electromagnetic environment impose severe constraints on LAS/DRSS communication system design and performance. In addition to the large distance between the vehicles, there can be strong interference due to earth reflection of transmitted signals and earth-originated RFI. It was shown above that the transmission of commands from the DRS to the LAS is virtually impossible without a communication channel free of earth-based, interfering transmitters. In the LAS-to-DRS telemetry channel, low level interference is tolerable due to the larger distance between the interfering source and the DRS receiver, but powerful interference sources must be internationally controlled.

4.1 SELECTION OF BASIC ANTIMULTIPATH TECHNIQUE

There are two basic approaches to improving communication when multipath, or earth reflection, interference is present: 1) utilize intelligently the reflected signal energy to enhance the detection process, or 2) discriminate against the reflected signal. A preliminary assessment of the first technique indicated that it was not consistent with the objective of minimum system complexity; and thus, it was not considered further in this study.

Four categories of techniques for discriminating against the reflected signal have been discussed in subsection 3.2. The requirement for omnidirectional antenna coverage eliminates the use of a directive antenna on the LAS, and the nature of the LAS-DRS reflection phenomenon and expected RF bandwidths in excess of 500 Hz makes discrimination with frequency filtering ineffective. The remaining, feasible, discrimination techniques include 1) polarization discrimination and 2) time-delay discrimination. It was shown in subsection 3.2 that polarization discrimination offers significant improvement potential, and it is discussed further in Section 9.

Three of the more common time-delay discrimination techniques considered for this application include 1) frequency hopping, 2) burst transmission, and 3) correlation coding. Although this study was devoted almost exclusively to the third, techniques 1 and 2 will be briefly described for completeness.

In the frequency hopping scheme, the carrier frequency of the transmitter is switched in a cyclic progression through several values. The receiver must be synchronized to the transmitter and, thus, rejects the delayed multipath signal whose frequency differs from that being instantaneously accepted by the receiver. To clarify this technique, consider an example where each frequency is to be transmitted for a period equal to one-fifth the maximum specular differential time delay, T_{dm} (see subsection 3.2). After completion of transmission at one frequency, the corresponding multipath signal may arrive at the receiver until T_{dm} seconds after completion of the transmission. Thus, $1.2\,T_{dm}$ seconds are required between the beginnings of transmissions at each frequency, and, since each transmission lasts $0.2\,T_{dm}$ second, six frequencies will be required.

Power requirements are the same as for continuous transmission at a single frequency, but the bandwidth must be increased to something larger than six times the original bandwidth. The relationship between the original bandwidth and the frequency hopping bandwidth depends on the size of the original bandwidth and the doppler shift effects. It should be noted that, in the above example, multipath interference can be eliminated when the multipath delay is greater than $0.2\,T_{dm}$, but, when it is less, interference will occur. If the LAS altitude is 500 miles, then according to Figure 3-13, the system in the above example would not eliminate interference for separation angles larger than about 80 degrees.

The burst transmission technique is related to the frequency hopping method. Only one transmission frequency is used, but data are transmitted in periodic bursts where a burst transmission period is a fraction, α, of the maximum specular differential time delay, T_{dm}. The time between bursts is $(1+\alpha)\,T_{dm}$, and so the data compression factor is given by $C_d = (1+\alpha)/\alpha$. If α is again chosen to be 0.2, then $C_d = 6$, and the RF bandwidth must be increased by this factor. For this system, the peak power increases also by the factor C_d, but the average power is the same as for continuous transmission. A preliminary LAS/DRSS VHF communication system preliminary design based on burst transmission techniques has been performed and is documented in Reference 6.

Both of the above techniques, as well as correlation coding, result in a bandwidth much greater than the data bandwidth.

4.1.1 Correlation Coding

Correlation coding is part of the general class of spread-spectrum techniques. It is one of the most attractive techniques and is the recommended approach to multipath discrimination in Reference 7. Before describing a total system concept and its implementation, the underlying principles and considerations will be briefly discussed.

Correlation coding has as its basis the properties of a particular class of binary sequences called maximum-length linear shift register sequences which are produced by shift registers with linear feedback. In Reference 8, these sequences are called "true pseudonoise" sequences,

and will be referred to here as PN sequences, but generally are not considered as the only PN sequences. These sequences satisfy the following properties.

1) In each period of the sequence, the number of ONEs differs from the number of ZEROs by one at most.

2) Among the runs of ONEs and ZEROs in each period, one-half of the runs of each kind are of length one, one-fourth of each kind are of length two, one-eighth are of length three, and so on as long as these fractions give meaningful numbers of runs.

3) If a period of the sequence is added modulo 2 with any cyclic shift itself, the number of agreements differs from the number of disagreements by one at most.

This last property can be restated as follows: For integral phase displacements, the autocorrelation function of a PN sequence is two valued. If s(t) represents a normalized PN sequence signal, the autocorrelation function is given by

$$R_s(\tau) = \frac{1}{T} \int_0^T s(t)\, s(t + \tau)\, dt$$

and is shown in Figure 4-1. It is the nature of the autocorrelation function which makes a PN sequence useful for signal detection.

By performing the correlation process on the received signal and detecting the peak of the autocorrelation function, multipath and RFI signals can be rejected. A fundamental requirement for a PN system to operate properly in the LAS/DRS multipath environment is that the code pulse length be shorter than a specified minimum delay between direct and reflected signals.

The output of a linear shift register with n two-state elements is a periodic binary sequence with a period equal to or less than $P = 2^n - 1$. Any output sequence with a period equal to P is called a maximum-length linear shift register sequence. It is shown in Reference 8 that the number, N, of these PN sequences with period P is equal to $\phi(P)/n$, where $\phi(\cdot)$ is the Euler function tabulated in Reference 9 for $P \leq 1000$. Table 4-1 shows P and N for values of n from 2 through 16.

Although maximum length sequences have an ideal autocorrelation function, the cross-correlation function for two specific sequences may not be favorable. That is, the cross-correlation function may have relatively large values compared with the autocorrelation function. Such a case would make correct synchronization difficult or impossible if two such PN sequence

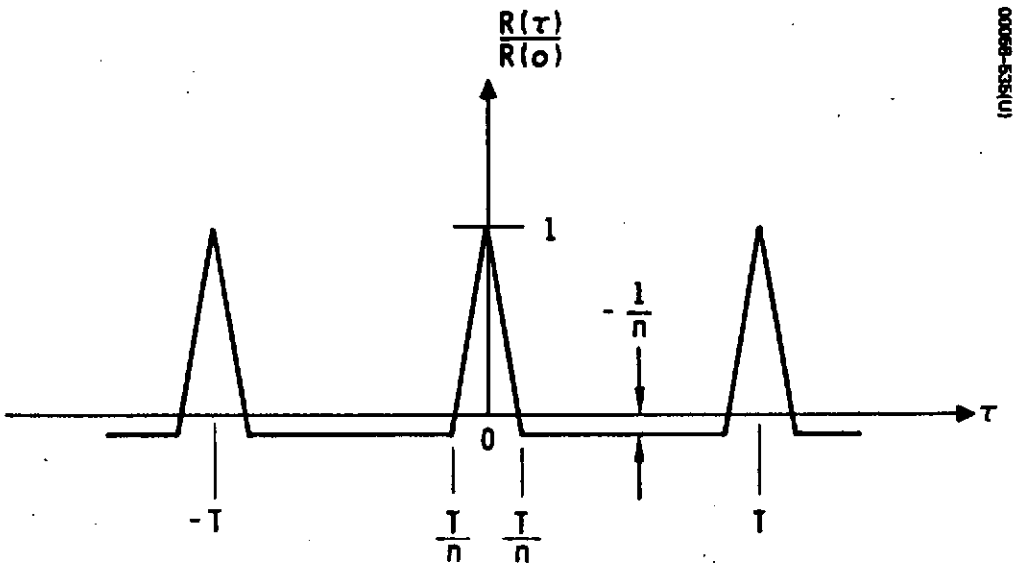

Figure 4-1. Autocorrelation Function of Pseudonoise Sequence

TABLE 4-1. PN SEQUENCE RELATED QUANTITIES

Shift Register Stages (n)	Period (P) 2^n-1	Number (N)
2	3	1
3	7	2
4	15	2
5	31	6
6	63	6
7	127	18
8	255	16
9	511	48
10	1023	60
11	2047	176
12	4095	144
13	8191	630
14	16383	756
15	32767	1800
16	65535	2048

modulated signals are received simultaneously as will occur in the system discussed shortly. The cross-correlation function for two signals s_i and s_j is given by

$$R_{ij}(\tau) = \frac{1}{T} \int_0^T s_i(\tau)\, s_j(t + \tau)\, dt$$

Gold, in Reference 10, has shown that it is possible to select pairs of PN sequences which have the following cross-correlation properties:

$$\left| R_{ij}(\tau) \right| \leq \frac{1}{2^{(n+2)/2} + 1} \qquad n \text{ even}$$

$$\leq \frac{1}{2^{(n+1)/2} + 1} \qquad n \text{ odd} \tag{1}$$

Gold has also devised a technique for generating large numbers of minimum cross-correlation codes utilizing linear shift registers. He has shown that there are $2^n + 1$ different sequences of period $2^n - 1$ such that the cross-correlation function of any pair is given by Equation 1 above. However, for these codes, the autocorrelation function is not ideal and, in fact, satifies Equation 1 with i = j, except that

$$R_{ii}(0) = 1 \tag{2}$$

These sequences will also be considered as part of the general class of PN sequences.

Another aspect of correlation coding is partial correlation. The above correlations are performed for the entire code length, however, for some systems, the correlation must be performed for only a portion of the code length. This case is discussed in Reference 7.

4.2 COMMUNICATION SYSTEM CONCEPT

This subsection presents an overview of a system concept for communication between the ground and a low altitude satellite (LAS) via a data relay satellite (DRS) system. This concept was developed with the objectives

and limitations of Section 2 as guidelines. The principal features of the system are listed below.

1) Correlation synchronization. This process discriminates against the multipath interference.

2) Clear command channel. As recommended in subsection 3.3, use of a clear channel appears to be the only feasible way of dealing with RFI in the DRS-to-LAS command link.

3) Coherent detection. This process allows range-rate determination from doppler drift measurement. It also allows the most efficient signal detection.

4) Biphase modulation. Biphase phase-shift keying (PSK) allows the most efficient detection with a carrier coherent system.

5) Different maximum-length linear sequences for each DRS and for direct ground command. A single sequence transmitted from a DRS to an LAS will allow continuous synchronization and carrier tracking of the DRS signal by each LAS as long as desired or as long as the two satellites are mutually visible. And it will eliminate interference from other DRS signals when the LAS is in view of more than one.

6) Distinct PN sequences for each LAS/DRSS link. A separate PN sequence for each LAS will allow simultaneous transmission and separation at the ground by correlation.

7) Code address command. Only one LAS at a time can be commanded from a single DRS. The total command signal will include an identification code activating the command system of the intended LAS.

In concept 5 above, each ground transmitter relaying commands through a DRS will modulate the command data with a different maximum length linear sequence. In addition, one such sequence will be reserved for direct ground command. Less than six sequences are needed, and although for the code length discussed later in Section 5 the existence of this many maximum-length sequences with minimum pairwise cross-correlation has not been proved, the existence of at least two is proved in Reference 10. Further study is required to establish the existence of six.

The particular one of these sequences to which a given LAS will synchronize for any period is selected by ground-relayed command. Thus, prior to handover from one DRS to another, the PN sequence corresponding to the next DRS must be activated by command. The LAS communication system then reverts to a sync acquisition mode and automatically acquires the PN sequence signal of the next DRS. This synchronization is maintained until the line of sight to the DRS is occulted or until another handover is

commanded. With the communication systems of the many LASs within view of a single DRS "locked on" to its signal, command may be sent at any time via this DRS to one of these LASs.

Each command message to an LAS from the ground station will contain an address to identify the LAS for which the command is intended. A series of commands to several low altitude satellites within view of the same DRS will be sequentially transmitted from the ground station, and each will contain the address code designating the intended LAS. Upon receiving a correctly addressed command, the LAS will store that command word until it receives an Execute command from the ground station. The LAS will immediately retransmit the received command message to the ground station for ground station verification of error-free receipt by the LAS. If verification is unsuccessful, the command will be retransmitted by the ground station. Otherwise, an Execute command will be transmitted to the LAS.

The system concept has been strongly influenced by the importance of low volume, weight, and cost of the LAS communication system. In order to achieve design simplicity for this system in a compact low-cost unit, the complexity of synchronization and receiver signal processing functions must be minimized. As a result, serial correlation of the PN sequence is employed because of the inherent simplicity even though serial processing implies relatively long sync acquisition times compared with parallel correlation.

Transmission of data from the LAS to the ground via a DRS presents fewer problems for the LAS system. The transmitter may be turned on and off by command, and a different PN sequence is assigned to each LAS to allow separation of signals transmitted simultaneously by several LASs. The transmitter is automatically activated when a command is sent, repeating the received command to the ground through the DRS. Further, if a command is sent to an LAS while it is transmitting data, the data transmission automatically is terminated and the received command is transmitted for verification. Data transmission is reactivated by command.

Tracking of the LAS can be performed while the LAS is transmitting data because the PN sequence transmitted by the LAS is synchronized to the command PN sequence received from a DRS. Thus, the LAS-DRS-ground range can be determined. And the transmitted carrier frequency biphase-modulated is a direct function of the received carrier frequency, thus allowing range rate determination from doppler shift measurements.

4.3 LAS COMMUNICATION SYSTEM IMPLEMENTATION

There are four commonly considered techniques for synchronizing with a received PN signal. These four, however, can be separated into two categories: 1) τ-jitter and 2) delay lock. Within the delay lock category, there are three methods of implementation 1) analog, 2) time-shared

analog, and 3) digital. Many comparisons have been made between the τ-jitter and delay lock systems, one of which can be found in Appendix II of Reference 7. It is noted there that the delay lock technique inherently provides better synchronization accuracy, thus making it superior when range determination is a requirement.

Comparisons between the three delay lock techniques indicate that, with present technology, the digital implementation results in a better system with respect to a combination of performance, simplicity, and reliability. Thus, the LAS communication system presented below employs a delay lock discriminator with reliable digital processing techniques.

Only the implementation of the correlation receiver and transmitter is presented in this section. Antenna-signal combining techniques were considered separately in this study, and the results are presented in Section 9.

The principal element of the LAS communication system is the double loop system for RF carrier and PN code sequence tracking, shown in Figure 4-2. One loop is a phase control loop (Costas loop) for automatically controlling the frequency and phase of a voltage-controlled crystal oscillator (VCXO). A second loop, termed the timing control loop, controls the clock pulse timing for the clock used to drive the command and telemetry link PN code sequence generators.

The VCXO provides a single source for all RF carrier, PN sequence, and data bit timing for the transponder. The frequency of this VCXO is automatically controlled by the phase control loop which maintains coherence of the oscillator and the received command link carrier once initial command link synchronization has been achieved and the VCXO is phase-locked to the incoming carrier phase. The locally generated carrier frequency, used for downconversion from RF to the command link PN code chip rate, is developed by multiplication of the VCXO output frequency by N, where N is the ratio between the nominal command link carrier frequency and the nominal VCXO frequency. Similarly, coherent generation of the LAS telemetry link transmit frequency is accomplished by multiplication of this same VCXO output frequency by M. M is the ratio between the nominal telemetry link carrier frequency and the nominal frequency of the VCXO. Therefore, the ratio N/M is the ratio of the receive and transmit carrier frequencies.

The LAS-generated replica of the command link PN sequence received from the ground station via a DRS and the telemetry link PN sequence generated by the LAS are coherently produced in sequence generators which are clocked at integer submultiples of the VCXO frequency. Although the LAS command link and telemetry link PN sequences differ in chip width, code pattern, and number of chips in the patterns, the time period (or sequence cycle time) of these patterns will be the same length to simplify synchronization and timing circuits. Additionally, the chip rate used in the telemetry link will be an integer multiple of that employed on the command link. Data bit rates for both command and telemetry links will be an integer

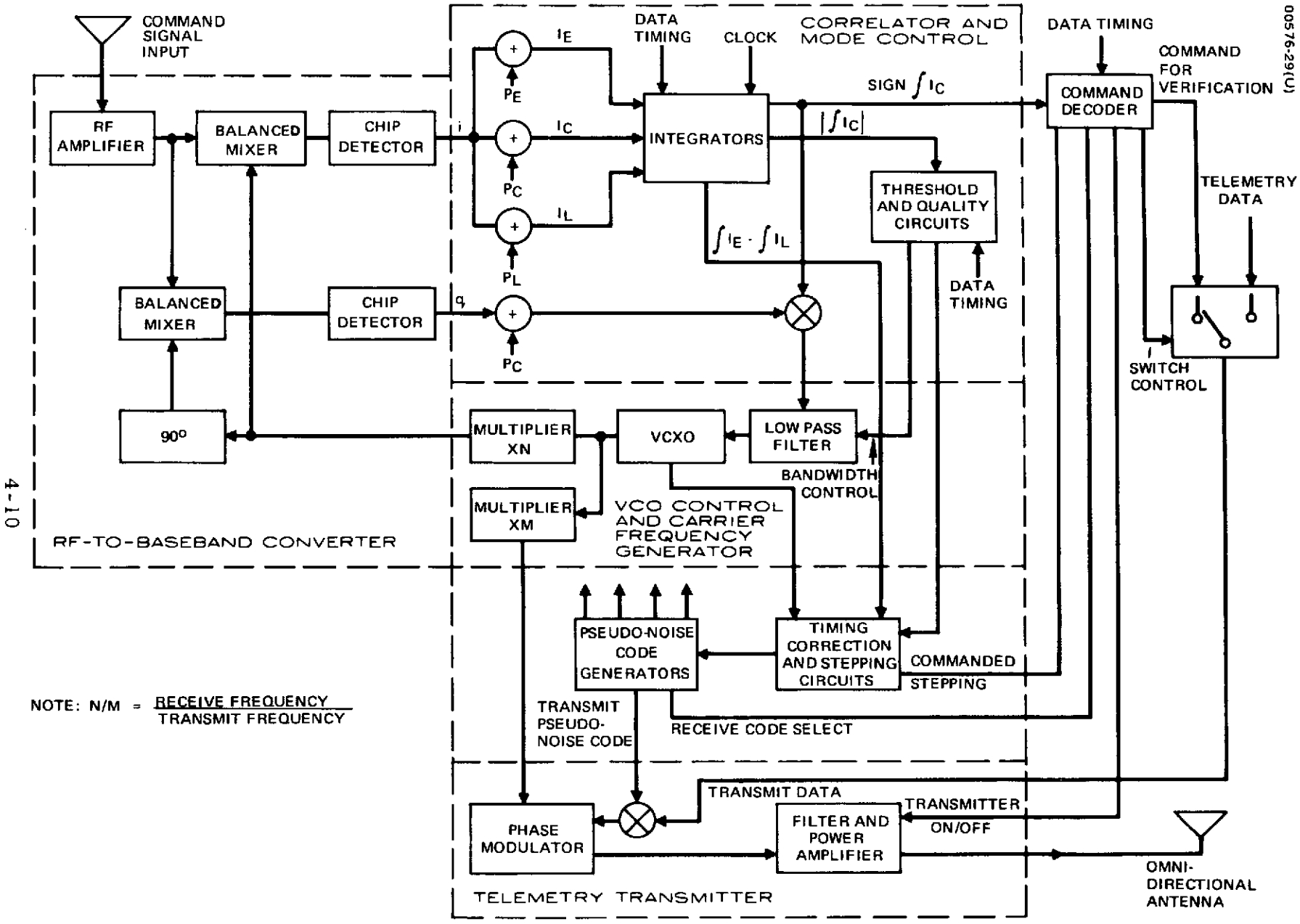

Figure 4-2. LAS Communication System

submultiple of the chip rates employed. These simple relationships permit the design of a series of LAS PN sequence generators that can be clocked coherently from a single timing source and synchronously track the received command link PN sequence by simple addition or deletion of pulses from that single timing source. The command link PN code is the same for each LAS receiving commands via the same DRS. However, multiple access to a ground station simultaneously from a number of low altitude satellites is achieved by utilization of a different telemetry PN sequence by each LAS. The ground station utilizes the autocorrelation and cross-correlation properties of these different sequences to distinguish between telemetry receptions from a number of low altitude satellites.

As illustrated by the block diagram of Figure 4-2, coherent detection and tracking of the received command link signal by the LAS communications transponder is performed utilizing a conventional correlation detector in the Costas loop. Error signals derived from the correlator output are utilized to control the output frequency of the VCXO, which in turn controls the timing of the entire system, as noted above. Received command link RF signals are amplified and supplied to a pair of balanced mixers. In-phase and quadrature components of the VCXO output, multiplied by N, drive these mixers, converting the received signal to two low pass signals separated in phase by 90 degrees. These are termed in-phase and quadrature components of the received signal.

Subsequent to chip (code pulse) detection, the in-phase (I) component is simultaneously supplied to three modulo-2 adders (exclusive-OR circuits). One compares the in-phase signal with the chip-synchronized locally generated replica of the command link PN sequence pattern and denoted by P_C in Figure 4-2. A replica of this same pattern time-shifted one-half chip interval earlier in time than P_C is denoted by P_E and is applied to a second adder. Similarly, a one-half chip late time-shifted version of P_C denoted by P_L is applied to the third adder. The outputs of these adders (I_C, I_E, and I_L in Figure 4-2) are integrated over one data-bit interval and used to develop error signals and mode control for the PN sequence generator clock.

Sync acquisition is achieved by performing a series of trial correlations between the received signal PN sequence and sequentially time-shifted replicas of the internally generated command link PN sequence. During this procedure, the PN sequence generator clock is stepped in one time-direction in one-half chip-width increments. At each position, the centered signal multiplier output (I_C) is integrated for one command bit period. If the result of this integration does not exceed a preset sync acquisition threshold, a delete signal is applied to the PN sequence generator clock source to delete one clock pulse. This serves to retard the sequence in time by one-half chip to establish a new trial time position for the sequence P_C.

This procedure is repeated until the integrated center signal output is larger than the acquisition threshold. Then, the stepping of the clock is discontinued and another correlation is performed to test for false acquisition or verify correct synchronization.

After sync acquisition has been verified by two successive correlations, the difference signal $D = \int I_E - \int I_L$ is used for fine phase control of the reference code generator. If D is positive, it indicates that the incoming signal correlated more strongly with the early output of the pattern generator P_E and the clock frequency is increased to advance the phase of the reference generator output. A negative value of D will retard the phase of the reference generator. The output of the centered signal integrator is also supplied to the telemetry encoder for data sampling and data word assembly.

For VCXO control, when the I_C integrator output is large and the Q_C correlator output is at or near zero, no error signal is supplied to the VCXO since this indicates an in-phase, on-frequency condition. When the Q_C correlator output is above a given threshold, the signal D is allowed to control the reference generator phase as described above. The time-coherent telemetry PN code sequence is also supplied from the PN code generator circuits.

Following a discussion and selection of the basic signal parameters in the next section, additional details on the implementation of this system are presented in Section 6.

5. PARAMETRIC ANALYSIS

The previous section described the proposed overall communication system concept and the implementation of the LAS system. However, the three following basic parameters must still be determined for both the command and telemetry links:

1) Chip rate: transmission/reception rate of the binary sequence

2) Data rate

3) Code length: length of the binary sequence

The primary considerations that influence the selection of these parameters include:

1) RF bandwidth

2) Multipath rejection capability

3) Number of satellite transmitters and cross-correlation effects

4) Acquisition reliability

5) Acquisition time

6) Range ambiguity

5.1 COMMAND SYSTEM ANALYSIS

5.1.1 Chip Rate

The chip rate determines both the percentage of orbital coverage for which multipath discrimination will be effective and the resulting system minimum RF bandwidth. In addition, this rate influences the range determination accuracy, acquisition time, code length selection, and command bit rate selection.

For the correlation process to be effective, the time duration (width) of a code sequence pulse (chip) must be less than the differential time delay between the direct and multipath signals at the LAS receiver.

As pointed out in subsection 3.1, if there are three DRSs symmetrically spaced in the equatorial plane, then there will always be a separation angle between the LAS and one of the DRSs less than or equal to 90 degrees. Thus, a nominal limit to the separation angle when other conditions are at their worst is 90 degrees. Referring to Figure 3-13, the multipath signal is delayed longer than the direct signal by 0.01 ms for a 100 mile LAS altitude with a separation angle of 90 degrees, which is near the 94 degree limit for this altitude.

The chip rate for biphase modulation is the reciprocal of the chip width. Thus, for correlation discrimination in an LAS with an altitude of 100 miles and separation angle of 90 degrees, the rate must be 100 kHz. This is an extreme case since for altitudes greater than 300 miles with $\phi = 90$ degrees, the differential time delay is greater than 0.15 ms which corresponds to 6.7 kHz chip rate. Referring again to Figure 3-13, an intermediate chip rate of 50 kHz will allow multipath discrimination at 100 miles altitude for separation angles up to 85 degrees. If there were only a single DRS, from Figure 3-3, this would allow an overall visibility or coverage of 45.5 percent as compared with the 53.5 percent limit.

Before a chip rate is chosen, the bandwidth must be considered. A clear (interference-free) frequency band is required as discussed in subsection 3.3. The difficulty in obtaining such a band will be partially a function of its size. The larger the required bandwidth, the more difficult it will be to obtain an allocation. However, if it is NASA's plan to use the DRS system as the primary means of communication with most low altitude satellites, then it is expected that a strong case can be made for such an allocation. Thus, a bandwidth of 100 kHz in the VHF frequency spectrum does not seem unreasonable.

Allowing 10 kHz for doppler shift as discussed in Section 3, the remaining 90 kHz will allow a maximum chip rate of 90 kHz. However, at this limit, special filtering is required in the LAS receiver. Considering both bandwidth allocation and multipath discrimination, the chip rate will be chosen to lie between 50 and 90 kHz and the RF bandwidth will be limited to 100 kHz. The exact choice of chip rate will depend on code length and data rate considerations discussed next.

5.1.2 Command Bit Rate and Sync Acquisition

The correlation process adds the outputs of the modulo-2 adders for the length of one command bit. Of primary interest in the correlation process is the ratio, G, defined by

$$G = \frac{\text{chip rate}}{\text{bit rate}} \qquad (1)$$

where the bit rate refers to the command binary bit rate. This ratio will be subsequently called the "rate ratio"* and is primarily determined by the requirements for acquisition reliability. Or conversely, the rate ratio will determine the probability of correct sync acquisition and the probability of false acquisition.

The relationship between the rate ratio and the probabilities of correct and false acquisition depends on many details of the system implementation. These details are beyond the scope of this study, but a preliminary analysis is possible. In the following nonrigorous analysis, the sources of noise and interference are considered first.

Depending on the number of DRSs and their placement, and depending on the LAS orbit, there are basically three interference cases to consider.

Case 1: Only one DRS is visible from the LAS. For this case, the worst case multipath must be considered.

Case 2: Two DRSs are visible from the LAS. The LAS will be commanded most often from the closest DRS. Thus, the separation angle to the second will be large, thereby reducing the multipath power according to Figure 3-11.

Case 3: Three or more DRSs are visible from the LAS. This case will probably occur only when the LAS is over or near to the earth's polar axis. Thus, the separation angles will be large with a resultant attenuation in received multipath power.

Evaluating these three cases together with the multipath and geometrical data of subsections 3.1 and 3.2, it appears that a conservative estimate of interfering power will be the sum of the direct power from three DRSs and the multipath power from one DRS with strength equal to the directly received power. In relating the rate ratio to acquisition probabilities, two basic cases must be considered: correct correlation and false correlation.

Correct Correlation Synchronization

If the locally generated code sequence is in phase with the received code sequence, the mixing process in the balanced modulator will transform the interference signals into Gaussian-like noise. In the total detection-correlation process of the system described in subsection 4.3, there are two sets of integration and threshold decision circuits. The first is used to detect code sequence pulses (chips) following the balanced modulator mixing, and the second is used to detect command bits. The integrator in the latter

*This ratio has been called "processing gain" in other literature (see Reference 7).

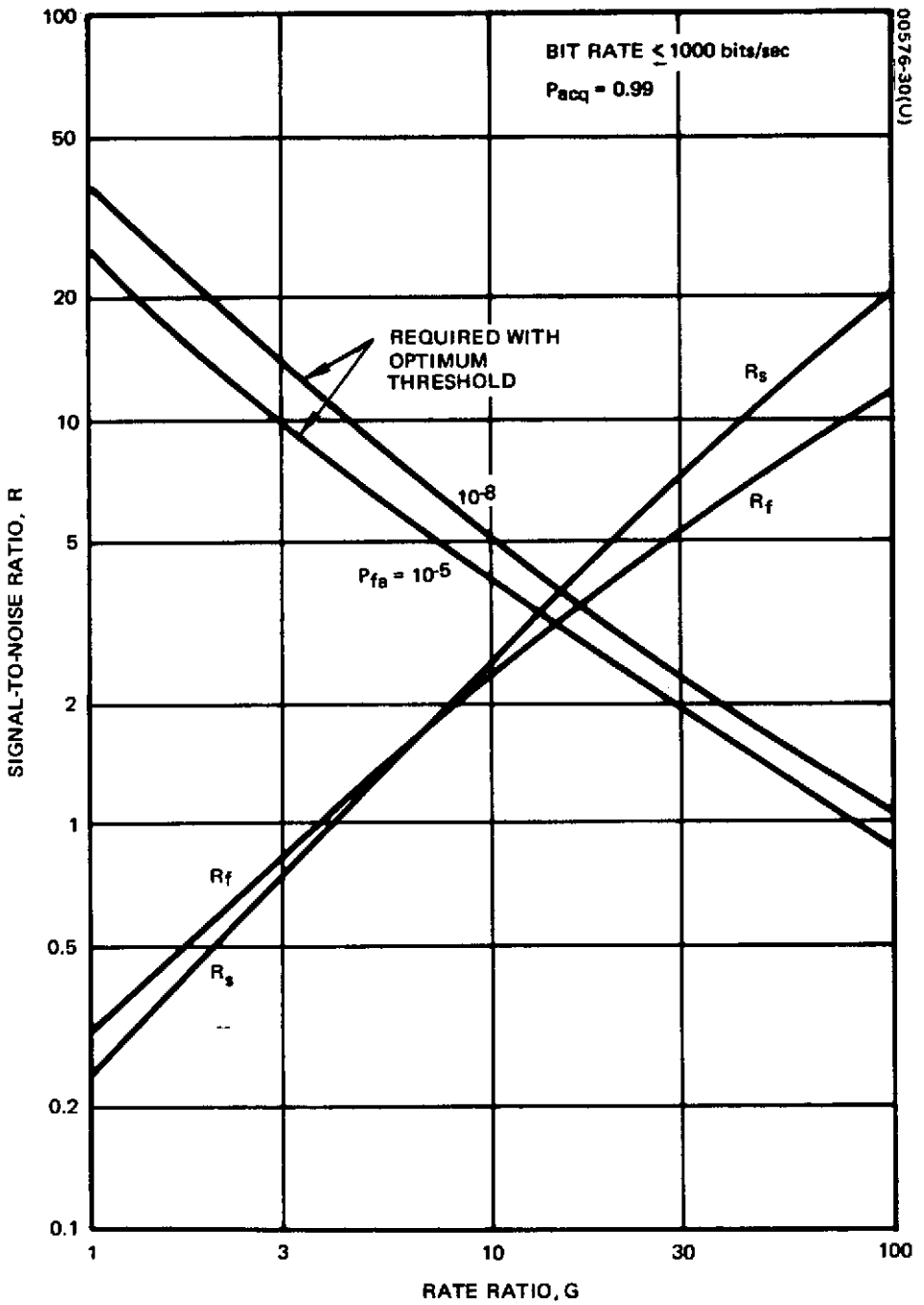

Figure 5-1. Signal-to-Noise Ratio as Function of Rate Ratio

detection is part of the code sequence correlator. Synchronization is detected when the output of the correlator is above a set threshold value. Although the chip detection process tends to complicate the overall analysis of bit detection, for preliminary analysis of this case, the correlator output can be considered as the sum of G samples of the command bit. Then the results of the radar detection analysis are applicable; the fundamentals may be found in References 11 and 12. The analysis and results of these references are employed in Reference 13 to relate signal-to-noise ratio, number of samples (rate ratio), probability of acquisition, P_{acq}, and probability of false acquisition P_{fa}. Modified results from Reference 13 are shown in Figure 5-1 for the proper choice of threshold value. The signal-to-noise ratio, R_s, corresponding to Figure 5-1 is given by

$$R_s = \frac{S_c}{N_T + \frac{N_I}{G}} \tag{2}$$

where S_c is the received command signal power, N_T is the thermal noise power corresponding to the command bit rate, N_I is the interfering noise power and G is the rate ratio; N_T is approximately the product of the system thermal noise density and the command bit rate.

As discussed above, a conservative design case assumes that $N_I = 4S_c$. Using this substitution in Equation 1, and simplifying the resulting expression,

$$R_s = \frac{1}{\frac{\eta_T R_b}{S_c} + \frac{4}{G}} \tag{3}$$

where η_T is the thermal noise density and R_b is the command bit rate. From the link analysis of Table 3-2, $S_c/\eta_T = 50$ dB-Hz; thus, for a bit rate of $R_b = 1000$ bps, $\eta_T R_b/S_c = 0.01$. Using this value in Equation 3 produces the relationship shown in Figure 5-1. For a probability of acquisition of 0.99 and a probability of false acquisition less than 10^{-8}, a rate ratio greater than 16 is required.

False Cross-Correlation Synchronization

The code sequences transmitted by the other DRSs will correlate to some degree with that of the desired command signal. The threshold of the detector must be set to reject these lower level false signals. The

signal-to-noise ratio for this case corresponding to the design interference conditions discussed above is given by

$$R_f = \frac{S_c}{N_T + C_c S_c + \frac{3S_c}{G}} \tag{4}$$

where the additional quantity, C_c, is the maximum value of any pairwise cross-correlation of the command code sequences.

By proper choice of the first G values of the binary sequences, it appears that the cross-correlation can be made as low as for maximum length linear sequences. Then, as mentioned in subsection 4.1, the cross-correlation can be made to satisfy the equalities

$$C_c \leq \frac{1}{2\sqrt{G+1}+1} \quad \text{Odd number of shift register stages} \tag{5}$$

$$C_c \leq \frac{1}{2\sqrt{2(G+1)}+1} \quad \text{Even number of shift register stages} \tag{6}$$

The value given by Equation 5 is larger than that given by Equation 6, and, hence, will be used in Equation 4 as a conservative case.

Making this substitution,

$$R_f = \frac{1}{\frac{N_T}{S_c} + \frac{1}{2\sqrt{G+1}+1} + \frac{3}{G}} \tag{7}$$

This relationship is shown in Figure 5-1 for $N_T/S_C = 0.01$, where it can be seen that a rate ratio greater than about 18 will limit the probability of false acquisition to 10^{-8} and will still maintain a 0.99 probability of correct acquisition.

Analysis Limitations

The above analysis was a simplified approach to the analysis of acquisition. It must be pointed out that the curves of Figure 5-1 are based on white Gaussian noise; whereas, the cross-correlation noise may not be approximated well by Gaussian noise. However, the above analysis does provide some basis for the lower bound on the rate ratio.

The actual nature of the correlation noise may require even larger rate ratios. For this reason, considerable margin is allowed in the value selected below. In addition, the exact effect of the chip detector should be accounted for in a rigorous analysis, but preliminary evaluation indicates that the chip detector enhances the acquisition process beyond that assumed in the simplified approach above.

5.1.3 Bit Rate and Rate Ratio

The above analysis assumed a bit rate less than 1000 bits/sec, but was relatively insensitive to this choice. The bit rate is limited by the received signal power-to-noise density ratio and the desired bit error probability.

A 10^{-6} error probability requires a received bit energy-to-noise density ratio, E_b/η, of 10 dB. From the link analysis of Table 3-2, the received E_b/η is 50 dB-Hz considering thermal noise only and allowing 6.5 dB for margin for the tolerances indicated, the link will support a 2.34 kilobit/sec rate after acquisition.

However, the interference noise due to multipath and other transmitting DRSs establishes an even lower limit for this rate. The value of E_b/η under conservative interference conditions discussed above in subsection 5.1.2 is equivalent to the value of R_s given by Equation 3. This can be seen as follows:

$$\frac{E_b}{\eta} = \frac{E_b}{\eta_T + \eta_I} \tag{8}$$

where E_b is the command bit energy, η_T is the thermal noise density, and η_I is the interference noise density. The latter is approximately the ratio of the interference power and the chip rate. Multiplying by the bit rate, R_b,

$$\frac{E_b}{\eta} = \frac{E_b R_b}{\eta R_b} = \frac{S}{N} = \frac{E_b R_b}{\eta_T R_b + \eta_I R_b} = \frac{S_c}{\eta_T R_b + \frac{N_I R_b}{R_c}} = \frac{S_c}{\eta_T R_b + \frac{N_I}{G}} = R_s \tag{9}$$

where S_c is the received command signal power and N_I is the received interference noise power. For the conservative design case, $N_I = 4S_c$. Thus, the final expression of Equation 9 is the same as that in Equation 3.

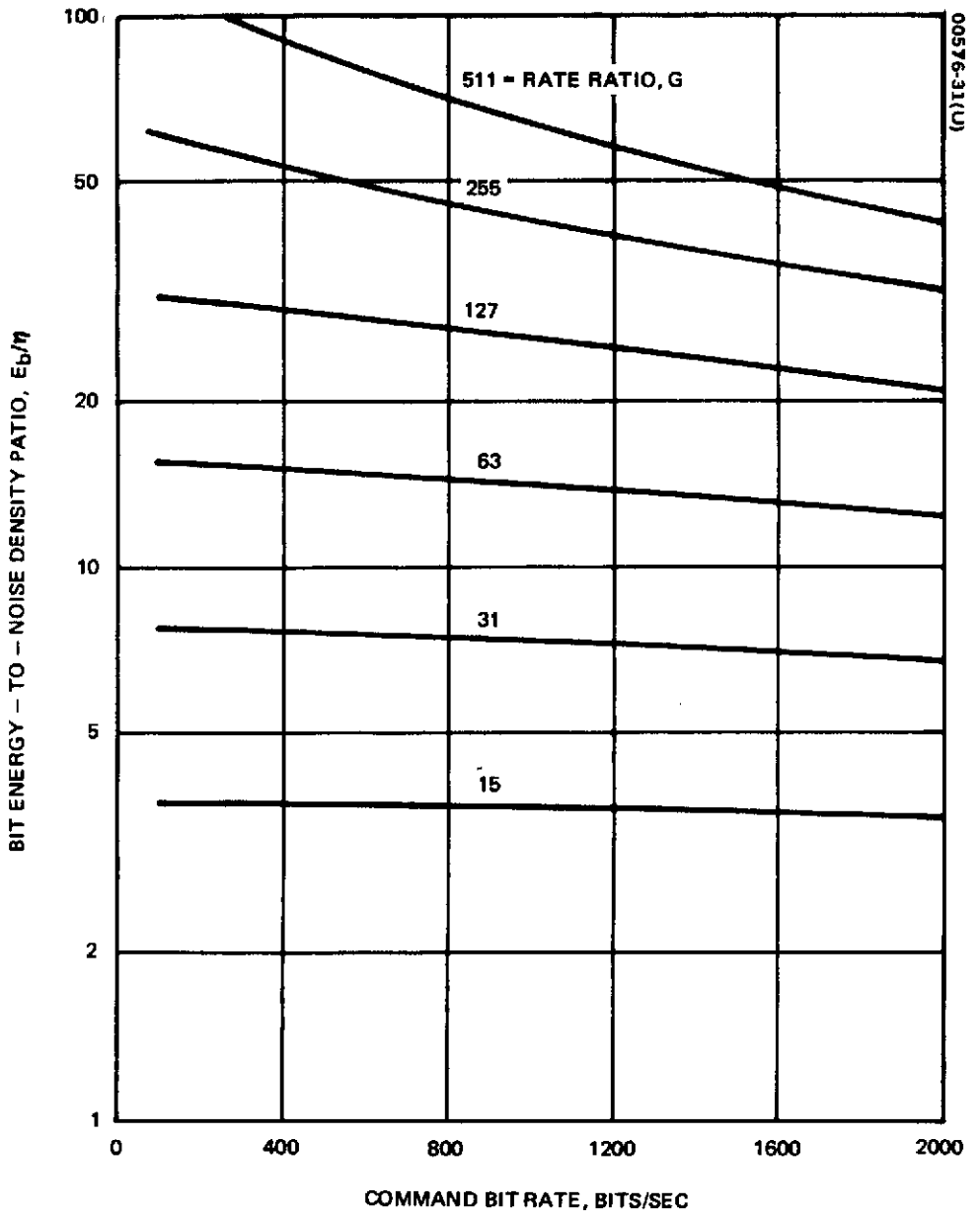

Figure 5-2. Bit Energy-to-Noise Density Ratio as Function of Command Bit Rate and Rate Ratio

From Table 3-2, $\eta_T/S_C = 1.0 \times 10^{-5}$ and using for G the maximum length numbers of Table 4-1, the relationship between R_s and bit rate is shown in Figure 5-2. From this figure, note that for the range of rate ratios shown, the value of E_b/η is much more influenced by the rate ratio than the bit rate. From Equation 9, it can be shown that for bit rates less than 2000 bits/sec, a rate ratio greater than or equal to 50 is required in order to ensure that E_b/η will be greater than 10 dB.

5.1.4 Code Length and Range Ambiguity

The length of the binary sequence, L, together with the chip rate, determines the distance within which the range can be determined by the code synchronization process but units of which must be determined by some other method. This distance is called the range ambiguity, A_r, and corresponds to the spatial length of the code. Since electromagnetic energy travels with the speed of light, the two-way (round-trip) ambiguity ($2A_r$) is given by

$$2A_r = \frac{cL}{R_c} \tag{10}$$

where L is the code length, an integer, and c is the speed of light = 186,272 miles/second.

In subsection 5.1.1, it was stated that the chip rate will lie between 50 and 90 kilobits/sec. For these two values, Figure 5-3 shows the relationship between the one-way ambiguity, A_r, and the code length. The maximum possible one-way range ambiguity for LASs with maximum altitudes of 2000 miles is approximately 6000 miles. From Figure 5-3, providing such an ambiguity resolution capability requires code lengths of 3000 to 6000 bits. However, it probably is not necessary to make the range ambiguity so large. After several orbits, the range of the LAS can be predicted within a few hundred miles as a function of time. But accurate prediction of the future orbit position as a function of time may not be desirable, in which case some significant portion of the possible 6000 mile ambiguity may be required.

5.1.5 Code Length and Multipath Rejection

The discussion of subsection 5.1.1 considered the rejection of multipath interference due to differential time delays greater than a chip width. But, if the code were delayed exactly one code length, interference fading may occur. This can be avoided if the code length is made longer in time than the maximum differential time delay. From Figure 3-13, it can be seen that the maximum delay occurs when the separation angle is zero, i.e., when the DRS is directly above the LAS. This maximum time

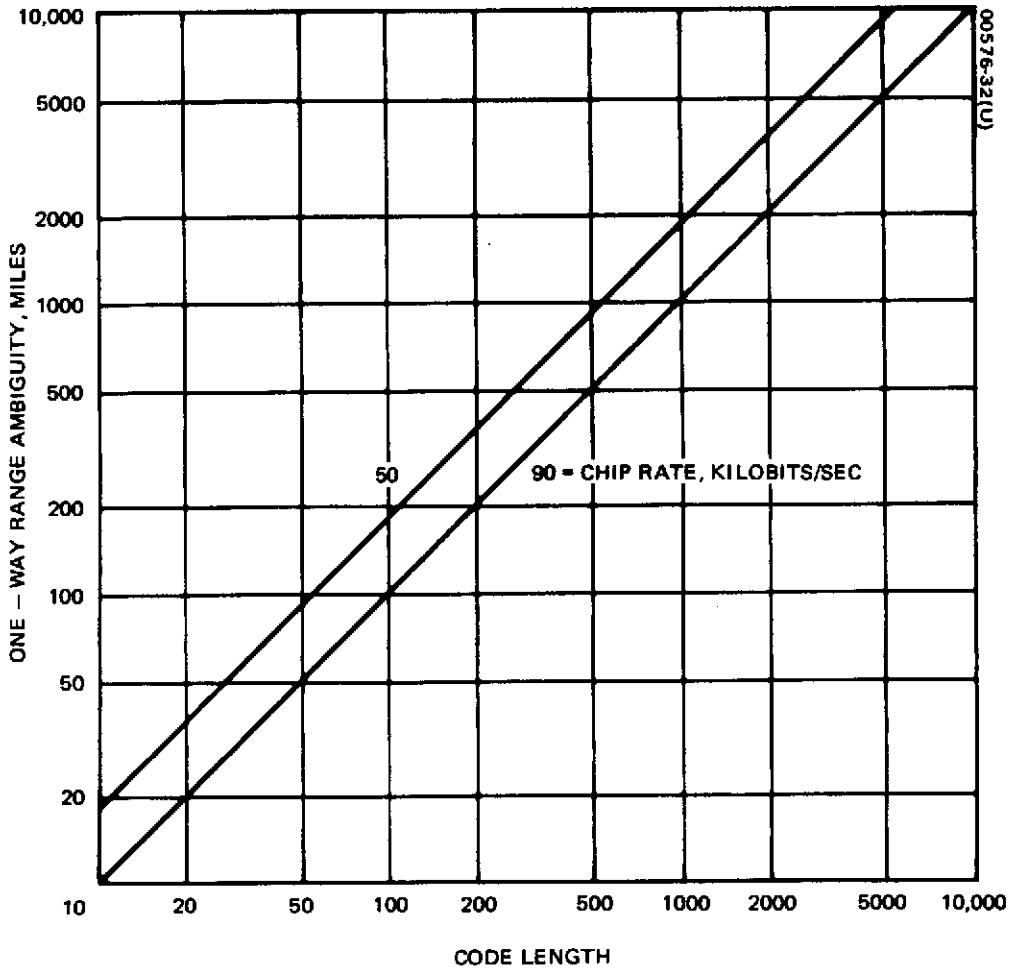

Figure 5-3. Range Ambiguity as Function of Code Length

delay is just the quotient of twice the altitude and the speed of light. This is easily related to the number of chips, N_c, transmitted during this interval by

$$2h = \frac{cN_c}{R_c} \tag{11}$$

where h is the LAS altitude. Note that this equation is the same as Equation 10 if A_r and L are replaced by h and N_c, respectively. Thus, given an altitude, Figure 5-3 can be used to determine the code length necessary to avoid code overlap. For an altitude of 2000 miles, code lengths between 1000 and 2000 must be used, depending on the chip rate.

5.1.6 Code Length and Acquisition Time

In subsection 5.1.2, the acquisition analysis did not account for the phase incoherency of the receiver near the beginning of the correlation process. A crude estimate of the time required to achieve phase lock can be obtained from a noise-free analysis of a second-order phase-lock loop (PLL).

In Reference 14, this is given by

$$T_p \approx \frac{(\Delta\omega)^2}{2\zeta\omega_n^3} \tag{12}$$

where $\Delta\omega$ is the difference between the received carrier frequency and the locally generated reference, and ζ and ω_n are PLL parameters. A typical value for ζ is 0.5, and if ω_m is the maximum expected difference between the two frequencies, then ω_n should be twice this value to both make the PLL effective and limit the noise. Thus, the maximum lock-up time is given by

$$T_{pm} = \frac{1}{8\omega_m}$$

As shown in subsection 3.1, the maximum one-way doppler shift is approximately 5 kHz, thus $T_{pm} \approx 2.5 \times 10^{-5}$ sec. The presence of noise may increase this value severalfold.

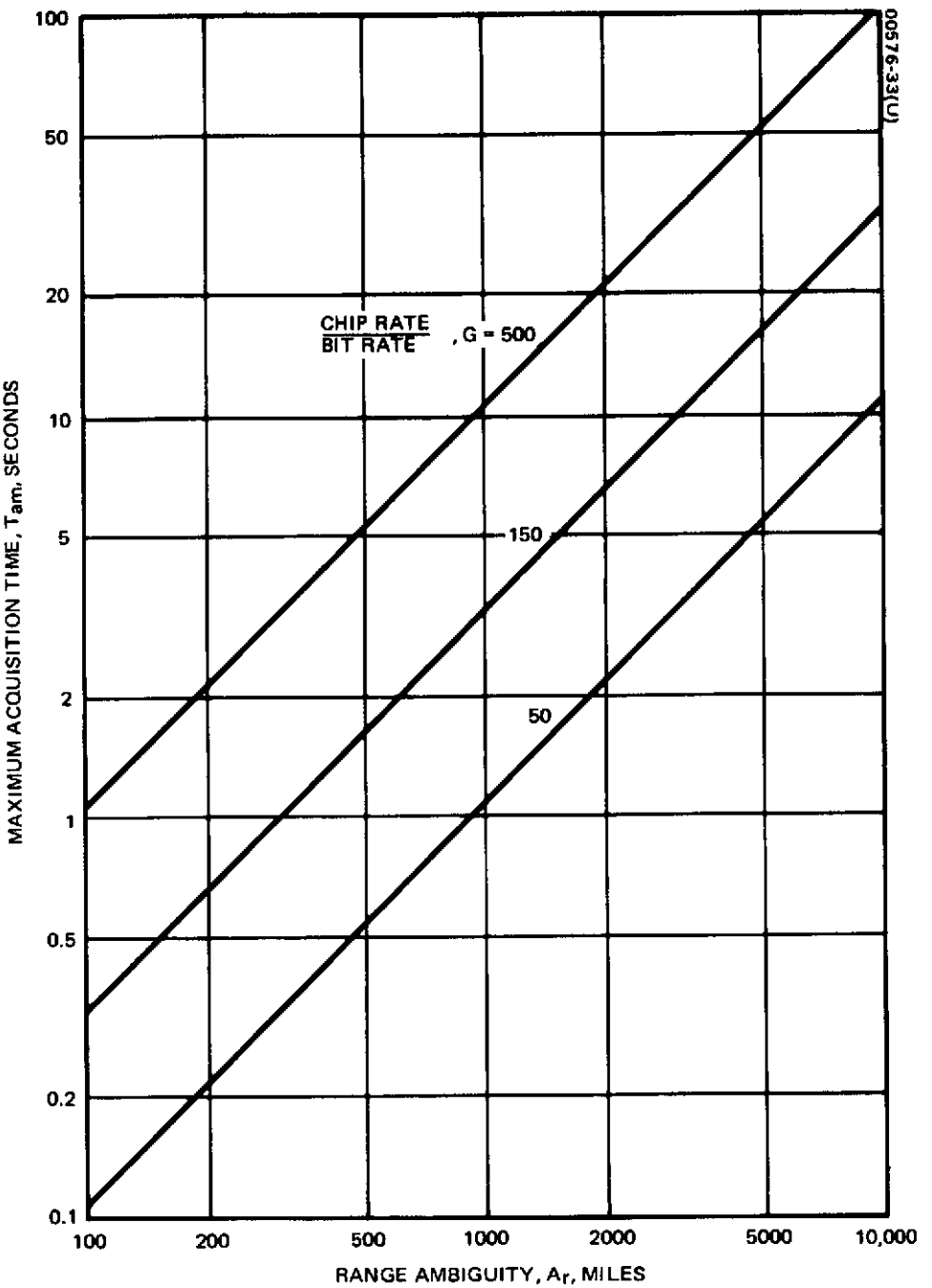

Figure 5-4. Maximum Acquisition Time as Function of Range Ambiguity and Rate Ratio

In the acquisition process, some small period may be allowed for phase lock prior to each trial correlation. From the above discussion and for the bit rates of interest here (less than 2000 bps), this will probably be less than 10 percent of the integration period. Thus, if the rate-ratio has a margin greater than this, a precorrelation phase-lock period should not be necessary. Assuming that this is the case, the correlation period is given simply by

$$T_c = \frac{1}{R_b} \tag{13}$$

where R_b is the bit rate.

In the serial correlation process, the local reference code is time-stepped in one-half chip increments; thus, a maximum of 2L correlations are required. The maximum sync acquisition time, T_{am}, is then given by

$$T_{am} = 2L\,T_c = \frac{2L}{R_b} \tag{14}$$

If, for example, R_b = 500 bits/sec and L = 2000 to eliminate multipath overlap, T_{am} = 8 seconds.

An interesting relationship can be formed between the range ambiguity and maximum acquisition time by combining Equations 10 and 14.

$$T_{am} = \frac{4A_r R_c}{cR_b} = \frac{4A_r G}{c} \tag{15}$$

Now, from previous discussion, $50 \leq G \leq 500$. For this range, T_{am} is shown as a function of A_r in Figure 5-4. From this figure, it can be seen that a range ambiguity of 2000 miles requires a maximum acquisition time of about 6.5 seconds if G = 150.

5.1.7 Parameter Selection

Based on all the above analysis and discussion, the following choices are made for the command system:

1)	Command bit rate	500 bits/sec
2)	Chip rate	70 kilobits/sec
3)	Code length	4095

With these basic selections, the following system characteristics are a consequence:

1)	RF bandwidth	≤ 100 kHz
2)	Acquisition time	≤ 18 seconds
3)	Range ambiguity	= 5450 miles
4)	Rate ratio	= 140
5)	Probability of bit error	= 10^{-6}

This selection was somewhat arbitrary, but was based on all the above discussed concepts and on the desire to achieve the above system characteristics while at the same time providing excellent multipath rejection and good acquisition reliability. Based on the discussions of subsections 5.1.2 and 5.1.3, the rate ratio of 140 provides significant margin beyond the minimum values needed for rejection of interference due to both multipath and signals from other DRSs.

5.2 TELEMETRY SYSTEM ANALYSIS

Once the command system parameters have been chosen, the telemetry parameters can be readily determined. A telemetry link analysis, based on thermal noise alone and corresponding to the DRS concept of Reference 1, is shown in Table 5-1. Requiring a value for E_b/η of 10 dB, this link will support a maximum data rate of 2.3 kilobits/sec, or if 4 dB margin is allowed, to cover the tolerances, the data rate limit is 910 bits/sec. The capacity of this link, considering thermal noise alone, is less than the command link because the transmitter power is much less. Depending on the particular omni-antenna implementation, the assumed ERP of 0.0 dBw in Table 5-1 implies a transmitter power between 1 and 3 watts.

The link capacity is reduced further by interference due to ground emitters (RFI) and signals transmitted by other LASs. The latter interference includes both the direct and multipath signals. In subsection 3.3, it was estimated that the mean interference power received by the DRS in the telemetry band (136 to 138 MHz) due to ground transmitters could be as large as -122 dBw. If this noise power were spread evenly over the band, the interference noise density, η_I, would be -185 dBw/Hz. This value of noise density, being much larger than that due to thermal noise, is the predominant factor in limiting the link capacity, and for a received bit energy-to-noise density of 10 dB, limits the data rate to about 50 bits/sec, an undesirably low limit. If the RFI noise density, η_I, is less than -200 dBw/Hz, then combined with the thermal noise density of Table 5-1, the total noise density will be less than 198 dBw/Hz which limits the data rate to 1000 bits/sec for the nominal link parameters.

TABLE 5-1. TELEMETRY LINK ANALYSIS

Parameter	Nominal Value	Worst Case Tolerance, dB
LAS ERP	0.0 dBw	-1.0
Free-space spreading loss	-168.0 dB	-0.5
Polarization loss	-0.5 dB	-0.5
Antenna pointing losses	-1.0 dB	-1.0
Miscellaneous losses	-0.5 dB	-0.5
DRS antenna gain	13.0 dB	-0.5
Received signal power	-157.0 dBw	-4.0
DRS system noise temperature	500°K	
DRS receiver thermal noise density, η_T	-201.6 dBw/Hz	
Signal power/noise density	44.6 dB-Hz	-4.0
Allowance for DRS-to-ground link degradation	-1.0 dB	0.0
Overall P/η_T	43.6 dB-Hz	-4.0

The RFI noise density can be limited to this value if international controls are employed to limit the number and power of earth transmitters in the telemetry band as recommended in subsection 3.3.3. The nature of the sharing criteria is beyond the scope of this study, but a simple computation will indicate the magnitude of the problem. A 1 watt omnidirectional earth-based transmitter with its power spread over the 2 MHz telemetry band will result in a power density received by a 16 dB DRS antenna of -215 dBw/Hz. Then 32 such transmitters with combined power spread evenly over the band will result in the -200 dBw/Hz RFI power density.

For the following analysis, it will be assumed that with imposition of appropriate band-sharing criteria on ground-based emitters in the 136 to

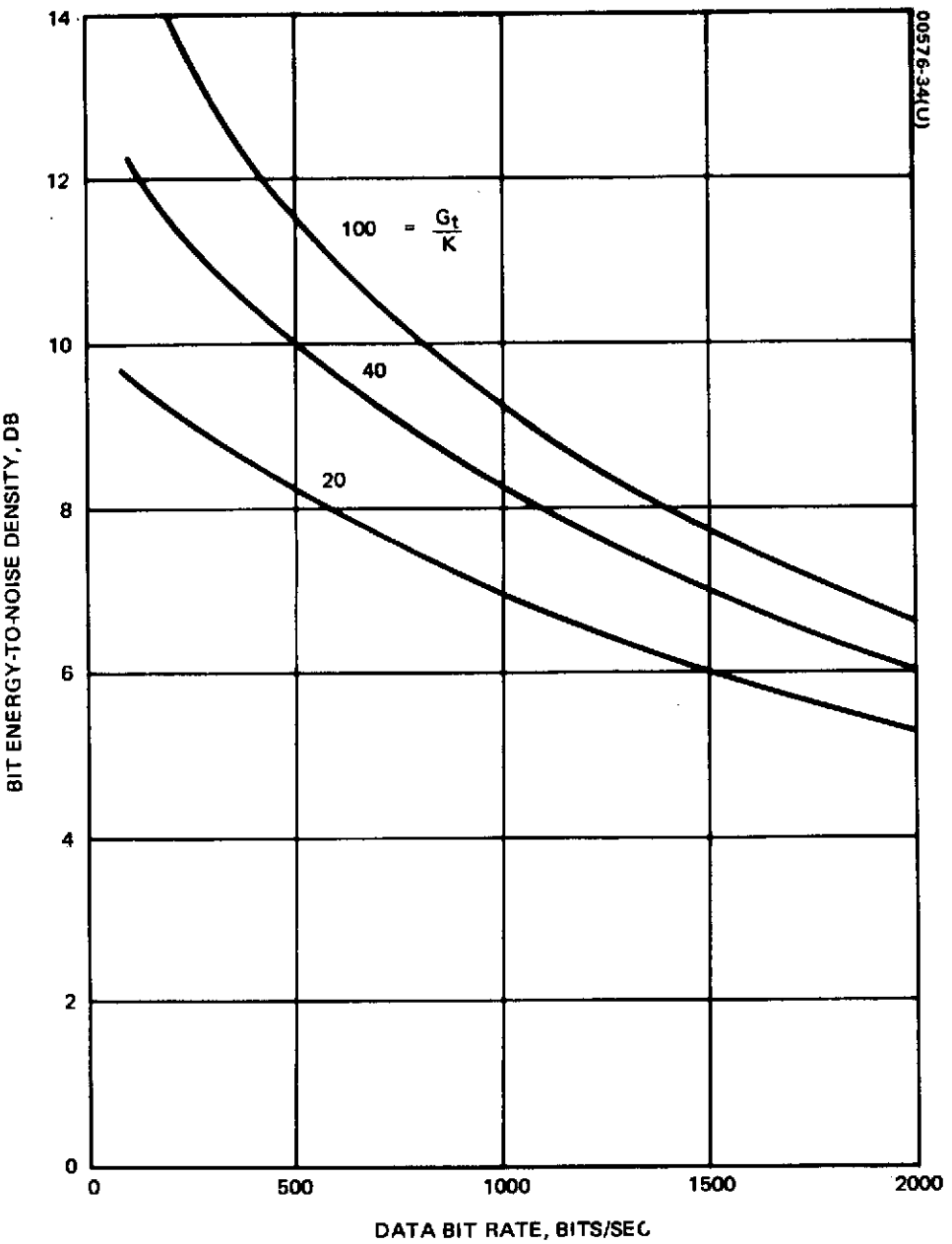

Figure 5-5. Bit Energy-to-Noise Density Ratio as Function of Data Bit Rate

138 MHz band, the interference can be reduced to a value comparable to the thermal noise density. Under this assumption, the total noise power density is given approximately by

$$\eta_T + \eta_E \approx -198 \text{ dBw/Hz}$$

Assuming that there are k LAS transmitters operating simultaneously and that the effective received multipath power is equal to the directly received power, an expression similar to that of Equation 9 can be developed for the ground received ratio of bit energy-to-noise density. This is given by

$$\frac{E_b}{\eta} = \frac{S_t}{\eta_T R_d + \frac{2kS_t}{G_t} + \eta_E R_d} \tag{16}$$

where R_d is the data bit rate, S_t is the equivalent ground received telemetry power, and G_t is the telemetry rate ratio. This expression can be rearranged yielding

$$\frac{E_b}{\eta} = \frac{1}{\left(\frac{\eta_T + \eta_E}{S_t}\right) R_d + \frac{2k}{G_t}} \tag{17}$$

Assuming a 10.0 dB DRS-to-ground degradation, and using the total noise density given above,

$$\frac{\eta_T + \eta_E}{S_t} = -198 + 158 = -40 \text{ dB/Hz } (10^{-4}) \tag{18}$$

Using this value in Equation 17, E_b/η can be determined as a function of R_d and G_t/k. This relationship is shown in Figure 5-5.

For the values of G_t/k shown in Figure 5-5, the required E_b/η of 10 dB is possible only if the data rate is less than 800 bits/sec. It can be shown from Equations 17 and 18 that if E_b/η is to have a value of 10 dB or greater then the data rate must be less than 1000 bits/sec, with G_t arbitrarily large. This limit is imposed by the assumed ground-based interference and the DRS receiving system noise temperature.

There are many implementation advantages to making the telemetry data rate and command bit rate have an integer multiple relationship. Since R_d must be less than 1000 bits/sec with the assumptions made above, and since the command rate was selected as 500 bits/sec, then the data rate should be chosen to be 500 or 250 bits/sec, etc. Before making this selection, the chip rate and number of simultaneously operating transmitters must be considered.

As noted above, there may be a significant advantage to limiting the RF bandwidth to less than the available 2 MHz bandwidth. An arbitrary limit of 1 MHz will allow some flexibility in selecting the exact portion of the band for this system so as to reduce interference. By doing so, the chip rate is limited to approximately 750 kilobits/sec. A data rate of 500 bits/sec then limits the rate ratio to 1500, and from Figure 5-5, the ratio G_t/k must be greater than 40. Hence, the number of simultaneously operating transmitters will be less than 37.

System simplicity is achieved if the telemetry code length, L_t, has a time period equal to the command code period. Imposing this requirement yields the following equation:

$$L_t = \frac{R_{ct}}{R_{cc}} L_c$$

where L_c is the command code length, R_{ct} is the telemetry chip rate, and R_{cc} is the command chip rate. Further, the ratio R_{ct}/R_{cc} should be an integer to simplify the LAS timing circuitry.

Taking all the above aspects into consideration, a reasonable and feasible set of parameters is listed below.

1) Telemetry data rate = 500 bits/sec

2) Chip rate = 700 kilobits/sec

3) Code length = 40,950

These selections result in the following system characteristics:

1) RF bandwidth $\leq$ 1 MHz

2) Maximum simultaneous transmissions = 35 per DRS field of view

3) Probability of bit error = 10^{-6}

4) Rate ratio = 1400

It should be noted that these selections are somewhat arbitrary and are based on 1) use of international band sharing controls, limiting the received interference noise power density due to earth-based transmitters in the telemetry band to -200 dBw/Hz and 2) a 0.0 dBw ERP limit for the LAS. There is a trade between the three parameters and characteristic 2 which depends strongly on the magnitude and spectrum of the interference in this band. If this interference were eliminated by the use of a clear channel, a data rate of up to 1500 bits/sec may be possible.

6. SUBSYSTEM IMPLEMENTATION

In Section 4, an overall system concept was discussed and a general implementation scheme presented. This section presents additional details concerning the implementation of portions of the LAS system, i.e., subsystems of the total LAS system shown in Figure 4-2.

6.1 RF-TO-BASEBAND CONVERSION

Figure 6-1 is a block diagram of the RF-to-baseband conversion subsystem. The received VHF command link signal is amplified before being converted to baseband. A diode limiter precedes the first RF stage to protect the input transistor from burnout due to strong signals or electrical transients at the antenna. The RF amplification provides the gain required to assure that the mixer and baseband amplifier noise figures do not appreciably degrade the total receiver noise figure. Low noise FET stages in the RF section will provide a low noise figure with a minimum amount of intermodulation distortion. The total RF gain should be approximately 20 to 30 dB to overcome the mixer and low pass filter losses and provide a sufficient signal amplitude to reduce the baseband amplifier contribution to receiver noise figure. If additional RF gain is used, strong interference signals may overload the last RF amplifier stage and mixer input, thereby degrading system performance by producing spurious intermodulation signals and blocking the response to the desired signal.

The balanced diode mixers convert the received RF signal to two baseband frequency (low pass) signals separated in phase by 90 degrees. The low pass filter bandwidths are matched to the command link PN code chip rate, and the in-phase and quadrature baseband channels have identical filters and baseband amplifiers. The baseband amplifiers have a bandpass greater than the low pass filter bandwidth. The total receiver bandwidth (and therefore, time delay) is thus set by the low pass filter, which has a more stable time delay and bandwidth characteristic than the amplifiers. The amplifier output signal levels are controlled by the AGC circuits and maintain a constant average signal plus noise level to the chip detector. This detector consists of an integrator and threshold circuit where the integration may be performed with an operational amplifier or by digital techniques (sample and hold). The AGC loop should be designed to control the gain for input signals ranging between the noise level and the maximum expected signal level.

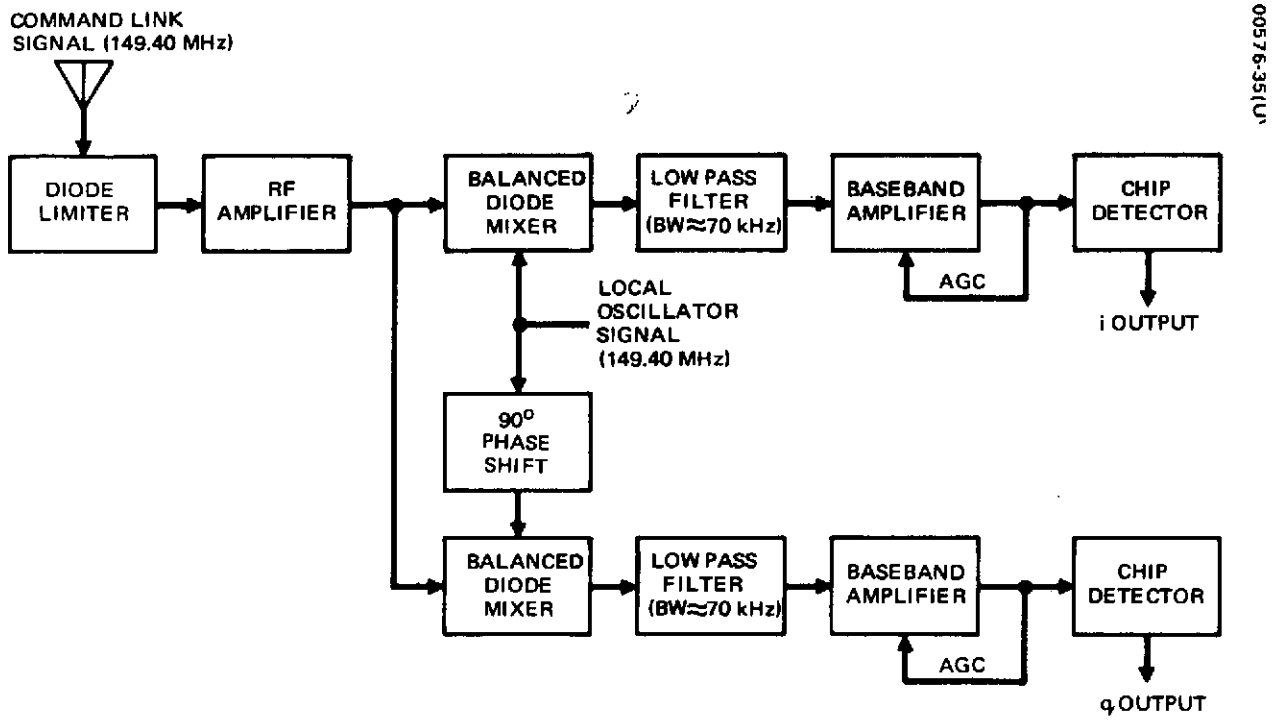

Figure 6-1. RF-to-Baseband Conversion

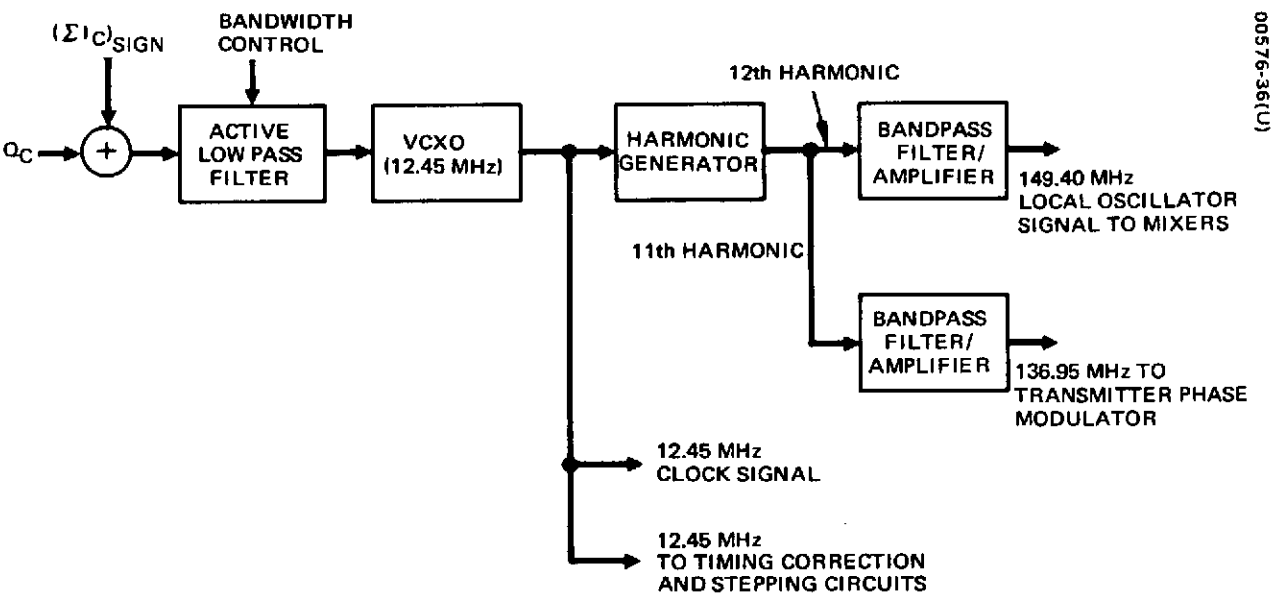

Figure 6-2. VCXO Control and Carrier Frequency Generation

6.2 VCXO CONTROL AND CARRIER FREQUENCY GENERATION

The transponder local oscillator (LO) signal is phase-locked to the received carrier by controlling the frequency of a voltage-controlled crystal oscillator (VCXO) with the product of the Q_C signal and I_C integrator sign bit shown in Figure 6-2. The resulting product, $(Q_C) \times (\text{sgn } I_C)$, is then integrated and represents the amount of signal in the quadrature channel. This result is used as an error signal to control the VCXO phase for a null in the quadrature signal. The integration of the VCXO control signal is accomplished in an operational amplifier type low pass filter which has its bandwidth controlled by the threshold and quality circuits. During the acquisition phase, the filter is held in the wideband mode, and during lock-on as the quality counter is advanced, the bandwidth is reduced until the minimum bandwidth state is achieved. If the quality of the I_C integrator output decreases, the bandwidth is widened slowly to prevent short fading of the signal from forcing the loop into the wideband state.

A crystal-controlled VCO is used to maintain a minimum drift of the VCO frequency when the loop is unlocked, which thereby reduces the required frequency acquisition range for the loop. The VCXO output drives a harmonic generator, which produces coherent harmonic outputs. The 12th harmonic is filtered and amplified for use as the command link receive local oscillator signal. The 11th harmonic, after filtering and amplification, drives the transmitter phase modulator and provides a transmitter carrier modulated by 11/12 of the received signal doppler. The 12.45 MHz also is used as the clock signal for the various digital circuits and thereby assures that the clock and the local PN code are compensated for the received signal doppler frequency.

6.3 PSEUDONOISE CODE GENERATION

The PN code generation subsystem block diagram is shown in Figure 6-3. The PN sequence chip-rate clock is derived from the VCXO in the receiver phase-locked loop and the chip rate is therefore corrected for doppler shift.

Timing correction and stepping of the receiver PN pattern are accomplished by adding or deleting clock pulses to the PN generation circuits. During the command link sync acquisition mode, the PN code is shifted in a single direction one-half chip interval each data bit period in search of a valid timelock. The auto-step command from the correlation and timing control logic enables this stepping. Once synchronization has been acquired, timing corrections in either direction are enabled by the advance/retard signals from the correlation and timing control logic.

The telemetry link PN code is produced by combining the output of a 16-stage shift register with the output of the 7-stage generator in an exclusive-OR circuit. The 7-stage generator is reset each frame time (pattern cycle time) of the 16-stage generator. Each LAS will have different

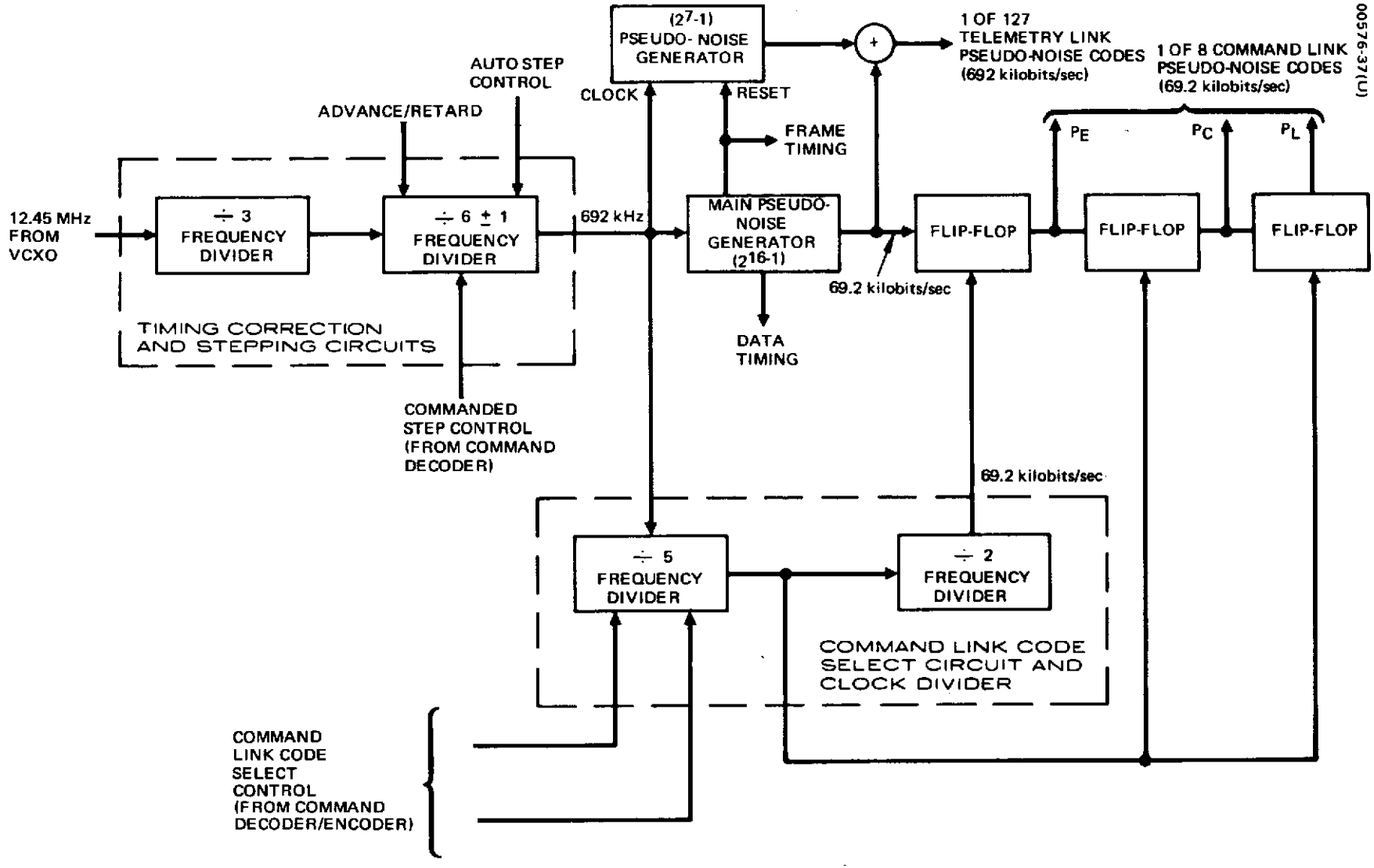

Figure 6-3. Pseudonoise Sequence Generators

feedback connections on its seven-stage generator, resulting in one of 127 unique telemetry PN patterns for identification at the ground station. The existence of 127 distinct codes generated in this manner with the cross-correlation properties assumed in subsection 5.1.2 has not been substantiated; however, trial and error code synthesis in previous PN system designs indiciates that the required cross-correlation properties can be obtained.

The command link PN codes are generated coherently with the telemetry codes by selecting every tenth main (16-stage) generator bit for the command code. Eight different command codes can be selected by the command decoder by sending the appropriate 3-bit word to select reset states in the divide-by-5 and divide-by-2 circuits that generate the timing to select the code. The time-shifted patterns are obtained by delaying the pattern with two flip-flops that are clocked at twice the command link PN rate to give a half-chip time separation between the three patterns (P_E, P_C, P_L).

6.4 CORRELATION AND MODE CONTROL

The correlation of the received PN code with the locally generated command link PN code is accomplished by the serial correlator system shown in Figure 6-4. The in-phase component of the baseband signal, I, is then compared to the PN code generator outputs in three exclusive-OR circuits. These circuit outputs are supplied to integrators that integrate the outputs over 140 chip intervals.

The phase and timing correction loops utilize the I_E, I_L, and I_C integrator outputs to determine the amount and direction of correction in phase and timing. The quality of the correlation process is determined by monitoring the magnitude of the I_C integrator output, and this magnitude is compared to a threshold level in the threshold/quality circuits where a decision is made as to the mode of operation for the phase and timing loops.

During sync acquisition, when the I_C integration magnitude exceeds a predetermined threshold, a valid timing point and phase lock are assumed and commands are sent to the two loops to change their operation to a tracking mode. This is accomplished in the timing loop by stopping the time stepping search for the correct PN code timing and enabling the $I_E - I_L$ correction of timing to allow tracking of the received signal. The phase loop is commanded to a new mode by switching the bandwidth of the loop low pass filter to a narrower (lower) bandwidth for a more precise tracking of the received signal phase.

After sync acquisition, the system switches to a sync tracking mode. The early/late PN code tracking is accomplished by correlation of half-chip early (P_E) and half-chip late (P_L) versions of the code with the received signal. The outputs of the early and late exclusive-OR circuits are integrated over the data bit time and the magnitudes are compared to generate an advance or retard timing correction signal. An

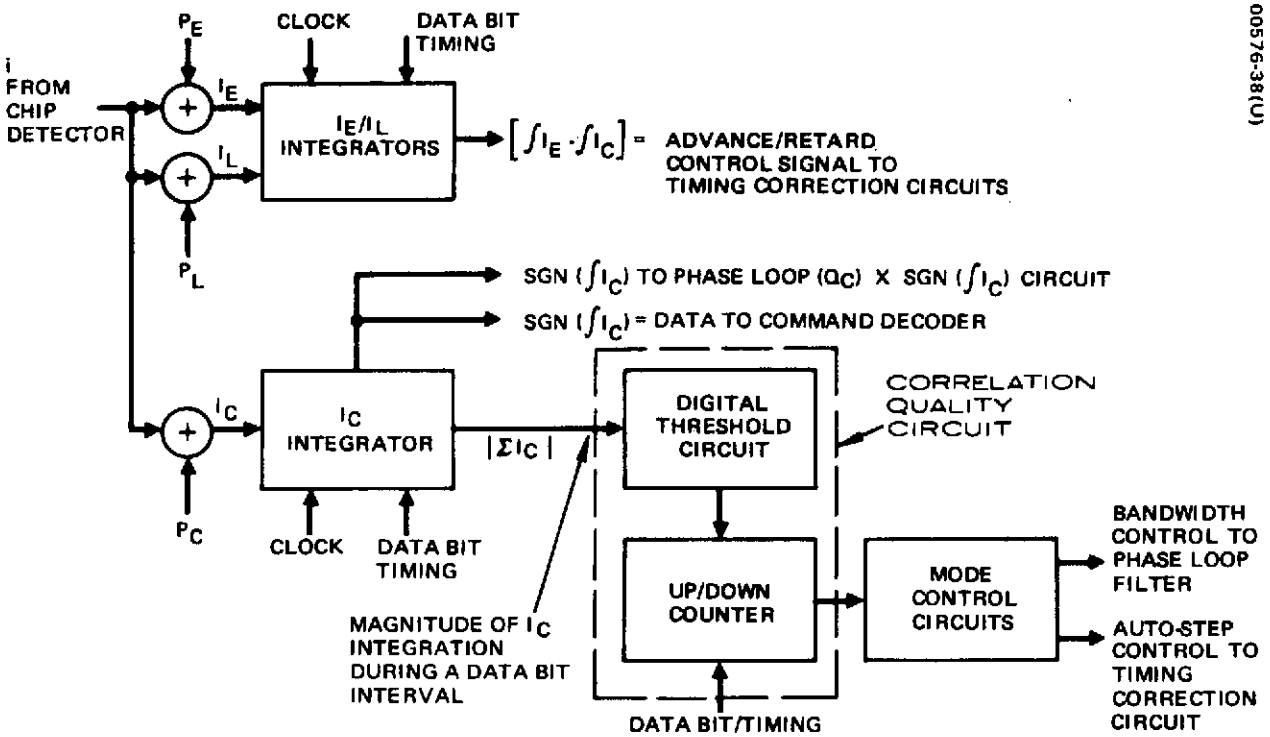

Figure 6-4. Correlation and Mode Control

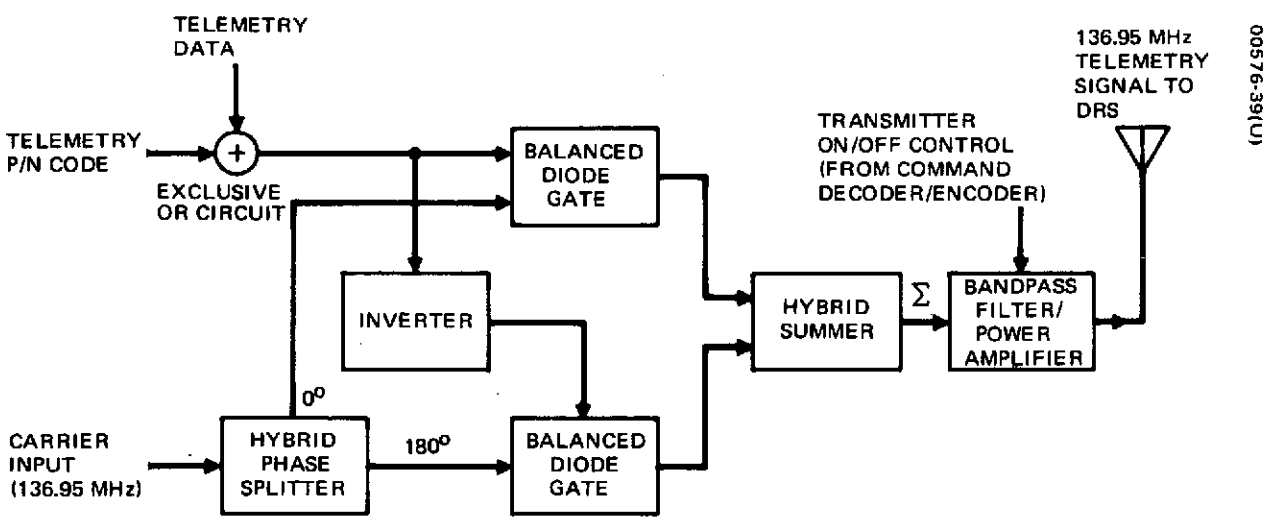

Figure 6-5. Telemetry Transmitter

up/downcounter (integrator) is used to accumulate the results of the exclusive-OR comparison of the center timed pattern, P_C, and the received signal. The counting range required in the integrators is equal to the clock rate divided by the data bit rate. The integrators are reset to zero at the start of each data bit time, and the results of the correlation over a data bit interval is read out at the end of the interval. The sign of the I_C integrator at the end of an integration establishes the data bit for that interval as a one or zero, and the magnitude of the I_C integrator output is a measure of the quality of the correlation process.

The correlation quality circuit consists of a digital threshold circuit and an up/down counter. This circuit is updated at the end of each data bit interval by adding one count to the counter each interval that the output of the I_C integrator is above the threshold until the upper limit of the counter is reached. A typical counter has three stages with an eight-count limit. For each data bit interval that the I_C magnitude is below threshold, the threshold-counter counts down until a zero count is reached. At the zero count, the phase loop filter is switched to the wide bandwidth mode and stepping of the PN code timing is initiated. The optimum threshold level and number of bits in the up/down counter require a detailed analysis of the system performance requirements and received signal characteristics before specific values can be established.

6.5 TELEMETRY TRANSMITTER

The doppler-shifted telemetry carrier developed by the carrier frequency generator is biphase-modulated by the product of the telemetry PN code and telemetry data as shown in Figure 6-5.

Multiplication of the telemetry link PN code by the telemetry data is accomplished in an exclusive-OR circuit. The exclusive-OR output is used to gate on or off the zero or 180 degree phase-shifted versions of the telemetry carrier to produce a biphase-modulated signal. The modulated signal is then filtered to attenuate the spread spectrum sidebands that are outside the telemetry channel bandwidth. After filtering, the signal is amplified in a solid-state power amplifier to the correct power output level. A transmitter on/off signal from the command decoder controls dc power to the power amplifier stages to conserve dc power when the LAS is not sending telemetry data.

6.6 LAS COMMUNICATION TRANSPONDER DC POWER, WEIGHT, AND VOLUME ESTIMATE

The LAS transponder hardware volume and dc power requirements were estimated based on the design outlined in the block diagrams. The estimates do not include the command decoder, telemetry encoder, antennas, or power supplies.

These estimates were developed by extrapolation from current operational hardware performing similar functions with currently available integrated circuit technology. Considerable reduction in volume and power

dissipation can be obtained utilizing new developments in low power, very high density integrated digital (LSI) and hybrid linear analog circuit techniques that are becoming available.

The estimated number and type of parts and volume are itemized in Table 6-1. In addition, the dc power required for the circuits included in this estimate is:

+12 vdc → 12.5 watts

+ 5 vdc → 9.25 watts

Total dc power = 21.75 watts

The estimated weight is 3.2 pounds.

TABLE 6-1. VHF COMMUNICATION SYSTEM COMPONENT QUANTITY AND VOLUME ESTIMATES

Item	Quantity	Volume, in^3
Integrated circuit flatpacks	100	10
Analog stages with TO-5 ICs*	17	8
Custom low power hybrid IC stages*	12	4.5
Custom high power hybrid IC stages*	2	2
Special purchased parts**		1
		Total volume - 25.5 in^3 (Does not include antennas, power supplies, command decoder, or telemetry encoder)

*A stage is an active device with associated R-L-C components

**Passive devices such as filter crystals, etc.

7. TRACKING PERFORMANCE

7.1 RANGE MEASUREMENT PERFORMANCE

Uncertainties in the measurement of two-way ground terminal-DRS-LAS range may be classified as either random or systematic. In a series of sequential range measurements, random uncertainties tend to be uncorrelated from measurement to measurement, while systematic uncertainties are typically invariant over periods long with respect to the observation interval. Thus, the effects of random uncertainties can usually be reduced by employing smoothing techniques (including simple averaging of the raw range data); while systematic uncertainties introduce offsets or biases in system range data which can be reduced by data preprocessing using an a priori model of the physical mechanisms that are the sources of these uncertainties. The fundamental sources of random uncertainties in the present case are additive system white thermal noise and oscillator phase jitter. The major sources of systematic uncertainties are long-term group delay variations in the ground terminal equipment, DRS, and LAS due to temperature changes, doppler shift, signal level variations, power supply variations, and miscellaneous aging effects.

A detailed analysis of all random and systematic uncertainties in the DRS VHF ranging system is beyond the scope of this report. However, based on previous experience, estimates of the magnitude of the principal uncertainties can be made; and, in particular, the results of a documented analysis of synchronization timing uncertainties (the limiting factor in the present system) are employed to develop bounds on system performance.

7.1.1 Synchronization Timing Uncertainty

For the delay-lock synchronization technique described in Sections 4 and 6, it is shown in Reference 7 that the rms timing uncertainty is given by

$$\sigma_t = \frac{T_c}{K\,(S/N)^{1/2}} \tag{1}$$

where T_c is the chip width in seconds, K is a constant depending on the ratio of RF bandwidth to chip rate, and S/N is the signal-to-noise ratio in the

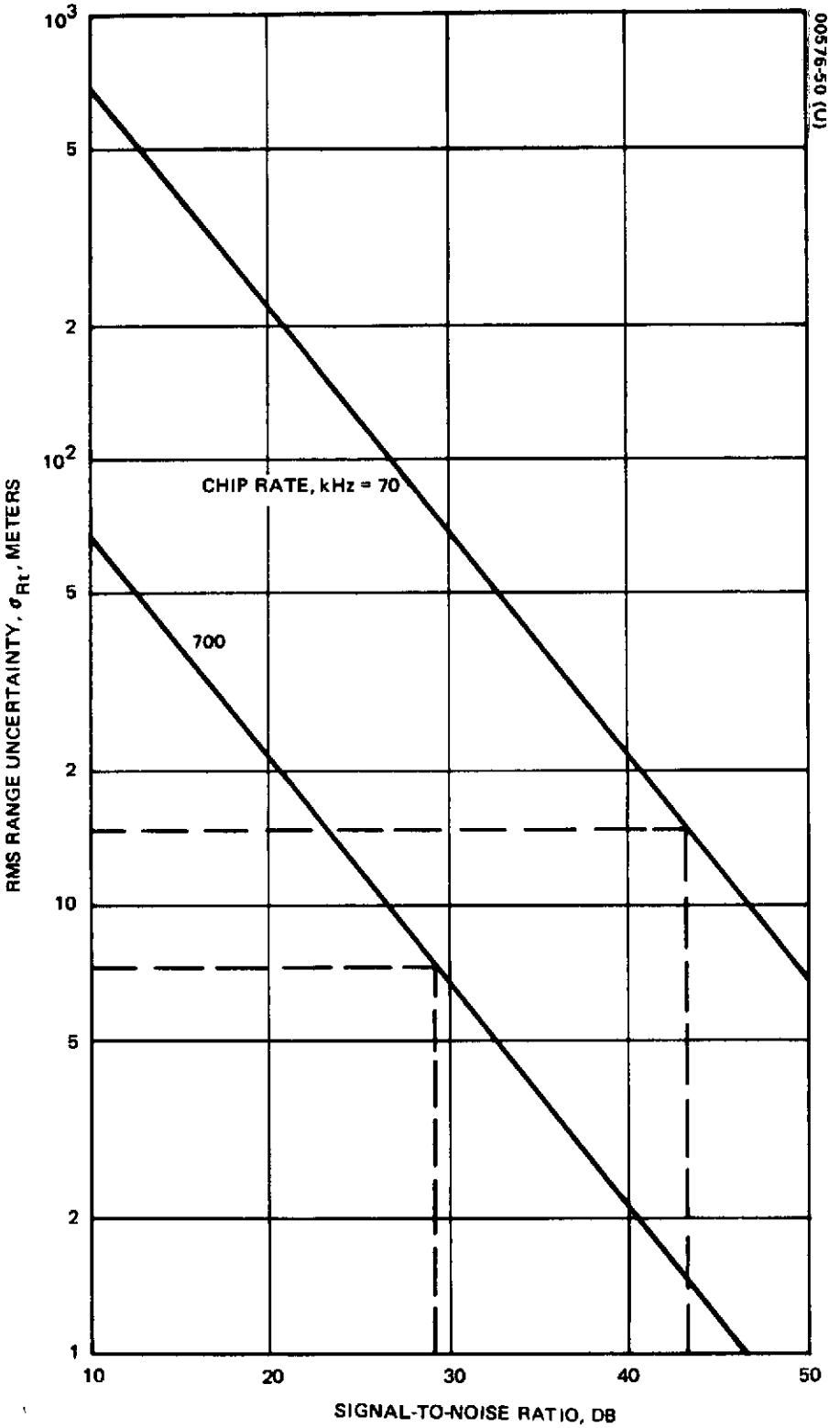

Figure 7-1. RMS Range Uncertainty Due to Synchronization Timing Uncertainty

carrier tracking phase lock loop. For the parameter selection of Section 5, this ratio has a value of 1.43, and from Appendix II of Reference 7, the value of K corresponding to this ratio is estimated to be about 2.0. For biphase modulation, T_c is just the reciprocal of the chip rate, R_c. With these substitutions, the rms range uncertainty due to synchronization timing uncertainty is given by

$$\sigma_{Rt} = c\sigma_t = \frac{c}{2R_c\,(S/N)^{1/2}} \tag{2}$$

where c is the speed of light (3×10^8 m/sec). This relationship is shown in Figure 7-1 for the command and telemetry chip rates selected in Section 5, i.e., 70 and 700 kHz, respectively.

Referring to Figure 3-9, the bandwidth of the phase lock loop on the LAS must be about 6 Hz and at the ground terminal must be 12 Hz to accommodate the doubling effect of two-way ranging. From Table 3-2,

$$(S/N)_{LAS} = -147.6 + 198.6 - 7.8 = 43.2 \text{ dB} \tag{3}$$

And from Table 5-1 and the analysis of Subsection 5.2,

$$(S/N)_{GND} = -157 + 198 - 1 - 10.8 = 29.2 \text{ dB} \tag{4}$$

From the above-mentioned values of S/N and Figure 7-1, the worst-case range uncertainties due to chip sync timing uncertainty in the LAS and ground receivers are given by

$$(\sigma_{Rt})_{LAS} = 14.8 \text{ meters}$$

$$(\sigma_{Rt})_{GND} = 7.5 \text{ meters}$$

7.1.2 Other Random Uncertainties

Apart from the range uncertainty due to the effects of additive system thermal noise on chip sync timing, there will be uncertainties due to phase jitter on the several oscillators used throughout the system. In the DRS configuration assumed, the ground terminal master oscillator is the basic phase reference for the overall system, and all frequency conversions in

both the DRS and LAS are phase coherent with respect to that reference. However, because signal propagation times in the DRS system geometry are long compared to the correlation times of the phase noise processes encountered at different points in the system, short-term phase jitter in the ground terminal oscillator, DRS frequency synthesizer/repeater, and LAS transponder will be uncorrelated and must be added on a variance basis to establigh a system value for the rms range uncertainty due to oscillator instability. Estimates are provided in Table 7-1, based on the DRS system concept of Reference 1 and the LAS subsystem implementation of Section 6. These are considered to be conservative values, in line with the objective of estimating a lower bound on system performance.

7.1.3 Systematic Uncertainties

The group delay stability of the overall ground terminal-DRS-LAS ranging system is difficult to estimate in the absence of more specifics regarding equipment design details. However, for the LAS (which will experience the most severe thermal environment), careful design will limit long-term variations in group delay to about 0.3 percent of the overall transponder group delay, the principal source of which is the 100 MHz IF filter in the receiver. Approximating its overall delay as the reciprocal of the filter bandwidth yields an estimated group delay uncertainty of 30 nanoseconds. The temperature environment on the DRS will be more stable, and the total bandwidth of the repeater-receiver in each direction will be at least 1 MHz. Thus, the total two-way DRS delay uncertainty can probably be kept less than 10 nanoseconds. Finally, the well regulated ground receiver should have a delay uncertainty less than 2 nanoseconds. These constitute the major contributions to overall system group delay uncertainty and are shown in Table 7-1 to yield an overall system rss systematic uncertainty of 9.6 meters.

7.1.4 Comparison with GRARR VHF System Performance

Comparing the performance of this system with that of the VHF Goddard range and range-rate (GRARR) system shown in Figure 2-2, it can be seen that the estimated DRS ranging system resolution is somewhat poorer than that of the 20 kHz GRARR tone implementation. The comparison is not straightforward since range measurement via a DRS involves four transmitters and receivers, whereas the GRARR direct-to-the-LAS system involves only two of each. In any case, the worst-case estimated range measurement uncertainty of the system presented in this report does not appear to be significantly greater than that of the GRARR system. Further, it should be emphasized that only estimates have been given here; and, if good design techniques are employed, the actual uncertainties will be significantly less than those shown in Table 7-1.

It should be pointed out that a major difference between the GRARR and DRS ranging systems is that the former must propagate VHF signals through the earth's troposphere and ionosphere. This invariably leads to ranging system performance much poorer than that predicted by the simple

TABLE 7-1. RANGE MEASUREMENT UNCERTAINTY DUE TO TIME-VARYING ERROR SOURCES

Source and Type of Uncertainty	Estimated Time Uncertainty, nanoseconds	Equivalent Range Error, meters
Rms code sync timing, LAS	49.3	14.8
Rms code sync timing, ground terminal	25.0	7.5
Rms phase jitter, LAS	10.0	3.0
Rms phase jitter, DRS	5.0	1.5
Rms phase jitter, ground terminal	2.0	0.6
Total rms random uncertainties, worst case	56.8	17.0
LAS group delay, LAS	30.0	9.0
DRS group delay, DRS	10.0	3.0
Group delay, ground terminal	2.0	0.6
Total rss systematic uncertainty	31.8	9.6
Two-way range instrumental accuracy, worst case	64.9	19.4

instrumental accuracy curves of Figure 2-2. The DRS VHF ranging system, on the other hand, will propagate signals through the troposphere and ionosphere at "window" type frequencies well above 2 GHz. As a result, it is legitimate to assume that actual DRS ranging system performance in the field will be very close to that measured in system instrumental accuracy tests on the ground. While it is difficult to put a quantitative figure of merit on this operational advantage, it must be reckoned with in any attempt to compare the two VHF ranging systems.

7.2 RANGE-RATE MEASUREMENT PERFORMANCE

Range-rate measurement is accomplished by counting the number of cycles of the received carrier or some lower, intermediate frequency, f_i, over a time interval, T. The ratio of the count to T is compared to the transmitted frequency, f_{io}, and the difference is the doppler shift, Δf. This doppler shift is the composite frequency shift due to relative motion between the ground station and DRS and between the DRS and LAS. The relationship between these two range rates, the carrier frequencies, and the total doppler shift is discussed in Reference 17. However, the motion between the former two terminals will be much less than that between the latter. Further, this smaller motion will be more precisely known. Thus, the dominant contributor to this composite doppler shift will be the LAS/DRS range-rate; likewise, the dominating contributor to the range-rate uncertainty will be the LAS/DRS range-rate uncertainty. This assumption is employed in the following preliminary analysis.

The major sources of uncertainty in the measurement of range-rate are: 1) additive noise in the phase lock loops, 2) ground terminal reference oscillator instability, and 3) time measurement quantization. In addition, there is uncertainty due to nonideal operation of signal processing and detection equipment. In this subsection, only the above three listed uncertainty sources are discussed and it is shown that sources 1 and 2 are the principal contributors. All of the causes mentioned above result in random uncertainty, as discussed in subsection 7.1. There are no apparent significant systematic uncertaintics.

7.2.1 Receiver Noise (White Gaussian Noise)

For a high gain, second-order, phase lock loop (PLL), the analysis of Reference 16 leads to a relationship between the rms range-rate uncertainty, R_u, the PLL signal-to-noise ratio, and the counting time given by

$$\dot{R}_u = \frac{\alpha\beta c}{f_o T}\,\sigma \tag{5}$$

where

$\dot{R}_u$ = rms range-rate uncertainty for a two-way coherency measurement, m/sec

f_o = nominal LAS/DRS carrier frequency, Hz

T = cycle counting interval (smoothing time), seconds

c = speed of light, m/sec ($\approx 10^9$)

σ = ideal filter relative rms phase noise, radians

$$= 2\left[\left(\frac{S}{N}\right)\right]^{-1/2} \tag{6}$$

(S/N) = signal to noise power ratio in phase lock loop two-sided noise bandwidth, numeric

$$\alpha = 2\pi f_n T \tag{7}$$

f_n = undamped second-order phase lock loop natural frequency, Hz

and β is shown as function of α in Figure 7-2 for several values of the loop damping ratio, ζ.

For high-loop gain, the S/N is given by the following relationship:

$$\left(\frac{S}{N}\right) = \left(\frac{S}{\eta f_n}\right) \frac{4\zeta}{1 + 4\zeta^2} \tag{8}$$

where

S = average received signal power after noise figure determining point, watts

η = power-spectral density of the additive-received noise measured at same point as signal power, watts/Hz

ζ = filter damping ratio, numeric

There are three phase lock loops to provide the round-trip phase coherency: one in the LAS, one at the ground station, and one in the DRS. In each of these, gaussian noise will produce phase uncertainty. Thus, Equation 5 can be rewritten with the additive effects of the three PLLs

$$\dot{R}_u = \frac{\alpha\beta c}{f_o T}\left(\sigma^2_{LAS} + \sigma^2_{DRS} + \sigma^2_{GND}\right)^{1/2} \tag{9}$$

Substituting from Equation 6,

$$\dot{R}_u = \frac{\alpha\beta c}{f_o T\sqrt{2}}\left[\frac{1}{(S/N)_{LAS}} + \frac{1}{(S/N)_{DRS}} + \frac{1}{(S/N)_{GND}}\right]^{1/2} \tag{10}$$

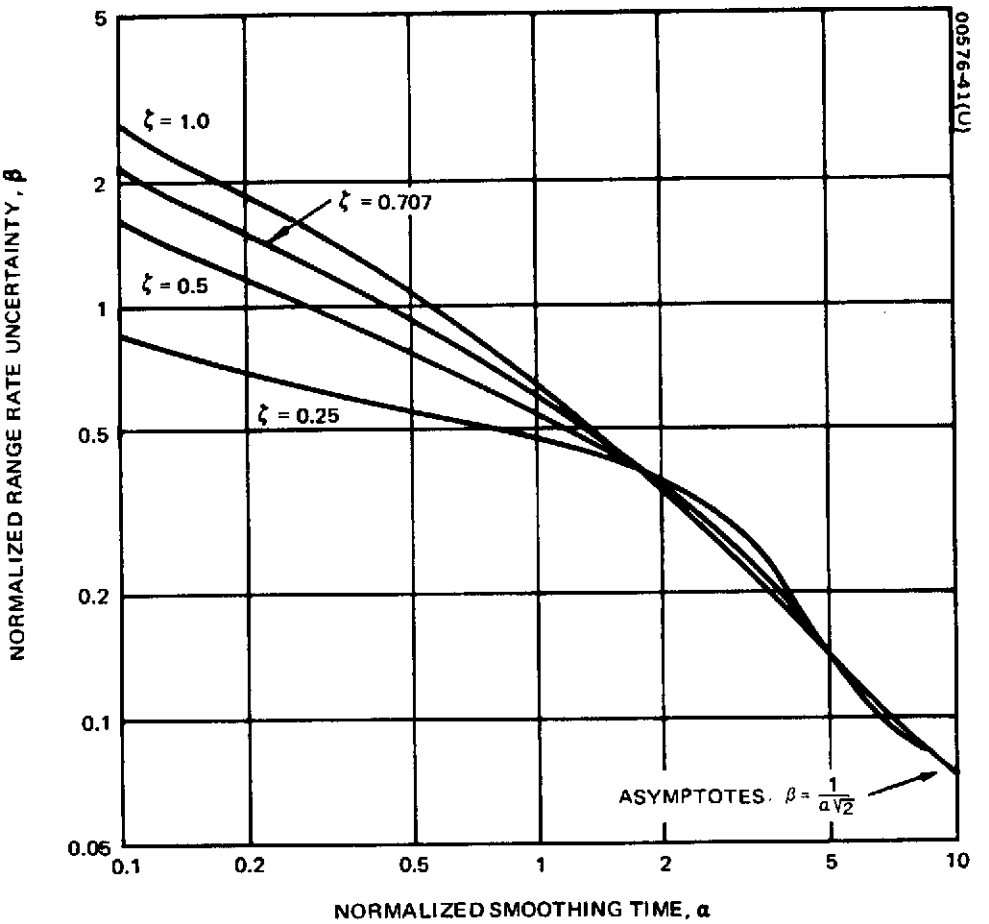

Figure 7-2. β Versus α

For sample calculations, assume that $\zeta = 0.5$; then from Equation 8, $(S/N) = (S/\eta f_n)$. And, f_n will be taken as the loop bandwidth necessary to track the doppler shift, i.e., the maximum rate of change of frequency. As previously stated, the bandwidths for the LAS and ground receivers are 6 and 12 Hz; respectively; and Equations 3 and 4 give the resultant signal-to-noise ratios. The large transmitter power and antenna gain available at the ground station will result in a signal-to-noise ratio much larger than that in either the LAS or ground receiver PLL. From Equations 3 and 4,

$$\frac{1}{(S/N)_{LAS}} + \frac{1}{(S/N)_{GND}} \approx 12.48 \times 10^{-4} \tag{11}$$

Substituting this result into Equation 10 and letting $f_o = 140$ MHz,

$$\dot{R}_u \approx 5.36 \frac{\alpha\beta}{T} \text{ cm/sec} \tag{12}$$

It may be noted from Figure 7-2 that $\alpha\beta = 1/\sqrt{2}$ for values of α larger than 10. For the determination of α from Equation 7, a value of $f_n = 12$ Hz will be used because the (S/N) at the ground receiver is dominant. For this parameter value, Figure 7-3 shows the relationship between the counting time, T, and the rms range-rate error due to receiver noise.

7.2.2 Oscillator Instability

The instability of the master oscillator at the ground terminal causes range-rate measurement uncertainty due to a phase drift during the round-trip propagation time. This phenomenon was analyzed in Reference 16 where it is shown that

$$\dot{R}_u \begin{cases} \frac{c}{2\pi f_o} \left(\frac{P}{2T}\right)^{1/2} & D > T \qquad (13a) \\ \frac{c}{2\pi f_o T} \left(\frac{PD}{2}\right)^{1/2} & D < T \qquad (13b) \end{cases}$$

where D is the round-trip propagation delay time and P is the rms value of the rate of change of carrier phase in rad/sec.

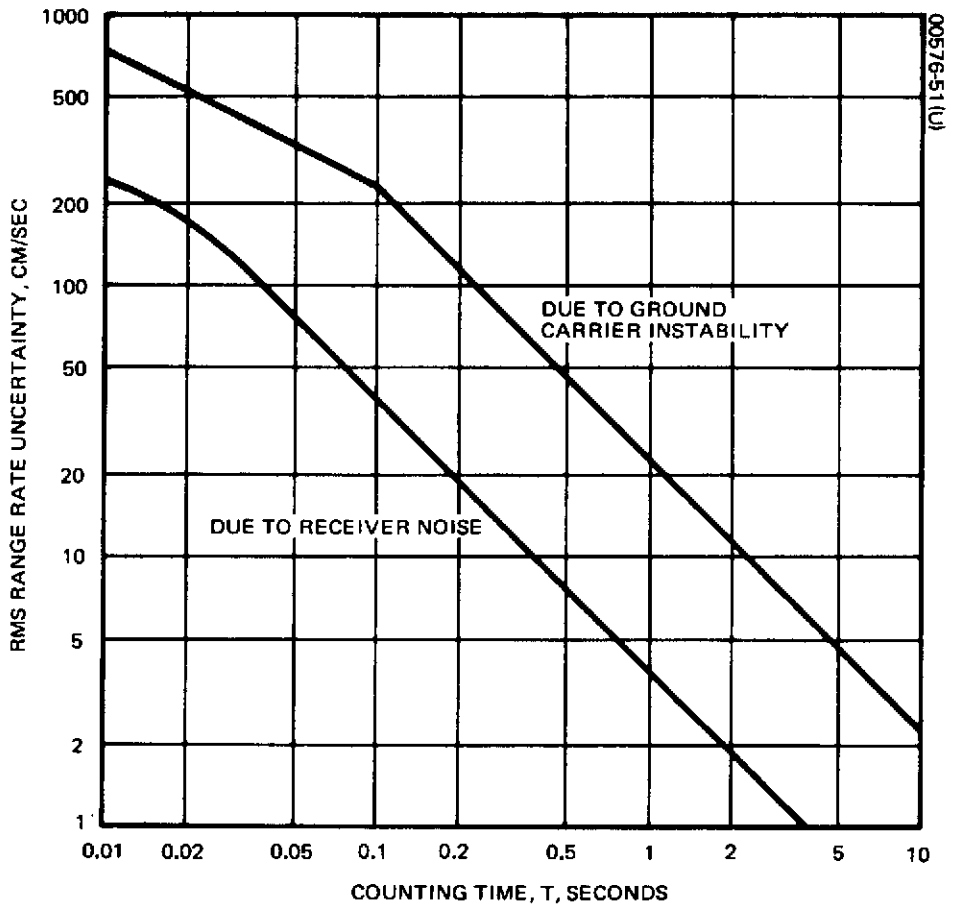

Figure 7-3. Range-Rate Uncertainty

The round-trip propagation distance lies between 28,500 and 33,000 n. mi., corresponding to a time delay, D, in range 0.095 to 0.11 second. Assuming D = 0.1 second and that T > D, Equation 13b becomes

$$\dot{R}_u = 7.64 \frac{\sqrt{P}}{T} \text{ cm/sec} \tag{14}$$

where f_o = 140 MHz has been used.

Since frequency translation in round-trip signal propagation is accomplished by mixing, the phase drift of the ground transmitter frequency is translated throughout the ground/DRS/LAS link. Thus, the rms phase drift rate, P, of the ground station carrier is critical to range-rate measurement performance; but data concerning this drift are scarce. For a given reference oscillator stability, P_x, at its frequency, f_x, the stability, P, at the transmitter carrier frequency, f_c, after frequency multiplication is given by

$$P = P_x \left(\frac{f_c}{f_x} \right)^2 \tag{15}$$

Thus, for a given reference oscillator, the carrier instability is proportional to the square of the carrier frequency. In Reference 2, the 350 MHz output of the frequency synthesizer has an rms drift rate of 0.018 rad/sec. If it is assumed that the ground station carrier is 8 GHz, then by Equation 15 a typical value for P is 9.4 rad/sec. Substituting this value into Equation 14,

$$\dot{R}_u = \frac{23.4}{T} \text{ cm/sec } (T \geq D = 0.1 \text{ second}) \tag{16}$$

Using Equation 13, $\dot{R}_u$ is shown as a function of T in Figure 7-3 for D = 0.1 second and P = 9.4 rad/sec.

7.2.3 Time Quantization Uncertainty

The zero crossings of the IF frequency, f_i, are counted; and while this counting proceeds, another reference frequency, f_r, is counted to establish the time interval T. The counting of f_r begins when the first count of f_i is registered and is terminated later at an integer count of f_i zero crossings.

In Reference 2, it is stated that the rms value of the uncertainty in determining the interval T is given by

$$\sigma_T = \frac{1}{f_r \sqrt{6}} \tag{17}$$

It can be shown that the rms range-rate uncertainty is given approximately by

$$\dot{R}_u = \frac{\dot{R}}{T} \sigma_T = \frac{\dot{R}}{f_r T \sqrt{6}} \tag{18}$$

In subsection 3.1.3, it is mentioned that the maximum range-rate is approximately 8500 m/sec (27,900 fps). Thus, if f_r = 10 MHz,

$$\dot{R}_u \leq 0.35/T \text{ cm/sec} \tag{19}$$

Note from Equation 17 that the uncertainty due to time quantization can be made small by making the reference clock frequency sufficiently large.

7.2.4 Combined Uncertainty

From Equation 7 and Figure 7-2, it can be seen that if f_n is taken as 12 Hz, as was done above, and if T > 0.1 second, the product $\alpha\beta$ in Equation 12 has the value $1/\sqrt{2}$. Then, with this value it can be seen by comparing Equations 12, 16, and 19 that the uncertainty due to receiver noise and ground carrier instability is much greater than that due to time quantization. The rss sum of the uncertainties is dominated by that due to oscillator instability and is thus given approximately by curve B in Figure 7-3.

The two parameters of greatest influence in the range-rate uncertainty were 1) the ground terminal's second-order phase lock loop natural frequency, f_n, and 2) the rms carrier phase drift rate, P, of the ground terminal. The first was taken as 12 Hz and the latter as 9.4 rad/sec. However, it may be possible to track the received frequency fairly accurately with a scheme employing ephemeris data, allowing f_n to be reduced by a factor of 10. This would both increase $(S/N)_{GND}$ and decrease the product $\alpha\beta$ in Equation 10. But, as can be seen from Figure 7-3, effort should be concentrated on an oscillator/synthesizer design which minimizes the carrier phase drift rate.

Comparing with the performance of the GRARR system given in Figure 2-3, the range-rate uncertainty as analyzed above will be slightly greater. For instance, for a 10 second measurement interval (counting time), Figure 2-3 indicates that the minimum range-rate uncertainty with the GRARR system will be about 2 cm/sec; whereas from Figure 7-2, it appears that the system presented here can be designed to have an uncertainty of approximately 2.34 cm/sec for the same measurement interval. Based on preliminary TDRS orbit determination studies in Reference 1, this accuracy should be sufficient to satisfy mission requirements.

8. GROUND TERMINAL AND RELAY SATELLITE CONSIDERATIONS

This section discusses a number of concepts associated with command transmission, the telemetry receiver, and range and range-rate tracking, and summarizes the assumptions made about the DRS in the above discussion and analyses.

A ground terminal is defined here as possessing a single antenna and hence capable of transmitting to, and receiving from, one DRS at a time. Depending on the number and positions of the DRSs, it may be possible to locate two ground terminals at the same geographic location and within the same building. The terminal consists of transmitting, receiving, and signal processing equipment, and associated support facilities.

8.1 COMMAND SYSTEM

Each ground terminal will be assigned a specific PN code which will be combined with the 500 bits/sec command data stream at a 70 kilobits/sec synchronized rate, as discussed in Sections 4 and 5. This combined binary signal phase modulates an RF carrier which is transmitted to a DRS where it is frequency translated to VHF and retransmitted toward the earth. Thus, all commands from this DRS are modulated by the same code; and the DRS may be thought of as an advantageous extension of the associated ground terminal. All LASs within view of a DRS whose correlation receivers have been set to its code can be commanded from the associated ground terminal. When a particular LAS is about to pass out of the view of a DRS, a new code setting is commanded from the ground terminal (see subsection 6.3), which allows the LAS to then be commanded via the next visible DRS from its associated ground terminal.

Each LAS whose receiver code has been set to match that of a visible DRS will automatically acquire the DRS signal in a matter of seconds, and so essentially continuous real-time command of every LAS is possible. If continuous availability is not required, command programming may be simplified by leaving the LAS receiver code matched to just one ground terminal. As the LAS comes within view of the corresponding DRS, signal acquisition is automatic. Such a scheme allows more than 50 percent command availability time and simplified command programming and coordination.

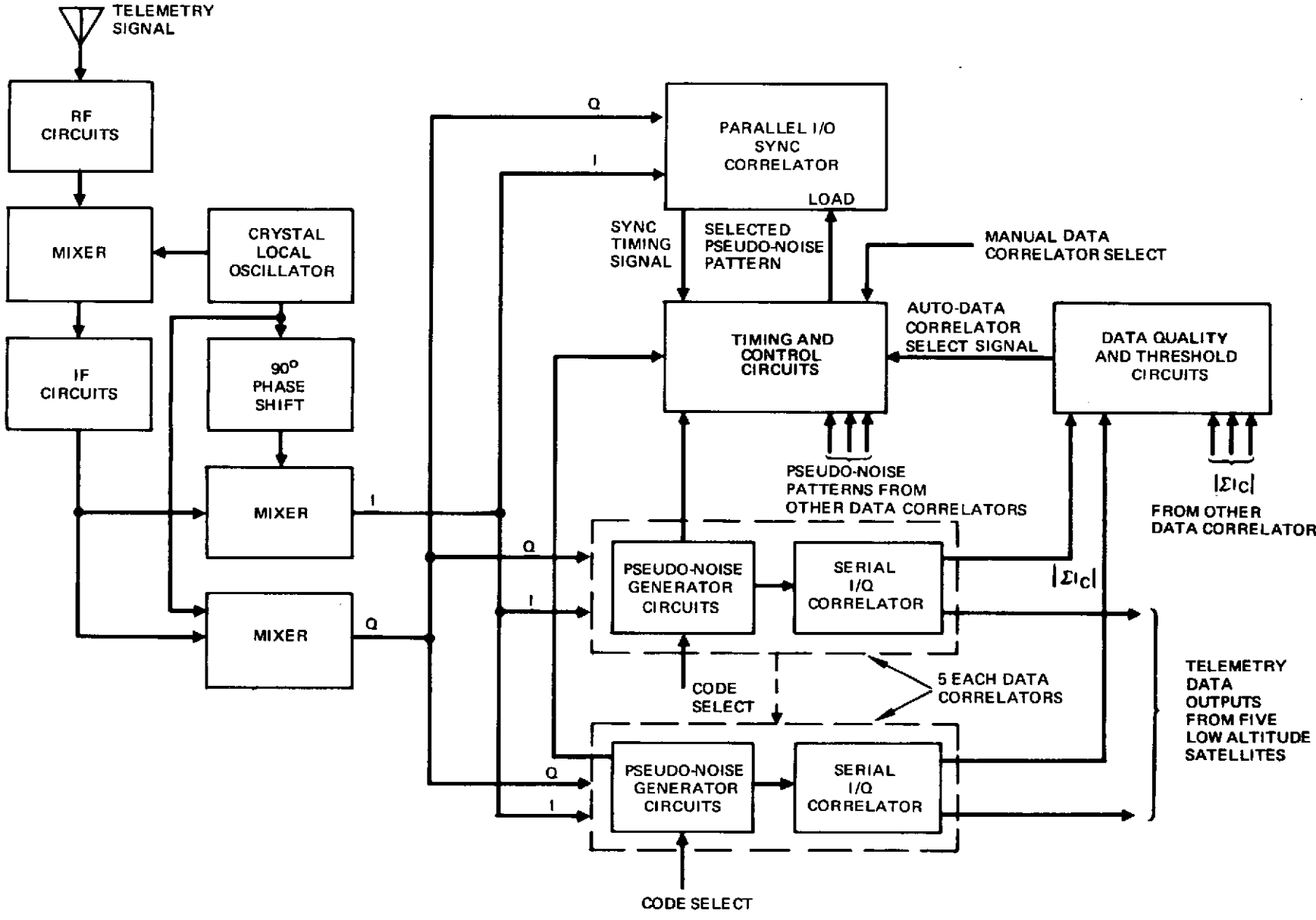

Figure 8-1. Ground Terminal Telemetry Receiver Simplified Block Diagram

In order for an LAS to accomplish automatic signal acquisition, the PN code modulated signal must be continuously transmitted from the ground terminal. Command data modulates this basic signal only when desired; but the RF signal, code modulated, must be continuous. Each LAS is assigned a unique binary address which comprises the first portion of the command data intended for any particular LAS. Reception of its address activates an LAS to store the remaining portion of the command and to immediately retransmit it to the ground terminal via the DRS for verification. After verification, an execute command is transmitted, preceded by the LAS address.

This command method allows complete flexibility. The commands and addresses need not conform to a specific format. Thus, each LAS or class of LASs may have a command format most appropriate for its particular mission and operation. Another option is the capability to transmit the same command simultaneously to several LASs and yet be able to command them individually when desired. This requires the implementation of the proper logic circuits in the receivers with resulting command capability similar to many locks with a master key as well as individual keys.

Commands must be sent sequentially, which conceivably could cause timing conflicts. However, it is anticipated that this problem will be minimal and can even be eliminated by programmed time sharing of the ground terminal command transmitter. A command sequencing system is not conceptually difficult to implement and requires principally buffer (temporary) storage, a clock, comparator circuits for time-tagged commands, and priority decision circuits.

8.2 GROUND TERMINAL RECEIVER

A representative ground terminal receiver concept is shown in Figure 8-1. The received telemetry signal is mixed down to an intermediate frequency by conventional techniques with both an in-phase (I) and a quadrature (Q) signal being produced. The I and Q signals are sent in parallel to the sync and data correlators. The salient feature of this concept is that a single, relatively complex sync correlator controls a number of simpler data correlators, with the sync correlator sequentially acquiring sync for each data correlator and the data correlators simultaneously tracking and decoding the data modulations on each PN sequence in the received signal. The number of data correlators that may be controlled by a single sync correlator is limited only by the complexity of the interface circuitry. However, practical limits also exist on the number of PN signals that may be processed simultaneously due to the signal processing gain required to decode the correct PN signal at each correlator in the presence of the other PN signals which appear as noise to the correlator.

The sync correlator is designed as a parallel I/Q correlator with active storage circuits (shift registers) for storing an entire telemetry

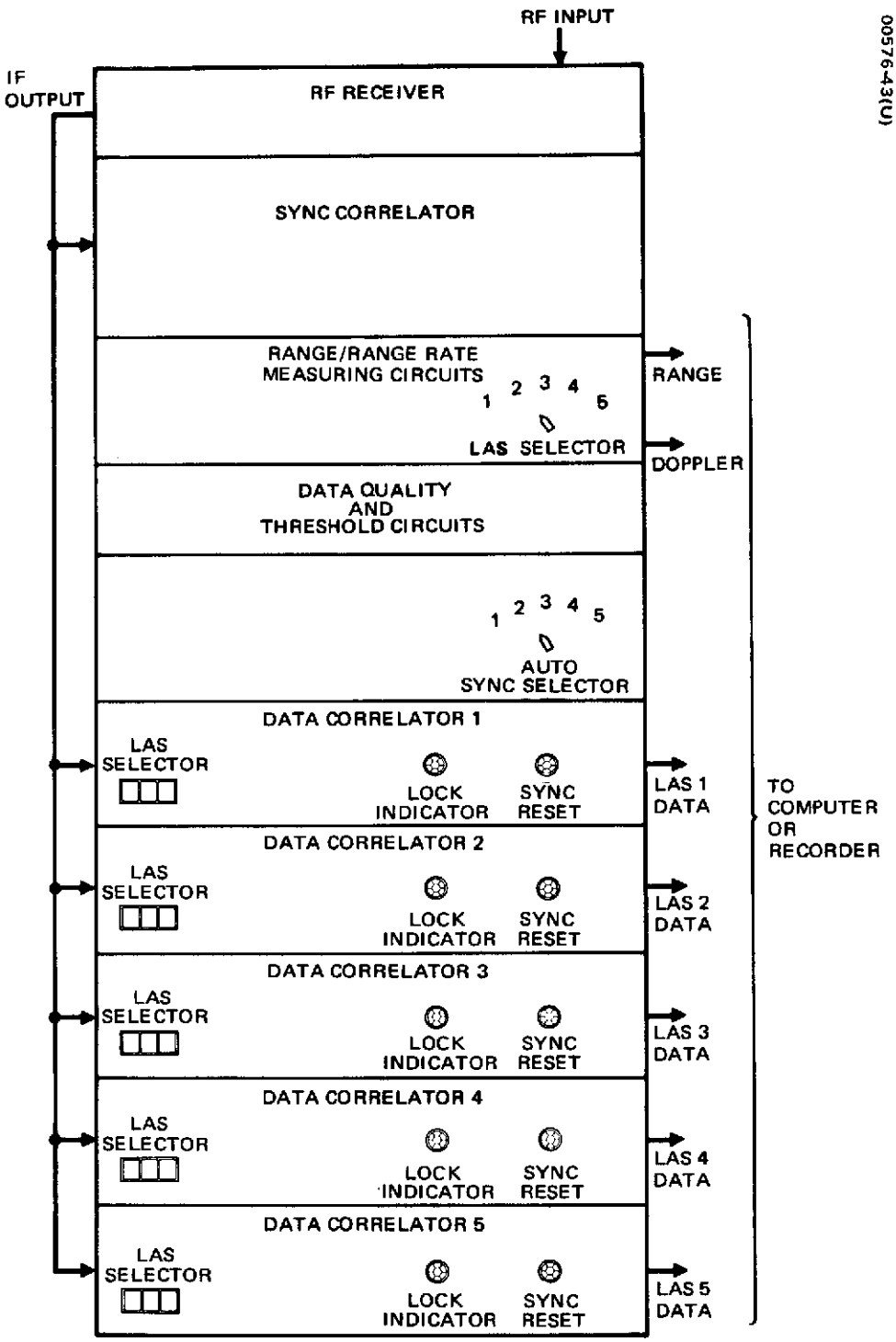

Figure 8-2. Typical Telemetry Receiver Cabinet for Ground Terminal

PN code. The pattern to be stored is selected by the timing and control unit which receives a pattern selection command from either an automatic data correlator selection circuit or from an operator-controlled switch. For automatic operation, the magnitude outputs from each correlator would be used as an indication of the quality of the data output from the data correlators. Whenever a correlator output dropped below a predetermined magnitude, the sync correlator would be loaded with the pattern corresponding to the low signal quality PN code for a resynchronization of the related data correlator on the next cycle of the received code.

The identical data correlators are serial correlators and have the ability of producing any one of the LAS telemetry codes being used. The PN generators, correlation circuits, phase loop, and timing-loop portions of the data correlators would be very similar to those in the LAS transponder. The quality thresholds and phase lock loop bandwidths may differ from the LAS values since sync acquisition is performed by the separate parallel correlator.

The data correlators supply the PN code to the sync correlator storage circuits whenever a sync acquisition is initiated for the particular data correlator being considered. Upon achieving proper sync (as indicated by the data quality monitor), sync timing signals to the data correlator are inhibited and this correlator tracks the received signal phase and timing, and decodes the data modulated on the PN code.

Figure 8-2 indicates the controls, indicators, and signals that would be found in a typical ground terminal receiver of the type described. The LAS signals to be monitored are selected on the data correlators by LAS number and the ranging measurements may be made on any one of the five LAS signals by selecting the corresponding data correlator (by adding additional range measuring units, simultaneous measurements may be made).

The data correlators also have indicators to show their operational status and would be used to tell the operator when the correlator is tracking a signal. During the sync acquisition mode, the acquisition process may be automatically sequenced between data correlators until all five correlators have valid signals, or acquisition of a particular correlator may be manually selected by a switch on the timing and control circuits. Additional indicators or controls may be incorporated to meet specific system requirements.

8.3 RANGE AND RANGE-RATE TRACKING

Round-trip transmission delay and doppler shift measurements provide the basic data for range and range-rate determination. Known communication system bias contributions to these measurements can be removed for an immediate estimate of the range and range-rate. Further processing of this data can reduce the error in this crude measurement due to systematic causes.

The round-trip time relay for a given LAS is simply the time difference between start of the transmitted PN code and start of the ground received LAS code. An addressed command signal to the LAS is not necessary, but the LAS transmitter must be operating. The LAS PN code, which is synchronized to the ground terminal PN code, combined with telementry data, biphase modulates the LAS carrier frequency. Thus, range measurements can be made during telemetry transmission. The telemetry data may consist of binary coded samples of spacecraft analog signals, binary outputs of payload instruments, or retransmission of received commands.

Doppler measurement is accomplished by mixing and frequency multiplication operations on the ground terminal local oscillator and the received carrier frequency which is tracked in a correlation receiver as discussed above. The resulting doppler frequency is determined by a zero-crossing counter.

It should be noted that telemetry data may be received by any ground terminal possessing a correlation receiver and antenna of sufficient size. However, tracking requires comparison of the timing and frequency of the received signal with that of the transmitted signal, and hence is most appropriately accomplished at a transmitting, i.e., command, ground terminal.

8.4 DATA RELAY SATELLITE

Below are the DRS assumptions made in the above analyses and discussion. They correspond to the DRS requirements listed in subsection 1.2.

VHF antenna gain	13 dB minimum
Transmitter power	20 watts
Receiver noise temperature	500°K
Coherent frequency conversion	

The assumption of coherent frequency conversion is necessary for range-rate determination from doppler shift measurement, and it is important for it requires a phase-tracking receiver that maintains frequency lock of the ground-transmitted signal. Phase-tracking is a well-established technique and should not present a serious problem; however, an alternate method is available. If a beacon signal, derived from the local oscillator of the DRS VHF system, is transmitted from the DRS directly to the ground, then the local oscillator drift can be compensated by ground processing. With this technique, the required third phase-tracking loop has been placed on the ground instead of on the DRS. However, either a separate beacon transmitter or frequency multiplexing is required to transmit the beacon signal to the ground.

9. LAS ANTENNA CONSIDERATIONS

Since the radiation pattern of any electromagnetic antenna with time-invariant parameters must have at least one null with respect to any fixed polarization, it is impossible to obtain essentially omnidirectional coverage with such an antenna. Through the use of time-variant interconnection of properly selected antennas, however, it is possible to extend coverage to include a full 4π steradians with only minor signal degradation. Several techniques are considered below for making this interconnection. Techniques that apply in the absence of multipath reflections from the earth are considered first. Situations in which such reflections will be absent include, for example, direct transmission from ground to satellite. In this case, the technique of maximal-diversity combining of the outputs of three orthogonally oriented antennas gives the optimum results independent of incident polarization. In the presence of secondary path signals from the surface of the earth, such a technique no longer appears desirable. In this latter case, the use of circularly polarized signals and six circularly polarized antennas on the satellite provides multipath rejection when used with selection-diversity combining techniques.

9.1 COMBINING TECHNIQUES IN THE ABSENCE OF MULTIPATH

In the absence of multipath signals, it is possible to combine the outputs of three mutually orthogonal antennas to improve reception of signals from arbitrary directions. In this study, three different combining techniques were considered. They have been referred to by Brennan (Reference 18) as 1) maximal-ratio diversity combining, 2) equal-gain diversity combining, and 3) selection-diversity combining. In the first technique, the signals received by the various antennas are combined with weighting coefficients that maximize the resulting signal-to-noise ratio. In the equal-gain diversity technique, the contribution of each antenna is weighted equally; in the selection-diversity technique, the strongest signal from the various antennas is used; the others are rejected.

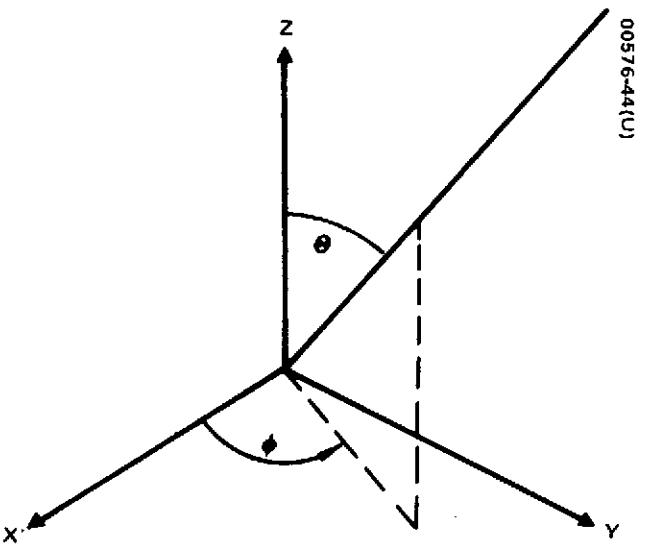

Figure 9-1. Orthogonal Dipoles and Coordinate System

9.2 ANALYSIS OF VARIOUS COMBINING TECHNIQUES

In order to analyze the response of the various combining systems to incident waves an antenna model consisting of three mutually orthogonal short dipoles was chosen. The dipoles were assumed to be directed along the X, Y, and Z axes as illustrated in Figure 9-1. The electric field strength radiated by the X-directed dipole is given by

$$\bar{E} = -A_x (\bar{u}_\theta \cos\theta \cos\phi - \bar{u}_\phi \sin\phi) \tag{1a}$$

The electric field strength from the Y-direct dipole is given by

$$\bar{E} = -A_y (\bar{u}_\theta \cos\theta \sin\phi + \bar{u}_\phi \cos\phi) \tag{1b}$$

That from the Z-directed dipole is given by

$$\bar{E} = A_z \bar{u}_\theta \sin\theta \tag{1c}$$

where the coordinates θ and ϕ are as shown in Figure 9-1, the A_i are the relative excitations of the individual dipoles, and $\bar{u}_\theta$ and $\bar{u}_\phi$ are unit vectors in the directions of increasing θ and ϕ, respectively. A plane wave of arbitrary polarization incident from the direction θ_i, ϕ_i can be represented as

$$\bar{E}_i = \bar{u}_\theta E_1 + \bar{u}_\phi E_2 \tag{2}$$

where the relative amplitudes and phases of E_1 and E_2 determine the polarization characteristics of the wave. The responses of the various dipoles to this incident wave may be written as follows

X-directed dipole:

$$V_x = -A_x (E_1 \cos\theta_i \cos\phi_i - E_2 \sin\phi_i) \tag{3a}$$

Y-directed dipole:

$$V_y = -A_y (E_1 \cos\theta_i \sin\phi_i + E_2 \cos\phi_i) \tag{3b}$$

Z-directed dipole:

$$V_z = A_z E_1 \sin \theta_i \tag{3c}$$

The various diversity-combining techniques adjust the weighting coefficients A_x, A_y, and A_z according to different rules. These techniques will be compared for various incident polarizations.

9.2.1 Maximal-Ratio Combining

If it is assumed that the mean noise power in each channel is the same, then, as shown in the Appendix, the optimum weighting of each channel is proportional to the amplitude of the received signal in that channel, with any phase shift between channels removed to bring all outputs in phase. Thus, the A's are given by

$$A_x = -K \left| E_1^* \cos \theta_i \cos \phi_i - E_2^* \sin \phi_i \right| \tag{4a}$$

$$A_y = -K \left| E_1^* \cos \theta_i \sin \phi_i + E_2^* \cos \phi_i \right| \tag{4b}$$

$$A_z = K E_1^* \sin \theta_i \tag{4c}$$

where K is an arbitrary constant. When these weightings are introduced into Equations 3 and the results are added, the total signal, V_t, becomes

$$V_t = K \left| |E_1|^2 + |E_2|^2 \right| \tag{5}$$

This output is independent of angle of arrival of the wave and depends only on the incident power density and not on polarization. Thus, maximal-ratio diversity combining results in optimum use of the available signal for all angles of arrival and for any incident polarization. The noise in the various channels is also weighted by the values in Equations 4 with the result that the mean square noise voltage in the weighted sum is proportional to

$$\overline{n_t^2} = \overline{n^2} K^2 \left| |E_1|^2 + |E_2|^2 \right| \tag{6}$$

where $\overline{n^2}$ is the mean squared noise voltage per channel (assumed the same for all channels). The signal-to-noise ratio is then given by

$$\left(\frac{S}{N}\right) = \frac{V_t^2}{\overline{n_t^2}} = \frac{|E_1|^2 + |E_2|^2}{\overline{n^2}} \tag{7}$$

which is the optimum possible signal-to-noise ratio. Use of the same weighting on transmission will result in a maximum power transfer back in the direction of arrival with the polarization matched to the receiving antenna.

9.2.2 Equal-Gain Diversity Combining

When equal-gain diversity is used, the magnitude of all the A's is equal, so that the resulting total signal voltage is given by

$$V_t = K\Big\{ \left| E_1 \cos\theta_i \cos\phi_i + E_2 \sin\phi_i \right| + \left| E_1 \cos\theta_i \sin\phi_i - E_2 \cos\phi_i \right| + \left| E_1 \right| \sin\theta_i \Big\} \tag{8}$$

The mean square noise voltage is

$$\overline{n_t^2} = 3\,\overline{n^2} \tag{9}$$

so that the signal-to-noise ratio is

$$\left(\frac{S}{N}\right) = \frac{|E_1|^2 + |E_2|^2 + 2F_1F_2 + 2|E_1| \sin\theta_1 (F_1 + F_2)}{3\,\overline{n^2}} \tag{10a}$$

where

$$F_{1,2} \equiv \tag{10b}$$

$$\sqrt{|E_1|^2 \cos^2\theta_i \cos^2\phi_i + |E_2|^2 \sin^2\phi_i \pm 2|E_1||E_2| \cos(\psi_1 - \psi_2) \cos\theta_i \sin\phi_i \cos\phi_i}$$

TABLE 9-1. COMPARISON OF PERFORMANCE OF DIVERSITY-COMBINING TECHNIQUES

Signal-to-Noise-Ratio / Polarization	Maximal-Ratio Diversity	Equal-Gain Diversity	Selection Diversity
ϕ - directed linear $E_1 = 0$ $E_2 = E$	$\frac{\lvert E\rvert^2}{\overline{n^2}}$	$\frac{\lvert E\rvert^2}{\overline{n^2}} \frac{1 + \lvert \sin\phi_i \cos\phi_i \rvert}{3}$ This S/N varies from $\frac{1}{3}$ to $\frac{1}{2}$ that of optimum case.	Greater of $\left\{ \frac{\lvert E\rvert^2 \sin^2\phi_i}{\overline{n^2}}, \frac{\lvert E\rvert^2 \cos^2\phi_i}{\overline{n^2}} \right.$ S/N equals the optimum when $\phi_i = 0°$, 90°, 180°, 270°. It has a minimum value of half the optimum when $\phi_i = 45°$, 135°, 225°, 315°.
θ - directed linear $E_1 = E$ $E_2 = 0$	$\frac{\lvert E\rvert^2}{\overline{n^2}}$	$\frac{\lvert E\rvert^2}{\overline{n^2}} \frac{1 + 2\lvert\cos\theta_i\rvert \left[\lvert \cos\theta_i \sin\phi_i \cos\phi_i \rvert + \sin\theta_i \left(\lvert\cos\phi_i\rvert + \lvert\sin\phi_i\rvert \right) \right]}{3}$ This S/N has a minimum value of 1/3 the optimum when $\theta = 90°$. The maximum ratio is equal to the optimum when $\theta_i = 35.2°$, 144.8° $\phi_i = 45°$, 135°, 225°, 315°	Greatest of $\left\{ \frac{\lvert E\rvert^2 \cos^2\theta_i \cos^2\phi_i}{\overline{n^2}}, \frac{\lvert E\rvert^2 \cos^2\theta_i \sin^2\phi_i}{\overline{n^2}}, \frac{\lvert E\rvert^2 \sin^2\theta_i}{\overline{n^2}} \right.$ S/N equals the optimum value at $\theta_i = 0°$, 90°, 180°. $\phi_i = 0$, 90°, 180°, 270°. It has a minimum value of 1/3 optimum at $\theta_i = 35.2°$, 144.8°. $\phi_i = 45°$, 135°, 225°, 315°.
Circular $E_1 = E_2 = E/\sqrt{2}$ $\psi_1 - \psi_2 = \pm\frac{\pi}{2}$	$\frac{\lvert E\rvert^2}{\overline{n^2}}$	$\frac{\lvert E\rvert^2}{\overline{n^2}} \frac{1}{3} \left\{ \sqrt{(\cos^2\theta_i \cos^2\phi_i + \sin^2\phi_i)(\cos^2\theta_i \sin^2\phi_i + \cos^2\phi_i)} + \sin\theta \left[\sqrt{\cos^2\theta_i \cos^2\phi_i + \sin^2\phi_i} + \sqrt{\cos^2\theta_i \sin^2\phi_i + \cos^2\phi_i} \right] \right\}$ This S/N has a maximum value equal to the optimum at $\theta_i = 54.8°$, 125.2°. $\phi_i = 45°$, 135°, 225°, 315°. It has a minimum value of 1/3 the optimum value when signal is incident along X, Y, or Z axis.	Greatest of $\left\{ \frac{\lvert E\rvert^2}{\overline{n^2}} \frac{(\cos^2\theta_i \cos^2\phi_i + \sin^2\phi_i)}{2}, \frac{\lvert E\rvert^2}{\overline{n^2}} \frac{(\cos^2\theta_i \sin^2\phi_i + \cos^2\phi_i)}{2}, \frac{\lvert E\rvert^2}{\overline{n^2}} \frac{\sin^2\theta_i}{4} \right.$ S/N has a maximum value of 1/2 the optimum at $\theta_i = 0°$, 90°, 180° for all ϕ and at $\phi_i = 0°$, 90°, 180°, 270° for all θ. It has a minimum values of 1/3 the optimum at $\theta_i = 54.8°$, 125.2° $\phi_i = 45°$, 135°, 225°, 315°.

The (+) goes with F_1 and the (-) goes with F_2. The symbol $\psi_1 - \psi_2$ is the phase difference between E_1 and E_2. The signal-to-noise ratio in this case is obviously dependent on both polarization and angle of arrival in a fairly complicated manner.

9.2.3 Selection-Diversity Combining

The third system of combining received antenna signals consists in merely selecting the highest signal channel and turning off the rest. In this mode of operation, the output voltage will be

$$\text{Greatest of} \quad \begin{cases} \left|E_1 \cos\theta_i \cos\phi_i + E_2 \sin\phi_i\right| \\ \left|E_1 \cos\theta_i \sin\phi_i - E_2 \cos\phi_i\right| \\ \left|E_1\right| \sin\theta_i \end{cases} \tag{11}$$

The signal-to-noise ratio will then be given by

$$\text{Greatest of} \quad \begin{cases} \dfrac{\left|E_1 \cos\theta_i \cos\phi_i + E_2 \sin\phi_i\right|^2}{\overline{n^2}} \\ \dfrac{\left|E_1 \cos\theta_i \sin\phi_i - E_2 \cos\phi_i\right|^2}{\overline{n^2}} \\ \dfrac{\left|E_1\right|^2 \sin^2\theta_i}{\overline{n^2}} \end{cases} \tag{12}$$

The signal-to-noise ratio is once again seen to depend on angle of arrival and on polarization. The responses of the various techniques to several different incident polarizations are compared in Table 9-I.

9.2.4 Effect of Dipole Length

The preceding analysis has been performed for a combination of short dipoles to facilitate the mathematics involved. Actual linear antennas that might be used are generally near self-resonant length ($\approx$ half-wavelength) to avoid the necessity of using additional tuning elements that would tend to complicate the feeding arrangement and to lower efficiency. Consequently, actual antenna patterns will differ somewhat from those of the short dipole so that the optimal-ratio combining will not yield complete insensitivity to polarization and angle of arrival. However, the results should not differ significantly from the results computed for the short dipole case.

TABLE 9-2. CHARACTERISTICS OF RIGHT-HAND CIRCULARLY POLARIZED ANTENNAS

s = distance of dipoles from groundplane
k = 2 π /wavelength

Crossed Dipole Antennas and Groundplane	Coverage Region	E_{RH}	E_{LH}	Axial Ratio	$\left(\frac{E_{RH}}{E_{LH}}\right)^2$
RHCP* along +Z axis	$0 \le \theta \le \frac{\pi}{2}$	$e^{-j\phi} \cos^2\left(\frac{\theta}{2}\right) \sin(k\, s \cos\theta)$	$-e^{-j\phi} \sin^2\left(\frac{\theta}{2}\right) \sin(k\, s \cos\theta)$	$\sec^2\theta$	$\cot^4\left(\frac{\theta}{2}\right)$
RHCP along -Z axis	$\frac{\pi}{2} \le \theta \le \pi$	$-e^{j\phi} \cos^2\left(\frac{\pi-\theta}{2}\right) \sin(k\, s \cos\theta)$	$e^{j\phi} \sin^2\left(\frac{\pi-\theta}{2}\right) \sin(k\, s \cos\theta)$	$\sec^2\theta$	$\cot^4\left(\frac{\pi-\theta}{2}\right)$
RHCP along +X axis	$0 \le \theta \le \pi$ $-\frac{\pi}{2} \le \phi \le \frac{3\pi}{2}$	$\frac{[\sin\theta + \cos\phi - j\cos\theta \sin\phi]}{2} \sin(k\, s \sin\theta \cos\phi)$	$\frac{[\sin\theta - \cos\phi - j\cos\theta \sin\phi]}{2} \sin(k\, s \sin\theta \cos\phi)$	$\frac{1 - \cos^2\theta \cos^2\phi}{\cos^2\phi}$	$\left(\frac{1 + \sin\theta \cos\phi}{1 - \sin\theta \cos\phi}\right)^2$
RHCP along -X axis	$0 \le \theta \le \pi$ $\frac{\pi}{2} \le \phi \le \frac{3\pi}{2}$	$\frac{-[\sin\theta - \cos\phi + j\cos\theta \sin\phi]}{2} \sin(k\, s \sin\theta \cos\phi)$	$\frac{-[\sin\theta + \cos\phi + j\cos\theta \sin\phi]}{2} \sin(k\, s \sin\theta \cos\phi)$	$\frac{1 - \cos^2\theta \cos^2\phi}{\cos^2\phi}$	$\left(\frac{1 - \sin\theta \cos\phi}{1 + \sin\theta \cos\phi}\right)^2$
RHCP along +Y axis	$0 \le \theta \le \pi$ $0 \le \phi \le \pi$	$\frac{[\sin\theta + \sin\phi + j\cos\theta \cos\phi]}{2} \sin(k\, s \sin\theta \sin\phi)$	$\frac{[\sin\theta - \sin\phi + j\cos\theta \cos\phi]}{2} \sin(k\, s \sin\theta \sin\phi)$	$\frac{1 - \cos^2\theta \sin^2\phi}{\sin^2\phi}$	$\left(\frac{1 + \sin\theta \sin\phi}{1 - \sin\theta \sin\phi}\right)^2$
RHCP along -Y axis	$0 \le \theta \le \pi$ $\pi \le \phi \le 2\pi$	$\frac{-[\sin\theta - \sin\phi - j\cos\theta \cos\phi]}{2} \sin(k\, s \sin\theta \sin\phi)$	$\frac{-[\sin\theta + \sin\phi - j\cos\theta \cos\phi]}{2} \sin(k\, s \sin\theta \sin\phi)$	$\frac{1 - \cos^2\theta \sin^2\phi}{\sin^2\phi}$	$\left(\frac{1 - \sin\theta \sin\phi}{1 + \sin\theta \sin\phi}\right)^2$

*Right-hand circular polarization

9.3 MULTIPATH CONSIDERATIONS

In the previous subsections, combinations of linearly polarized antennas were considered and three combining techniques were compared. Such systems can be designed to work well in the presence of a single incident signal. However, if a multipath condition occurs in which the secondary path signal is strong and delayed relative to the direct path signal then, except for the equal gain system, the combining system may be confused by the composite signal. In addition, if the secondary path signal is doppler-shifted from the direct path signal, there will be beating at the difference frequency that may interfere further with the proper combining operation. In this case, some method must be used for multipath rejection by the antennas themselves prior to combining their outputs. Rejection can be built into such a system if the transmitted signal is circularly polarized (CP) since the multipath signal reflected by the earth will have its sense of rotation reversed over most angles of incidence (see subsection 3.2). The amount of secondary path signal that remains unreversed will thus be small and may not interfere significantly with combiner operation. Any physical antenna will not radiate a perfectly circularly polarized wave, at least not over its complete coverage region, so that complete rejection of the opposite sense polarization will not be realized. However, for axial ratios of up to 5 dB, the relative acceptance by the antenna of opposite sense circularly polarized waves is less than -10 dB. A curve of relative acceptance versus axial-ratio is shown in Figure 9-2. By using this figure, it can be seen that if the opposite sense CP signal is 3 dB down from the correct sense, and the axial ratio of the antenna is 2 dB, the opposite sense CP signal will be about 22 dB below the correct sense CP signal. This comparison assumed that the antenna gain is the same in the directions of arrival of both signals. In subsection 3.2, additional data concerning polarization ellipticity and multipath rejection are presented (see Figure 3-24).

A diversity-combining system that uses circular polarization discrimination requires six antennas. Three antennas would look along the positive directions of three mutually orthogonal axes, while three would look along the negative directions of these axes. For example, combinations of crossed dipoles fed in time quadrature above ground planes yield circularly polarized radiation in directions normal to the ground planes and elliptically polarized radiation elsewhere. The responses of these antennas to incident right-hand and left-hand circular polarizations are listed in Table 9-2. From this table, the response of the antennas for incident circularly polarized waves can be determined. The effect of multipath signals can also be estimated. If a spacing of $\lambda/3$ is used between the crossed dipoles and the groundplane, a relatively flat angular response is obtained for right-hand circulary polarized (RHCP) signals out to about 54.8 degrees, which is the lowest crossover level of patterns of adjacent antennas. At this point, the RHCP signal is down only 1.25 dB below its on-axis value, and the left-hand CP signal response is down 11.5 dB below the RHCP response. These values are shown on curve B of Figure 9-3.

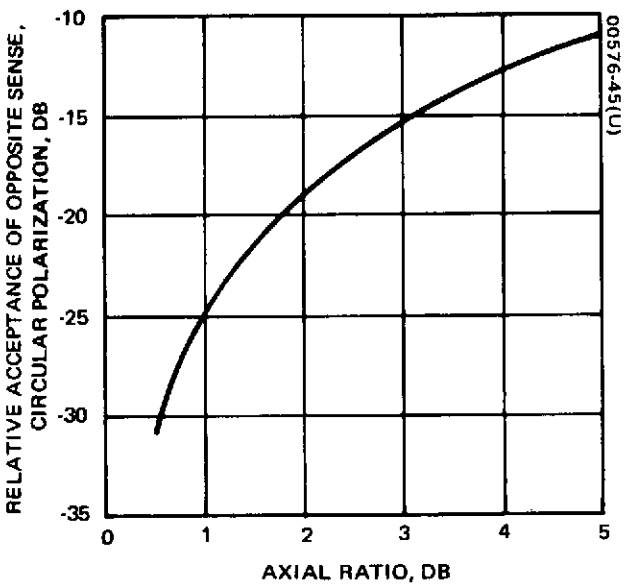

Figure 9-2. Relative Acceptance of Opposite Sense Circular Polarization Versus Axial Ratio

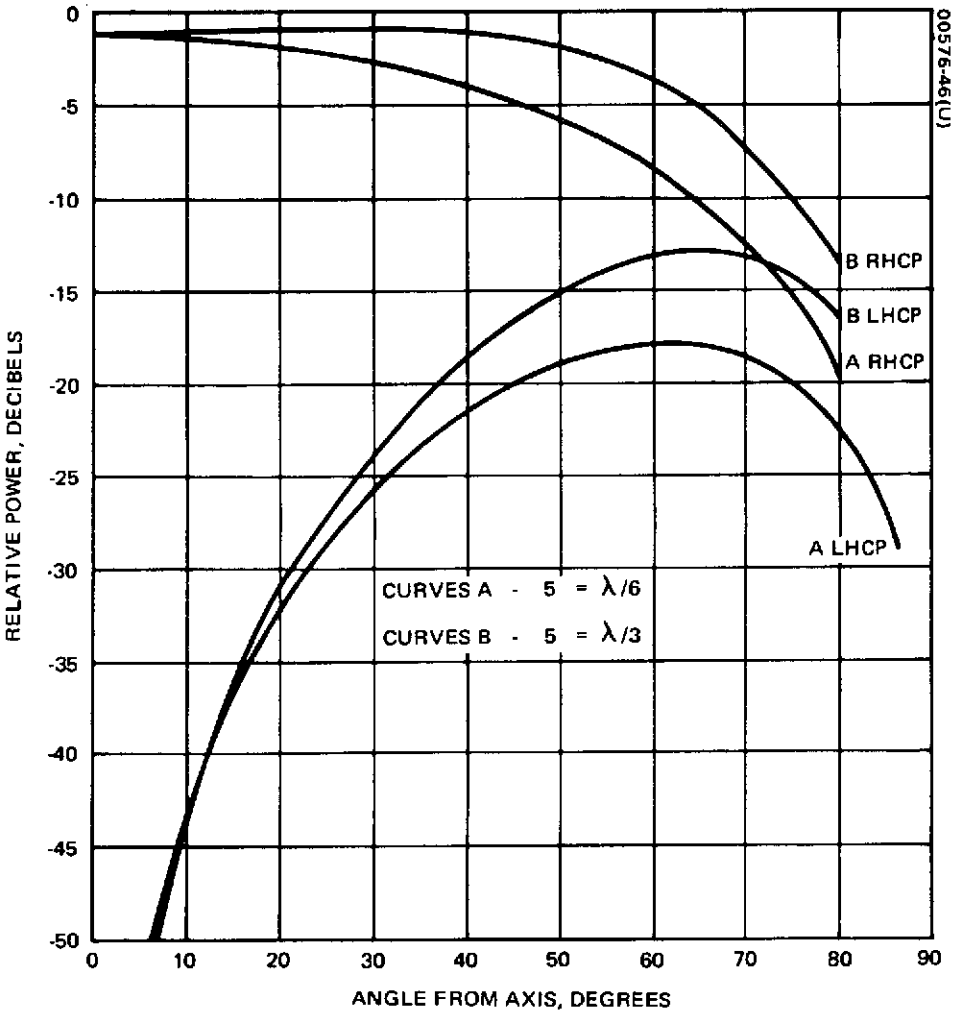

Figure 9-3. Relative Response of Crossed Short Dipoles Above Ground Plane to Both Right-Hand and Left-Hand Circularly Polarized Incident Waves

9.4 CONSIDERATION OF COMBINING TECHNIQUES

The use of maximal-ratio diversity combining or equal-gain diversity combining would allow all antennas to contribute to the signal, even those in which the multipath rejection would not be very great, and rather than improving the signal-to-interference ratio, would actually degrade it. Consequently, it appears that with an arrangement such as this, use of circular polarization with selection diversity combining would be a desirable technique to employ. With this technique, direct path signal variation would be small (no greater than 1.25 dB for the idealized case considered here), and the antennas themselves would provide multipath rejection.

There are six coverage regions that correspond to the coverage provided by each of the six circularly polarized antennas:

① and ② ±Z-axis

Bounded by planes

$$\begin{cases} \cot\theta = \pm\cos\phi & -\frac{\pi}{4} < \phi < \frac{\pi}{4} \\ \cot\theta = \pm\sin\phi & \frac{\pi}{4} < \phi < \frac{3\pi}{4} \\ \cot\theta = \mp\cos\phi & \frac{3\pi}{4} < \phi < \frac{5\pi}{4} \\ \cot\theta = \mp\sin\phi & \frac{5\pi}{4} < \phi < \frac{7\pi}{4} \end{cases}$$

where upper signs apply to +Z axis and lower signs to -Z axis

③ + X-axis

Bounded by planes

$$\begin{cases} \phi = \pm\frac{\pi}{4} \\ \cot\theta = \pm\cos\phi \end{cases}$$

④ -X-axis

Bounded by planes

$$\begin{cases} \phi = \frac{3\pi}{4} \\ \phi = \frac{5\pi}{4} \\ \cot\theta = \mp\cos\phi \end{cases}$$

⑤ + Y - axis

Bounded by planes

$$\begin{cases} \phi = \dfrac{\pi}{4} \\ \phi = \dfrac{3\pi}{4} \\ \cot\theta = \pm \sin\phi \end{cases}$$

⑥ - Y - axis

Bounded by planes

$$\begin{cases} \phi = \dfrac{5\pi}{4} \\ \phi = \dfrac{7\pi}{4} \\ \cot\theta = \mp \sin\phi \end{cases}$$

The implementation of the selection-diversity combiner for the circularly polarized case would be similar to that used for the no multipath case discussed previously, except that one of six signals would be selected rather than one of three. The implementation of the combining techniques is discussed in the next subsection.

9.5 IMPLEMENTATION OF DIVERSITY-COMBINING TECHNIQUES

The type of signal that is anticipated as incident on the spacecraft is biphase modulation with no residual carrier. The signal bandwidth is expected to be 100 kHz.

9.5.1 Maximal Ratio Combiner

A maximal-ratio combining receiving system for such a modulation scheme is illustrated in Figure 9-4. Each channel contains a preamplifier to establish the noise figure. The signal is then split two ways. One part of the signal is mixed with a reference local oscillator that is operating at the IF frequency but is phase-modulated by the detected signal. Consequently, when this signal is mixed with the incoming signal, the phase modulation is removed leaving only a sinusoidal signal whose phase shift from channel to channel is the same as the phase shift from channel to channel of the incoming signal and whose amplitude in each channel is proportional to that of the incoming signal in the channel. This signal is amplified in a narrow-band linear amplifier to increase its level and filtered to improve its signal-to-noise ratio. It is then multiplied by the incoming modulated signal in that channel to provide an IF signal that is in phase with the signals from all other channels and amplitude-weighted to give the maximum signal-to-noise

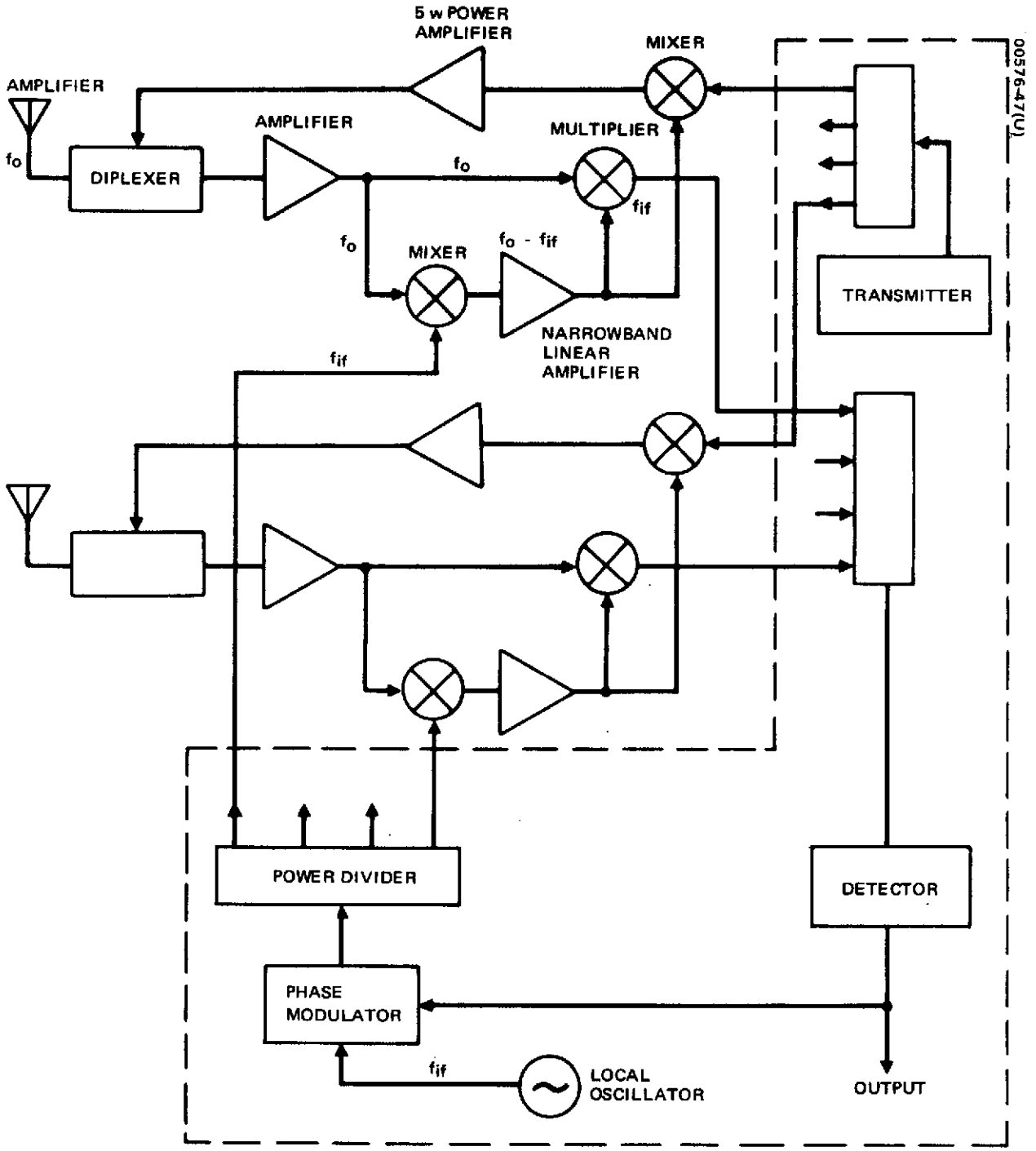

Figure 9-4. Arrangement for Maximal-Ratio Combining on Receive, Equal-Gain Combining on Transmit

Section with dashed lines is common to all channels.

ratio. The signal can then be summed and detected by the usual techniques. Table 9-3 lists the components necessary to implement such a technique. On transmission, equal-gain combining is employed because efficient weighting of high power is not presently feasible.

The determination of the exact performance characteristics of such a technique would require additional analysis and experimentation.

TABLE 9-3. COMPONENTS REQUIRED FOR MAXIMAL-RATIO DIVERSITY COMBINING* ON RECEIVE, EQUAL-GAIN COMBINING ON TRANSMIT

Component	Number	Weight/Unit, ounces	Power Required, watts
Diplexer	N	9	
RF amplifier	N		
2-way power divider	2 N		
Mixer	N	4	0.4
Narrowband linear amplifier	N		
Multiplier	N		
Mixer	N	9	
Power amplifier, 5 watts	N		
1-to-N power divider	3	2	
Phase modulator	1	2	
Local oscillator	1	2.5	

*All components for equal-gain diversity are the same except that the narrowband linear amplifiers are replaced by narrowband limiting amplifiers, and multipliers are replaced by mixers.

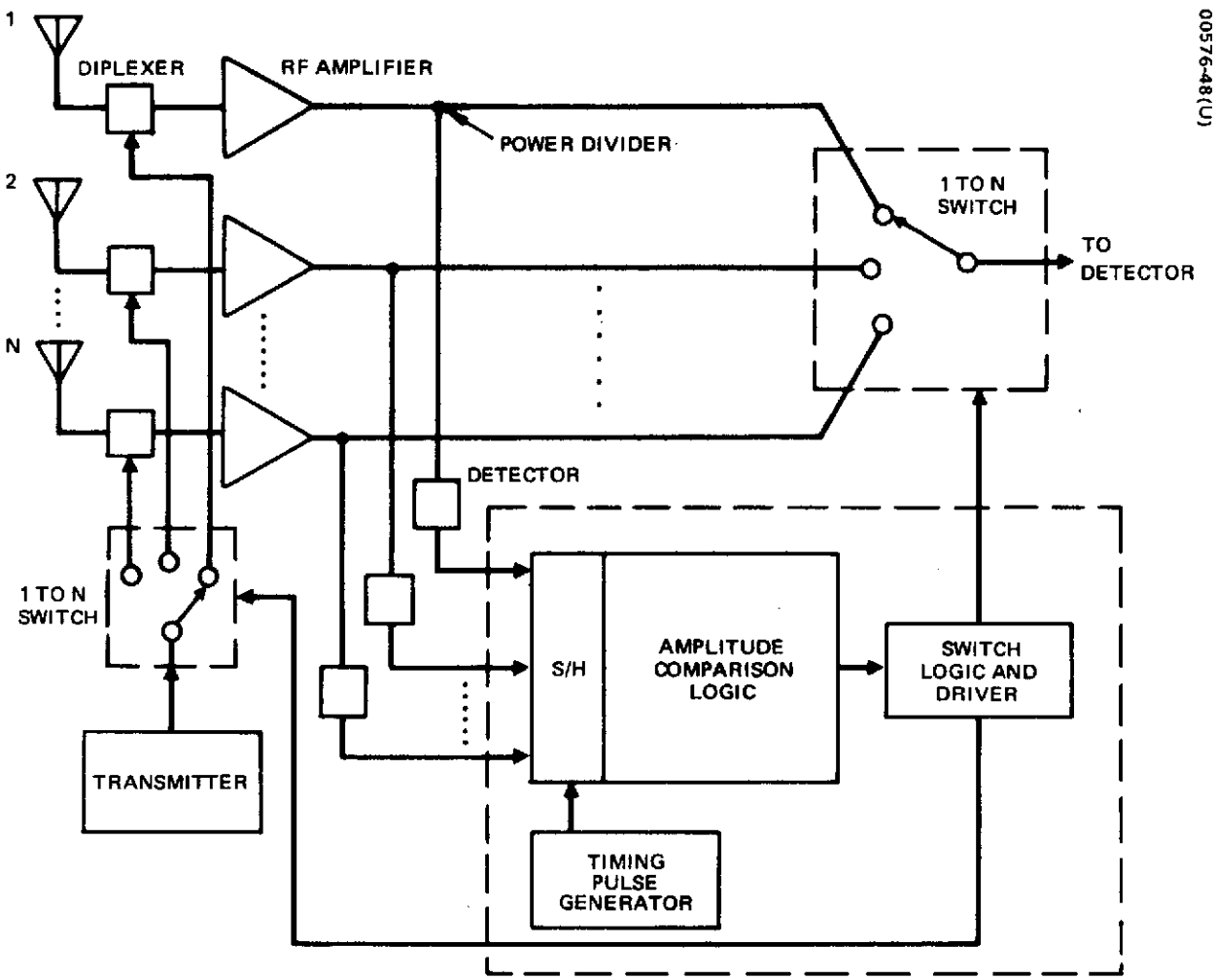

Figure 9-5. Selection-Diversity Combiner

9.5.2 Equal-Gain Combiner

An equal-gain combiner results when the narrowband linear amplifier used in the maximal ratio combiner is replaced by a limiting amplifier with a fixed amplitude output. In this latter configuration, the amplitude weighting is no longer proportional to the amplitude of the incoming signal but is the same for all channels. Table 9-3 lists the components required for equal-gain diversity.

9.5.3 Selection-Diversity Combiner

A selection diversity combining technique requires the comparison of relative signal amplitudes and connection of the channel with the greatest signal amplitude to the detector. The system illustrated in Figure 9-5 periodically samples the signals from the various channels and stores them in a sample-hold circuit. The various amplitudes are then compared in the amplitude comparison logic section. The channel with the greatest amplitude is selected. The switch logic and drivers then control the 1-to-N way switch so that the channel with the greatest signal amplitude is connected to the detector. The same channel is also used for transmitting. The components required for implementing such an arrangement are listed in Table 9-4.

TABLE 9-4. COMPONENTS REQUIRED FOR SELECTION-DIVERSITY COMBINER

Component	Number Required	Weight/Unit, ounces	Power/Unit, watts
Diplexer	N	9	
RF amplifier, Coupler, Detector	N	4	0.4
N-way switch	2	4, N = 3 6, N = 6	--
Amplitude logic, Timing generator	1 (package in 1 module)	5	0.3, N = 3 0.5, N = 6
Switch driver	1	5, N = 3 7.5, N = 6	0.1, N = 3 0.15, N=6

9.5.4 Radiating Elements

Relatively simple radiating elements are envisioned for application to these techniques. In the absence of multipath, an arrangement of three mutually perpendicular dipoles would be used. In order to avoid a possibility of blockage by the spacecraft, two such arrangements might be required. The weight of each combination of three dipoles including feeds, baluns, etc. is estimated at somewhat less than 1 pound.

For the multipath case, each of the six antennas might consist of two crossed half-wave dipoles mounted approximately $\lambda/3$ above a $3\lambda/4 \times 3\lambda/4$ ground screen. The estimated weight of each such antenna including baluns is in the neighborhood of 1 pound or less.

9.5.5 Comments

Several techniques for diversity combining have been discussed that are applicable to omnidirectional coverage by satellite antennas. The general characteristics of such systems have been considered, including the problem of reducing the effects of multipath propagation. Before any such techniques could be implemented, a more detailed examination should be made. The effects of amplitude modulation introduced by satellite spin should also be considered. The tolerance to these effects may dictate other antenna configurations to give smoother coverage in the plane of scan.

APPENDIX. SIGNAL WEIGHTING

The weighting of noisy signals to provide maximum signal-to-noise ratio is considered in this appendix. It is assumed that there are N noisy channels each with the same signal but with independent noises. The voltage of the i^{th} channel can be written as

$$v_i(t) = a_i f(t) \cos\left[\omega t + \phi(t) + \psi_i(t)\right] + n_i(t)$$

where f(t) and $\phi(t)$ represent amplitude and phase modulations, respectively, a_i is the amplitude of the signal, ψ_i its phase, and $n_i(t)$ is the noise voltage. The signals from each channel must be put in phase with each other before combining. The resulting combined voltage is given by

$$v_t = \sum_{i=1}^{N} A_i a_i f(t) \cos\left[\omega t + \phi(t)\right] + \sum_{i=1}^{N} A_i n_i(t)$$

where the A_i are the weighting coefficients. The signal-to-noise ratio is therefore given by

$$\frac{S}{N} = \frac{\frac{1}{2} f^2 \left(\sum_i A_i a_i\right)^2}{\sum_i n_i^2 A_i^2}$$

The values of the A_i that maximize S/N must satisfy the following condition, derived by requiring that

$$\frac{\partial(S/N)}{\partial A_i} = 0 \qquad i = 1, \cdots, N$$

$$A_i = \frac{\left(\sum n_j^2 A_j^2\right)}{\left(\sum_j a_j A_j\right)} \frac{a_i}{n_i^2} = K \frac{a_i}{n_i^2}$$

Thus the weighting coefficients must be proportional to the ratio of the amplitude of the signal in the i^{th} channel to the mean noise power in that channel. If the mean noise powers in all channels are equal, then the A_i are proportional to the signal amplitudes in their respective channels. The resulting signal-to-noise ratio is just the sum of the signal-to-noise ratios in each channel.

REFERENCES

1. "GSFC Mark I Tracking and Data Relay Satellite (TDRS) System Concept," Phase A Study Final Report, Goddard Space Flight Center, November 1969.

2. "Goddard Range and Range System, Design Evaluation Report," General Dynamics, Electronics Division, NASA Contract No. NAS 5-10555, 13 December 1967.

3. D. J. Eggert, "Multipath Study for a Low Altitude Satellite Utilizing a Data Relay Satellite System," Hughes Aircraft Company Report for NASA, Contract No. NAS 5-11602, October 1970.

4. D. J. Eggert, "Study of a Low Altitude Satellite Utilizing a Data Relay Satellite System, Phases I and II," Hughes Aircraft Company Report for NASA, Contract No. NAS 5-11602, January and August 1969.

5. J. W. Bryan, "RFI Characteristics of a Delay Relay Satellite System," Proceedings of the International Telemetering Conference, Vol. V, 1969.

6. "Final Report for Multipath Modulation Study – Adaptive Techniques," Hekemian Laboratories Report for NASA, GSFC, Contract No. NAS5-10749, March 1970.

7. J. N. Birch, "Multipath/Modulation Study for the Tracking and Data Relay Satellite System," Magnavox Company Report for NASA, Contract No. NAS 5-10744, January 1970.

8. S. W. Golomb, Shift Register Sequences, Holden-Day, 1967.

9. Handbook of Mathematical Functions, National Bureau of Standards, Applied Mathematics Series - 55, June 1964.

10. R. Gold, "Optimal Binary Sequences for Spread Spectrum Multiplexing," IEEE Transactions on Information Theory, IT-13, October 1967, pp 619-621.

11. J. I. Marcum, "A Statistical Theory of Target Detection by Pulsed Radar," with mathematical index, RAND Research Memo RM-754, 1 December 1947.

12. J. Pachares, "A Table of Bias Levels Useful in Radar Detection Problems," IRE Trans. on Information Theory, IT-4, No. 1 (1958) pp 38-45.

13. D. J. Eggert, "Antenna Acquisition by Scanning," Hughes Interdepartmental Correspondence No. 2290/820, 7 May 1970.

14. F. M. Gardner, Phase Lock Techniques, John Wiley and Sons, 1966.

15. G. C. Kronmiller, Jr. and E. J. Baghdady, "GRARR Tracking System – Concept Design and Performance," NASA, GSFC Report No. X-531-65-403, October 1965.

16. J. A. Develet, Jr., "Fundamental Accuracy Limitations in a Two-way Coherent Doppler Measurement System," IRE Transactions on Space Electronics and Telemetry, Sept. 1961, p 80-85.

17. R. H. Pickard and P. J. Heffernan, "ATS-F/Nimbus-E Tracking and Data Relay Experiment," AIAA Paper 70-1306, Houston, Texas, October 1970; NASA GSFC Document X-751-70-361.

18. D. G. Brennan, "Linear Diversity Combining Techniques," Proc. of the IRE, Vol. 47, No. 6, June 1959, pp 1075-1102.